
Doctoral Dissertations

Student Theses and Dissertations

Fall 2020

Modeling and optimization of froth flotation of low-grade phosphate ores: Experiments and machine learning

Ashraf Alsafasfeh

Follow this and additional works at: https://scholarsmine.mst.edu/doctoral_dissertations



Part of the [Mining Engineering Commons](#)

Department: Mining Engineering

Recommended Citation

Alsafasfeh, Ashraf, "Modeling and optimization of froth flotation of low-grade phosphate ores: Experiments and machine learning" (2020). *Doctoral Dissertations*. 2948.
https://scholarsmine.mst.edu/doctoral_dissertations/2948

This thesis is brought to you by Scholars' Mine, a service of the Missouri S&T Library and Learning Resources. This work is protected by U. S. Copyright Law. Unauthorized use including reproduction for redistribution requires the permission of the copyright holder. For more information, please contact scholarsmine@mst.edu.

MODELING AND OPTIMIZATION OF FROTH FLOTATION OF LOW-GRADE
PHOSPHATE ORES: EXPERIMENTS AND MACHINE LEARNING

by

ASHRAF ALSAFASFEH

A DISSERTATION

Presented to the Graduate Faculty of the
MISSOURI UNIVERSITY OF SCIENCE AND TECHNOLOGY

In Partial Fulfillment of the Requirements for the Degree

DOCTOR OF PHILOSOPHY

in

MINING ENGINEERING

2020

Approved by:

Dr. Lana Alagha, Advisor
Dr. Taghi Sherizadeh
Dr. Mark Schlesinger
Dr. Shoaib Usman
Dr. Venkata Sriram Siddhardh Nadendla

© 2020

Ashraf Alsafasfeh

All Rights Reserved

ABSTRACT

In this research work, bench-scale and micro-scale flotation tests were conducted to separate phosphate minerals from silicate minerals using direct and reverse flotation approaches, respectively. Experiments were conducted at different flotation conditions including reagents' type, reagents' dosages, pulp's pH, and flotation time.

In the direct flotation process, two polymers were selected to promote the depression of silicates: hybrid polyacrylamide-based polymers (Hy-PAM) and chitosan. Results indicated that the highest recovery of P_2O_5 (86.82%) was obtained when the Hy-PAM polymer was used compared with 66.7% and 40% when chitosan and commercial inorganic depressant were used, respectively. The experimental datasets obtained from the direct flotation tests were assimilated to develop an artificial neural network (ANN) model to predict the flotation efficiency of phosphate minerals in relation to various process parameters. The developed ANN model predicted that optimum flotation performance can be achieved at 4 min of flotation time, 250-300 g/ton of reagents' dosages, and pH 9.

The reverse flotation tests were conducted using two types of ionic liquid collectors (THAI and HMLHF) in micro-flotation system wherein pure apatite and quartz were used as an example of phosphate and silicate minerals, respectively. Results obtained from mixed minerals flotation showed that quartz's recovery and grade were ~90% and ~64% when HMLHF was used at pH 11. When THAI was used, the recovery and grade of quartz were 87% and 70.3%, respectively, compared with 87% and 65.3% when commercial amine collector was used.

ACKNOWLEDGMENTS

I would like to express my greatest acknowledgment to my advisor Dr. Lana Alagha for her precious advice, motivation, and continual support throughout this study. This thesis was impossible to be completed without her academic guidance, fairness, and responsiveness. Her modest and prudent spirit always influences me and reminds me to work harder.

I would like to extend my deep gratitude to the thesis committee members, Dr. Mark Schlesinger, professor of materials science & engineering. Dr. Shoaib Usman, associate professor of nuclear engineering, Dr. Taghi Sherizdeh, assistant professor of mining engineering, and Dr. Venkata Sriram Siddhardh Nadendla, assistant professor of computer science, for accepting to be members of my Ph.D. dissertation committee. My appreciation is also expressed to all the staff members in the departments of Mining and Nuclear Engineering and Material Science and Engineering for their help. My appreciation is also extended to the graduate students in Dr. Alagha's research group, Ms. Keitumetse Monyake, and Mr. Jose Corchado Albelo for their support and useful discussions.

Finally, I would like to dedicate this thesis to my dearest family. The constant support and encouragement from my father and mother were always the greatest motivation for me to accomplish all. I want to thank my wife, Ala Alzidaneen, for her love and constant support, for all the late nights and early mornings, and for keeping me sane over the past few months. Most of that work occurred on weekends, nights, while on vacation, and other times that were inconvenient to my family. Thank you for being my wife. I owe you everything.

TABLE OF CONTENTS

	Page
ABSTRACT.....	iii
ACKNOWLEDGMENTS	iv
LIST OF ILLUSTRATIONS.....	ix
LIST OF TABLES.....	xiii
 SECTION	
1. INTRODUCTION.....	1
1.1. PHOSPHATE DEPOSITS AND ORE PROCESSING	1
1.2. STATEMENT OF THE PROBLEM	3
1.3. OBJECTIVES OF THE CURRENT WORK.....	4
1.4. BROADER IMPACTS AND INTELLECTUAL MERIT OF THE PRESENT WORK	5
1.4.1. Broader Impact.	5
1.4.1.1. Economic benefits.....	5
1.4.1.2. Environmental benefits.....	6
1.4.2. Intellectual Merit.....	6
1.5. RESEARCH STRATEGY	7
1.5.1. Phase I: Investigations on Mineralogical and Morphological Characteristics of Low-Grade Phosphate Ore.....	7
1.5.2. Phase II: Investigations on the Adsorption Characteristics of Reagents on Phosphate and Silicate Surfaces.....	8

1.5.3. Phase III: Investigations on the Flotation Behavior of Phosphates and Silicates Minerals using Alternative Reagents	9
1.5.4. Phase IV: Machine Learning (ML) Modeling to Predict the Flotation Performance of Phosphate-Silicate Ores.	11
1.6. ORGANIZATION OF DISSERTATION.....	12
2. LITERATURE REVIEW.....	14
2.1. FROTH FLOTATION FUNDAMENTALS.....	14
2.2. PHOSPHATE FLOTATION PROCESS	16
2.2.1. Direct Flotation	17
2.2.2. Reverse Flotation	17
2.3. VARIABLES AFFECTING FROTH FLOTATION EFFICIENCY	18
3. ENHANCED RECOVERY OF PHOSPHATE MINERALS FROM LOW-GRADE ORE USING DIRECT FROTH FLOTATION	23
3.1. BACKGROUND.....	23
3.2. METHODOLOGY AND MATERIALS	25
3.2.1. Mineral Samples and Flotation Reagents	25
3.2.2. Characterization of the Flotation Feed.....	26
3.2.2.1. Particle size distribution.....	26
3.2.2.2. Mineral liberation analysis (MLA).....	27
3.2.2.3. X-ray diffraction (XRD).....	34
3.2.2.4. Scanning electron microscope (SEM).....	34
3.2.2.5. Zeta potential measurements.....	35
3.2.3. Flotation Experiments.....	36
3.3. RESULTS AND DISCUSSIONS	39

3.3.1. Zeta Potential Measurement.....	39
3.3.2. Investigations on the Potential of Polymers to Aid Silicate Depression in Phosphate’s Flotation Process.....	41
3.3.2.1. Baseline experiments.....	41
3.3.2.2. Flotation experiments in the presence of sodium silicate dispersant.....	42
3.3.2.3. Flotation experiments in the presence of Hy-PAM depressant.....	44
3.3.2.4. Flotation experiments in the presence of chitosan depressant.....	47
4. RECOVERY OF PHOSPHATE MINERALS USING IONIC LIQUIDS IN REVERSE FLOTATION PROCESS.....	51
4.1. BACKGROUND.....	51
4.2. METHODOLOGY AND MATERIALS	53
4.2.1. Materials.....	53
4.2.2. Zeta Potential Measurement.....	53
4.2.3. Adsorption Studies.....	53
4.2.4. Micro-flotation Experiments.....	54
4.3. RESULTS AND DISCUSSIONS	56
4.3.1. Adsorption Studies.....	56
4.3.2. Zeta Potential Measurements.....	63
4.3.3. Micro-flotation Experiments.....	65
4.3.3.1. Single mineral flotation experiments in the presence of tetrahexyl-ammonium iodide (THAI) collector.....	66

4.3.3.2. Single mineral flotation experiments in the presence of 1-hexyl-3-methylimidazoli hexafluorophosphate (HMLHF) collector.....	67
4.3.3.3. Comparison of single mineral flotation performance of apatite and quartz in the presence of ionic liquid collectors and commercially used dodecylamine collectors.....	67
4.3.3.4. Comparison of flotation performance of binary mineral system in the presence of ionic liquid collectors and commercially used dodecylamine collectors.....	69
5. APPLICATIONS OF ARTIFICIAL NEURAL NETWORK MODELING TO PREDICT THE FLOTATION PERFORMANCE OF PHOSPHATE-SILICATE ORES.....	71
5.1. BACKGROUND.....	71
5.2. DATASETS DEVELOPMENT.....	73
5.3. NEURAL NETWORK DESIGN.....	74
5.4. RESULTS AND DISCUSSION.....	76
6. CONCLUSIONS AND RECOMMENDATIONS.....	89
6.1. CONCLUSIONS.....	89
6.2. RECOMMENDATIONS FOR FUTURE WORK.....	91
BIBLIOGRAPHY.....	94
VITA.....	103

LIST OF ILLUSTRATIONS

	Page
Figure 1.1 Worldwide phosphate reserves and deposits.....	1
Figure 1.2 Schematic representation of tasks performed in Phase I.....	8
Figure 1.3 Schematic representation of tasks performed in Phase II.....	9
Figure 1.4 Schematic representation of tasks performed in Phase III.....	10
Figure 1.5 Schematic representation of tasks performed in Phase IV.....	11
Figure 2.1 Principle of the froth flotation process.....	14
Figure 2.2 Different variables in froth flotation process.....	15
Figure 2.3 Simplified flowsheets of a typical flotation circuit.....	16
Figure 2.4 Flow diagram of the direct flotation process at Florida’s phosphate mines ...	17
Figure 2.5 Flow diagram of reverse flotation process at Florida’s phosphate mines	18
Figure 2.6 Flotation process flowsheet adopted at Agrium Inc.–Kapusksing Phosphate Operations (KPO)	21
Figure 2.7 Flotation recovery of phosphate minerals as a function of particle size of flotation feed	22
Figure 3.1 Structure of hybrid polyacrylamide polymer (Hy-PAM).....	24
Figure 3.2 Structure of chitosan polymer	25
Figure 3.3 Particle size distribution of the flotation feed.....	27
Figure 3.4 Model mineralogy.....	28
Figure 3.5 MLA-calculated elemental composition (Wt.%).	29
Figure 3.6 Mineral grain size distributions of apatite phases.....	31

Figure 3.7 Composite mineral liberation by particle composition for the apatite, mixed apatite/fluorite, and quartz.....	31
Figure 3.8 Mineral liberation of apatite phase by sieve fraction in the flotation feed.....	32
Figure 3.9 Mineral liberation of the mixed apatite phase by sieve fraction in the flotation feed.....	32
Figure 3.10 Mineral liberation of the quartz phase by sieve fraction in the flotation feed.....	33
Figure 3.11 X-ray diffraction (XRD) patterns of the flotation feed.....	34
Figure 3.12 A photograph of zetasizer nano ZS instrument used in this study.....	36
Figure 3.13 A photograph of denver flotation cell used in this study.....	37
Figure 3.14 Zeta potential measurements of apatite and quartz at different pH.....	39
Figure 3.15 Zeta potential measurements of apatite and quartz after mixing with different reagents at natural pH (A) and pH 9 (B).....	41
Figure 3.16 Baseline flotation experiments at different flotation conditions.....	42
Figure 3.17 Flotation recovery of P_2O_5 in the presence of sodium silicate at different flotation conditions.....	43
Figure 3.18 Concentrate grade of P_2O_5 in the presence of sodium silicate at different flotation conditions.....	44
Figure 3.19 Flotation recovery of P_2O_5 in the presence of Hy-PAM at different flotation conditions.....	45
Figure 3.20 Concentrate grade of P_2O_5 in the presence of Hy-PAM at different flotation conditions.....	46
Figure 3.21 Comparisons of flotation performance of P_2O_5 in the presence of sodium silicate and Hy-PAM at pH 9.....	47
Figure 3.22 Flotation recovery of P_2O_5 in the presence of chitosan at different flotation conditions.....	48
Figure 3.23 Concentrate grade of P_2O_5 in the presence of chitosan at different flotation conditions.....	49

Figure 3.24 Comparisons of flotation performance of P ₂ O ₅ in the presence of sodium silicate and chitosan at pH 9.	50
Figure 3.25 A comparison between the flotation performance of P ₂ O ₅ in the presence of commercial dispersant sodium silicate, Hy-PAM, and chitosan at pH 9. .	50
Figure 4.1 Chemical structure of A) Tetrahexylammonium iodide (THAI), and B) 1-Hexyl-3-methylimidazoli hexafluorophosphate (HMLHF).	52
Figure 4.2 A photograph of hallimond micro-flotation tube used in this study.	55
Figure 4.3 FTIR spectra of pure THAI and HMLHF.	57
Figure 4.4 FTIR spectra of pure apatite(1-A), A-THAI (1-B), A-HMLHF (1-C), pure quartz(2-A), Q- THAI (2-B), and Q-HMLHF (2-C).	58
Figure 4.5 XPS spectra for (A) THAI, (B) N 1s of THAI, (C) HMLHF, and (D) N 1s of HMLHF.	59
Figure 4.6 XPS spectra for (A) pure quartz and (B) pure apatite.	60
Figure 4.7 XPS spectra of N 1s of pure IL and IL treated quartz and apatite.	61
Figure 4.8 the XPS curve fitting of N (1S) of pure minerals and HMLHF treated quartz and apatite.	63
Figure 4.9 Zeta potential measurements of mineral suspensions before and after adsorption of ILs.	65
Figure 4.10 Recovery of apatite and quartz at different flotation conditions with THAI.	66
Figure 4.11 Recovery of apatite and quartz at different flotation conditions with HMLHF.	67
Figure 4.12 Recovery of apatite and quartz at optimum flotation conditions (pH 9 and 11, and 150 g/ton collector dosage).	68
Figure 4.13 The recovery and grade of quartz in the presence of ionic liquids and Dodecylamine collectors.	70
Figure 4.14 The recovery and grade of apatite in the presence of ionic liquids and Dodecylamine collectors.	70

Figure 5.1 Datasets developed from laboratory scale batch flotation experiments of phosphate ore.....	73
Figure 5.2 Flowchart of the machine learning strategy applied in this study.....	74
Figure 5.3 Real vs. predicted values of the training phase of the ANN model for both of recovery and grade.....	78
Figure 5.4 Real vs. predicted values of the testing phase of the ANN model for both of recovery and grade.....	79
Figure 5.5 Predicted and experimental values of P ₂ O ₅ recovery using three-hidden layer ANN.....	80
Figure 5.6 Predicted and experimental values of P ₂ O ₅ grade using three-hidden layer ANN.....	81
Figure 5.7 Predicted recovery and grade vs the random normalized input data in the presence of sodium silicate.....	82
Figure 5.8 The relationship between the flotation inputs and expected flotation outputs in the presence of sodium silicate, recovery (A) and grade (B).	83
Figure 5.9 Predicted recovery and grade vs a random normalized input data in the presence of Hy-PAM.....	85
Figure 5.10 The relationship between the flotation inputs and expected flotation outputs in the presence of Hy-PAM, recovery (A), and grade (B).....	86
Figure 5.11 Predicted recovery and grade vs a random normalized input data in the presence of chitosan.....	87
Figure 5.12 The relationship between the flotation inputs and expected flotation outputs in the presence of chitosan, recovery (A), and grade (B).	88

LIST OF TABLES

	Page
Table 2.1 Common collectors used in phosphate flotation operations	19
Table 2.2 Common depressants used in phosphate flotation operations	20
Table 3.1 A list of reagents used throughout this study.	26
Table 3.2 Phosphorus distribution by mineral type.	30
Table 3.3 Phosphate mineral associations in the flotation feed.	33
Table 3.4 EDS analysis of flotation feed.	35
Table 3.5 Different conditions and parameters used in this study.	38
Table 4.1 Experimental conditions used to investigate the flotation efficiency of apatite and quartz in the reverse flotation process.	56
Table 4.2 Binding Energy Shifts of the N 1s of ILs before and after adsorption on apatite and quartz.	62
Table 5.1 Statistical analysis of trained and tested data.	77
Table 5.2 Statistical analysis of normalized trained and tested data.	77
Table 5.3 Model evaluation of the three hidden layers.	80

1. INTRODUCTION

1.1. PHOSPHATE DEPOSITS AND ORE PROCESSING

Phosphate rocks are one of the non-renewable resources in the earth's crust [1]. There are three major types of phosphate deposits in the world: sedimentary, igneous, and metamorphic [1], [2]. Approximately 80 % of these deposits are sedimentary, 15% are igneous, and 5% are metamorphic. The sedimentary deposits are mainly located in the Middle East, China, the United States, and Morocco. Igneous deposits are distributed in South Africa and Russia, while the metamorphic deposits are located in India [1], [3], [4]. The worldwide phosphate reserves are shown in Figure 1.1. As shown, Morocco and Western Sahara in North Africa contain approximately 50% of the world's phosphate reserves [4].



Figure 1.1 Worldwide phosphate reserves and deposits [4].

Phosphate ore bodies are usually associated with other minerals of no economic values [4]–[8]. These minerals include clays, silicates, calcites, and dolomite [4], [9], [10]. Dolomite and silicates are the major gangue minerals that need to be removed at the early stages of processing since their presence has a negative impact on downstream processing. Their low solubility may cause blinding or bogging of filters, which could increase the pumping costs [4], [11].

Several beneficiation techniques are usually applied to enrich phosphate minerals in the ore. The choice of the beneficiation technique depends on the mineralogical and morphological characteristics of the ore body. These techniques include size reduction and screening, electrostatic separation, magnetic separation, and froth flotation [4], [11], [12]. The size reduction and screening method is a traditional technique used to upgrade phosphate minerals. It utilizes the differences in the friability factor between phosphate minerals and the associated gangue minerals, but a high percentage of phosphate minerals is lost in the coarse size fraction [13]. The electrostatic separation method is a combination of attrition, gravity separation, and desliming that has been successfully used to remove silicates and carbonates minerals from phosphate ore. This method has less efficiency at larger scale production operations due to the low capacity of the electrostatic separators [13]. The magnetic separation method is practically used when processing igneous phosphate rocks that contain significant amounts of magnetic gangue minerals [4], [12], [14]. The Froth flotation process is usually used to upgrade phosphate minerals in most phosphate production plants. The Froth flotation process exploits the difference in surface hydrophobicity of mineral particles. In this process, mineral particles are selectively captured and carried by air bubbles to the froth product, whereas hydrophilic minerals are

discharged as tailings or reject. Therefore, it is considered one of the most selective and versatile techniques for mineral enrichment. [4], [12], [14]–[16].

1.2. STATEMENT OF THE PROBLEM

Phosphate is one of the most common minerals essential to human, animal, and plant life [17]–[19]. It is an important mineral commodity used in phosphoric acid production, which is used to make phosphate salts for fertilizers [12], [20]. The phosphate ore bodies are usually associated with other minerals (gangue minerals) such as siliceous, calcareous, and clayey minerals. These minerals are generally removed during the beneficiation processes of phosphate ores [4], [12], [21]. Silicate minerals are the most common gangue minerals associated with phosphates ores and present several technical challenges and complex processing, especially in the processing of lower-grade ores [4]. To make the chemical extraction process of phosphates economically feasible, phosphate minerals must be physically enriched to remove the majority of silicates prior to chemical dissolution [12], [22]. Since silicates are liberated at finer sizes, the froth flotation process is usually used to separate phosphates from silicates [23], [24].

Phosphate minerals can be separated from silicates using either direct froth flotation (i.e., phosphates are floated, and silicates are depressed) or reverse flotation process where phosphates are depressed, and silicates are floated [4], [23]. Despite the extensive and successful application of this process in phosphate separation, selective depression silicate minerals remain a serious challenge. This is primarily due to changes in ore quality, crystalline phases, and water quality over time – all of which affect the interfacial micro-processes taking place in liquid-solid-gas interfaces that govern the froth flotation behavior

of constituent minerals. Therefore, there is an urgent need for the utilization of “flexible” and sustainable reagents that remain selective and perform efficiency in different conditions.

Furthermore, phosphates' flotation efficiency is influenced by several key process variables [e.g., water chemistry, reagents chemistry, feed characteristics, cell type, and aeration rate]. Although each of these parameters influences the flotation process outcomes (recovery and grade) independently, their interdependence makes the process control very difficult. Therefore, it is of central importance to develop and employ adaptive intelligent control tools that consider the diversity of these variables and their mutual interaction to ensure process stability and desired outcomes.

1.3. OBJECTIVES OF THE CURRENT WORK

This research proposes different approaches to improve the separation of silicate minerals from low-grade phosphate ore by froth flotation process. The specific objectives are:

1. To investigate the potential of using organic-inorganic hybrid polyacrylamides (functional synthetic polymers) and chitosan (biodegradable polymer) as selective depressants of silicates in the direct flotation process of low-grade phosphate ore.
2. To investigate the potential of using ionic liquid (IL) as selective collectors of silicates in the reverse flotation process of a model phosphate ore.
3. To investigate the effect of key process variables on the recovery of phosphate minerals (in terms of P_2O_5) and the grade of the concentrate products; and

4. To develop and employ a machine learning (ML) platform to predict the flotation process outcomes in relation to various process variables, which in turn can be used to optimize the flotation efficiency of phosphate minerals.

1.4. BROADER IMPACTS AND INTELLECTUAL MERIT OF THE PRESENT WORK

1.4.1. Broader Impact. This research will contribute immensely to the existing body of knowledge on froth flotation efficiency in mineral processing. Results generated from this study will be beneficial at different frontiers:

1.4.1.1. Economic benefits. Selection of the reagents plays a significant role in evaluating the economic feasibility of the froth flotation process of minerals at industrial scale. Commercial flotation depressants that are currently used in industrial operations need at least two flotation stages, in most cases, for either direct or reverse flotation. This is to enhance the process efficiency and to upgrade the phosphate concentrates to the required economic production-grade, which should be at least 24% of P_2O_5 [25]. Based on the results obtained from this work, the proposed reagents could produce the target economic grade of P_2O_5 in a single-stage flotation, which could reduce the energy and reagent consumption. For example, a flotation plant with double-stage flotation needs 15 KW.h per ton [26]. The average industrial electricity rates are 8.82¢/KW.h [27]. The energy cost is \$1.323 per KW.h/ton. In a single-stage flotation, the hourly energy consumption is 7.5 KW.h per ton. This should reduce the energy cost to \$0.6615 per KW.h/ton. In addition, the proposed techniques and alternative reagents helped significantly to improve the flotation outcomes at shorter flotation time. This potential

reduction in the energy consumption is critical at an industrial scale where energy cost is a determinant factor to assess the economic feasibility of flotation processes.

1.4.1.2. Environmental benefits. As the waste produced from the phosphate industry presents many challenges due to the environmental impacts of their disposal, the new reagents should improve the environmental profile of the flotation process and reduce the tailing discharge. For example, the proposed reagents have the potential to reduce the amount of tailing products since they are able to significantly increase the recovery of phosphates in the concentrate products. This will help to reduce the cost of tailing disposal. Also, in the direct froth flotation practice, sodium silicate is usually used as a dispersant of silicate minerals to suppress their flotation [9]. Although sodium silicate has shown good performance in depressing the flotation of silicate minerals, recent studies indicated that sodium silicate is toxic to aquatic and terrestrial organisms [28]–[30]. Moreover, it may cause irritation to the skin and eyes [30]. Therefore, its replacement with green reagents from sustainable resources is appealing. Furthermore, chitosan polymer used as an alternative depressant of silicates is considered a green biodegradable reagent. Recent research approved that chitosan is very safe for human uses like dietary and approved for pharmaceutical manufacturing, and no adverse effects reported in the skin or eyes [31], [32].

1.4.2. Intellectual Merit. The proposed research should result in a better understanding of the factors that impact the froth flotation process. Considerable information will be generated through the different phases of this work that will broaden the knowledge in the field of phosphate mineral flotation. The findings of this study should also advance the fundamental knowledge in different areas of science and engineering as

follows: Understanding the interaction mechanism between mineral particles in the flotation pulp and the reagents through electro-kinetic measurements, Fourier-Transform Infrared Spectroscopy (FTIR), and X-ray Photoelectron Spectroscopy (XPS) will contribute to the field of applied surface science.

- Understanding the mineralogical and morphological characteristics as well as grain liberation of the flotation feed will assist in selecting the best separation method and thus will contribute to the fields of process mineralogy and separation science.
- Development of machine learning and artificial intelligence models for reliable prediction of flotation performance will pave the path for developing “smart systems” for better control of phosphate flotation in industrial plants, especially when polymers are used as process aids. Such control is vital to ensure peak performance and process stability with no significant amplification in cost and time—especially in industry- scale froth flotation procedures, which feature continuous variation in feed characteristics and water quality.

1.5. RESEARCH STRATEGY

The following explains how the project was accomplished through the implementation of four major research phases.

1.5.1. Phase I: Investigations on Mineralogical and Morphological Characteristics of Low-Grade Phosphate Ore. Characterization studies such as X-ray Diffraction (XRD), X-ray Fluorescence (XRF), Scanning Electron Microscopy (SEM), and Mineral Liberation Analysis (MLA) were first conducted to identify the mineralogical and morphological characteristics as well as grain liberation to understand the behavior of the

flotation feed better. In this phase and as shown in Figure 1.2. the tasks focused on preparing phosphate samples by mixing, collecting, drying, and sieving according to ASTM C136-14 protocol, then extensive characterization studies on different size fractions were performed using XRD, XRF, SEM, and MLA.

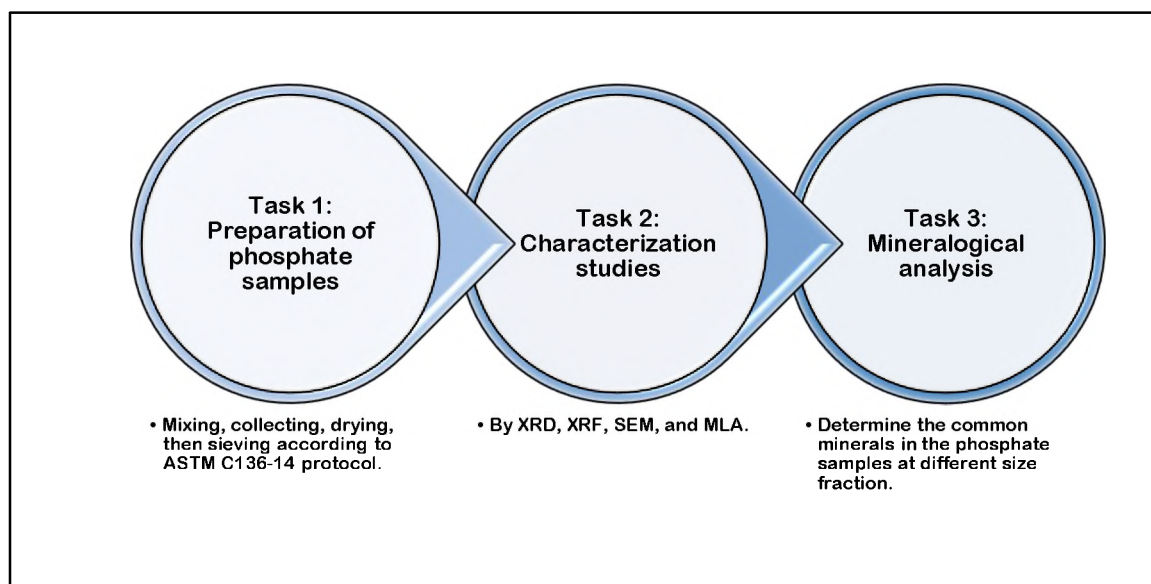


Figure 1.2 Schematic representation of tasks performed in Phase I.

1.5.2. Phase II: Investigations on the Adsorption Characteristics of Reagents on Phosphate and Silicate Surfaces. This phase aimed to build a strong foundation to design an appropriate experimental procedure that were implemented in the following phases to achieve the optimum separation of silicates from phosphate minerals. In this phase, the fundamental features of reagents adsorption on minerals surfaces were investigated. Quartz was used as an example of silicate minerals, while apatite was used as an example of phosphate minerals. All the tasks of this phase are outlined in Figure 1.3.

Sodium silicate dispersant and amine collector were selected as conventional reagents for comparison purposes. Chitosan, organic-inorganic hybrid polyacrylamide (Hy-PAM), tetrahexylammonium iodide (THAI), and 1-Hexyl-3-methylimidazoli hexafluorophosphate (HMLHF) were tested as alternatives to the conventional reagents. Zeta potential measurements were performed on mineral surfaces before and after the addition of reagents to study the influence of these reagents on the electrical characteristics of the selected minerals and understand the flotation behavior of minerals.

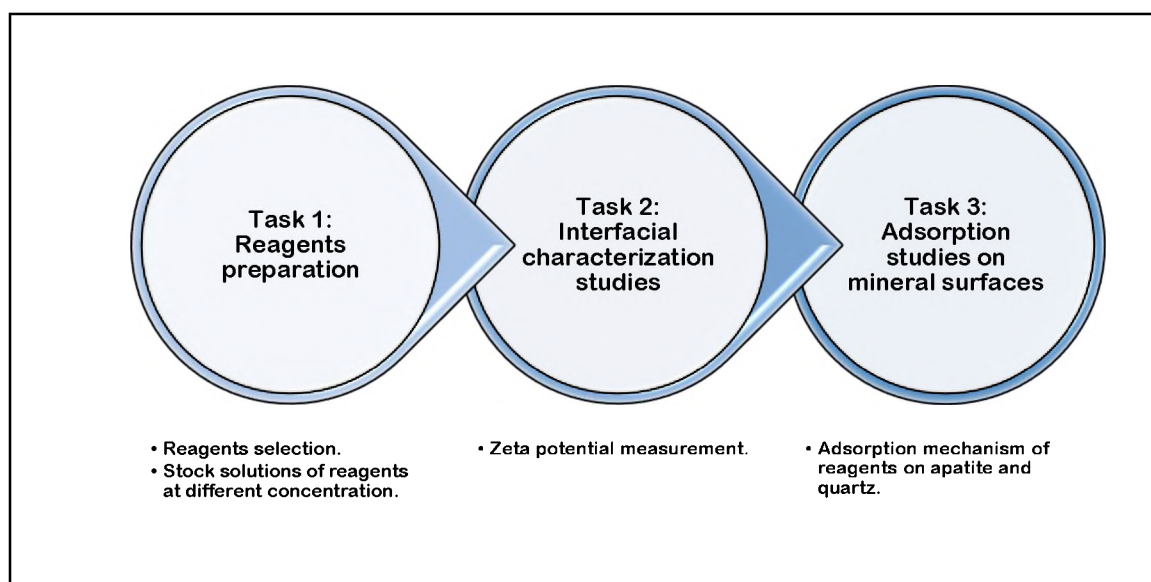


Figure 1.3 Schematic representation of tasks performed in Phase II.

1.5.3. Phase III: Investigations on the Flotation Behavior of Phosphates and Silicates Minerals using Alternative Reagents. In this phase, froth flotation experiments were conducted using conventional and alternative reagents. As stated earlier, two different approaches were investigated to enhance the separation of phosphates from silicates (Figure 1.4).

The first approach investigated the applicability of functional and green polymers as alternatives to conventional depressant of silicates minerals in the direct flotation of phosphate ore. Two different polymers were selected in this study: hybrid polyacrylamide-based polymers (Hy-PAM) as an example of functional synthetic polymers and chitosan polymer as an example of sustainable, biodegradable natural polymers. Batch flotation experiments were conducted using a laboratory-scale Denver cell. Baseline experiments were performed periodically based on specific conditions in order to define a base recovery and to ensure the reproducibility of the results as well as a congruity of the experimental parameters. The flotation process outcomes were studied as a function of various process variables, including pulp's pH, flotation time, reagent type, and reagent dosages.

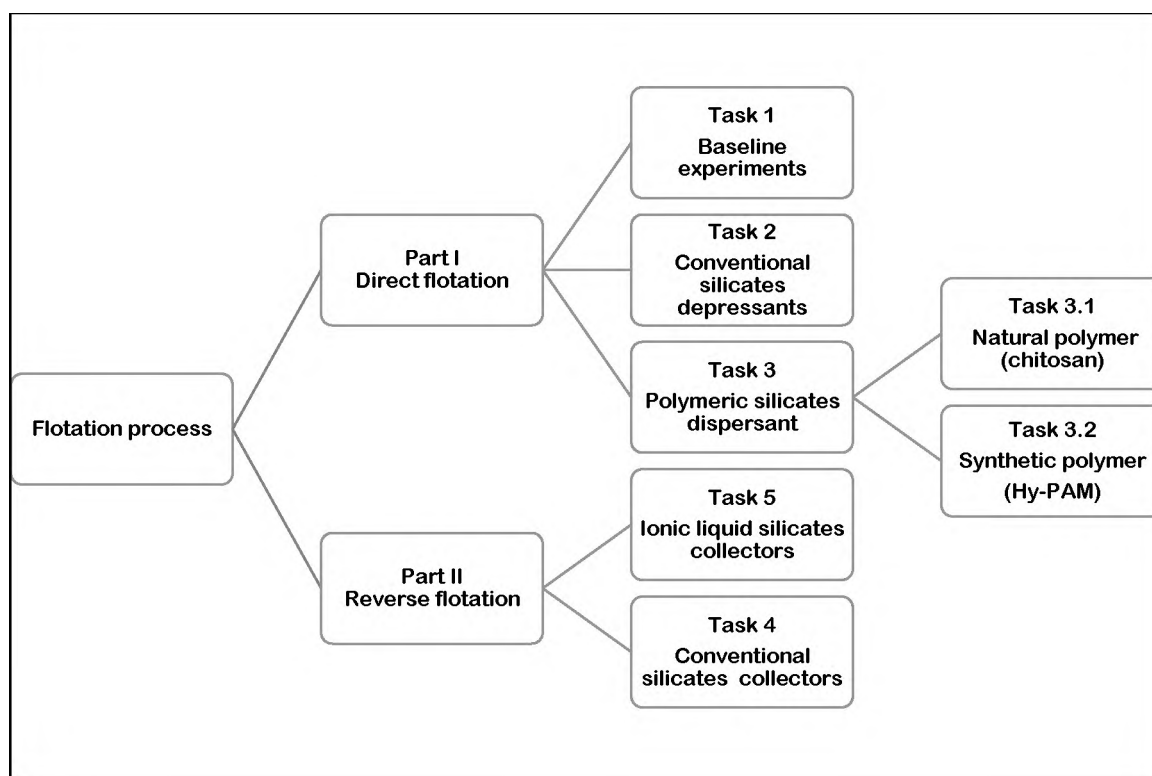


Figure 1.4 Schematic representation of tasks performed in Phase III.

The second approach was to explore the ability of ionic liquids (ILs) to serve as selective collectors of silicate minerals in the reverse phosphate flotation process. Micro-flotation tests were conducted using a Hallimond tube to understand the effect of ILs on the flotation of apatite and quartz without external factors such as mechanical parameters; thus, it is an excellent tool to assess the suitability of a particular reagent in the froth flotation process. Concentrate and the tailing products obtained were weighed, dried, and analyzed using X-ray Fluorescence Spectroscopy (XRF) and X-ray Diffraction (XRD).

1.5.4. Phase IV: Machine Learning (ML) Modeling to Predict the Flotation Performance of Phosphate-Silicate Ores. In this phase, as shown in Figure 1.5, the experimental datasets and information pertaining to the influence of experimental variables were processed under the progressive-and-adaptive framework of machine learning (ML). Artificial neural networks (ANN) were used in this study to model the flotation behavior of phosphate and silicate minerals in direct froth flotation processes.

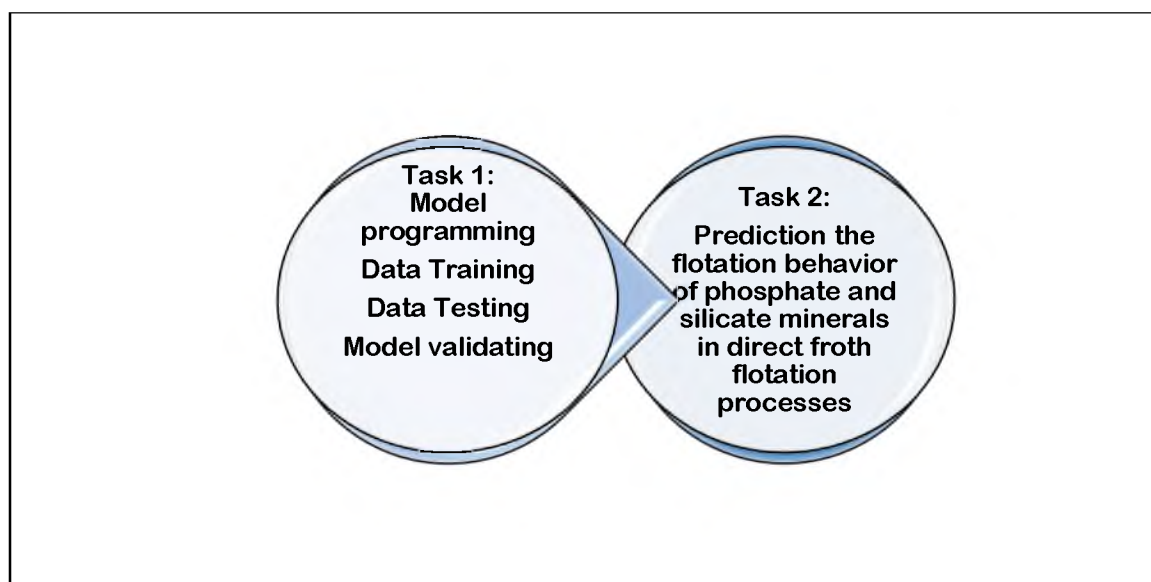


Figure 1.5 Schematic representation of tasks performed in Phase IV.

ANN has been used recently to predict the metallurgical performance of the flotation process in various applications with excellent accuracy [33]–[38]. Python was used to code the ML model. The mean absolute error (MAE), coefficient of determination (R^2), and root-mean-square error (RMSE) were used as performance indicators of the ANN model.

1.6. ORGANIZATION OF DISSERTATION

This dissertation contains six sections. The key contents of each section are provided below.

Section 1: This section provides the overall introduction of the thesis, including the background, statement of the problem, research objectives, broader impacts and intellectual merit of the work, and finally, the research scope and strategy.

Section 2: This section presents a comprehensive literature review on the fundamental principles of froth flotation process, an overview of industrial froth flotation practices applied to phosphate ores, and a thorough review of the factors that impact the flotation efficiency of phosphate minerals.

Section 3: This section discusses the direct froth flotation process of low-grade phosphate ore in the presence of synthetic and natural polymeric depressants in batch flotation systems. The section also provides a detailed characterization of phosphate ore used in this study and a fundamental investigation of the electrical characteristics of minerals at water-solid interfaces.

Section 4: This section discusses the application of ionic liquids (ILs) as alternatives collectors of silicate minerals in the reverse flotation process of phosphate

minerals in the micro-flotation system. The section also provides systematic investigations on the fundamental features of ILs' adsorption on mineral surfaces.

Section 5: This section presents the application of machine learning (Artificial Neural Network, ANN) to predict the process outcomes (i.e., recovery and grade) in the direct froth flotation of low-grade phosphate ores in relation to a process variable. Process optimization is also discussed.

Section 6: This section provides the overall conclusions, contributions of this work, and recommendations for future research.

2. LITERATURE REVIEW

2.1. FROTH FLOTATION FUNDAMENTALS

In 1897, the first industrial commercial flotation process was established at Glasdir mine by Elmore's brothers for sulfides minerals [26]. Since that time, the froth flotation process has become one of the most selective techniques used in mineral separation processes. Froth flotation is extensively used to enrich sulfide minerals (i.e., galena, chalcopyrite, sphalerite, molybdenite, and pentlandite) as well as non-sulfides such as phosphate minerals, iron ores, and fine coal [23], [39]–[42]. Froth flotation utilizes the differences in wettabilities of minerals in a three-phase system that consists of solids, gas, and water [10]. In this process, hydrophobic particles attach to air bubbles to form a froth, which is basically solid-air aggregates containing entrapped water. Hydrophilic minerals tend to stay in the pulp as waste products or flotation tailings [4], [43]. Figure 2.1 represents the concept of the froth flotation process [44].

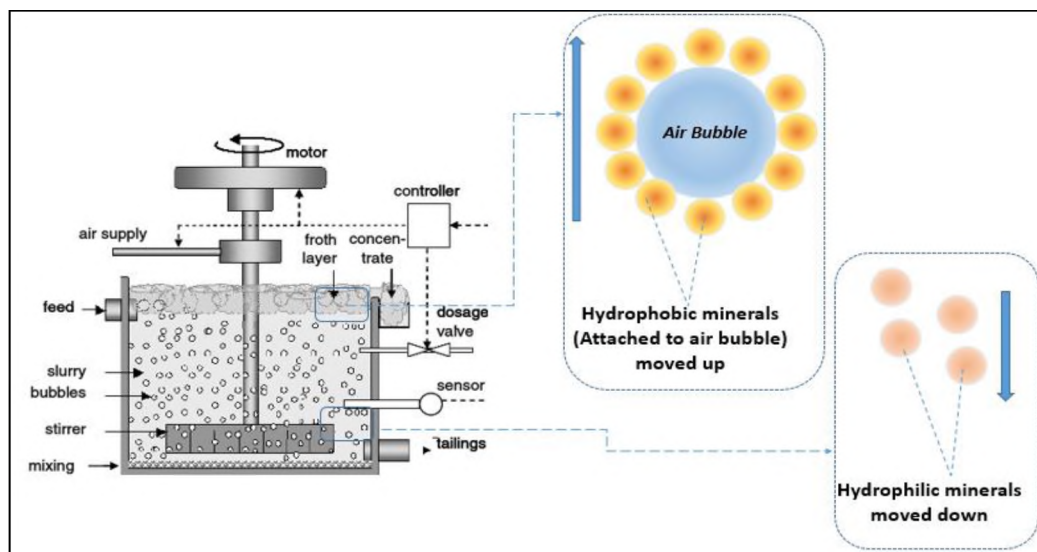


Figure 2.1 Principle of the froth flotation process.

There are three closely correlating components in any froth flotation system – all of which affect the flotation process efficiency (Figure 2.2) [9]. The first component is mechanical, which includes cell design, agitation speed, and airflow rate. The second is chemical, which comprises flotation reagents such as collectors, frothers, and depressants, as well as the pH of the flotation pulp. The third is operational, which includes feed flow rate, the particle size of the flotation feed, and flotation time [4], [45].

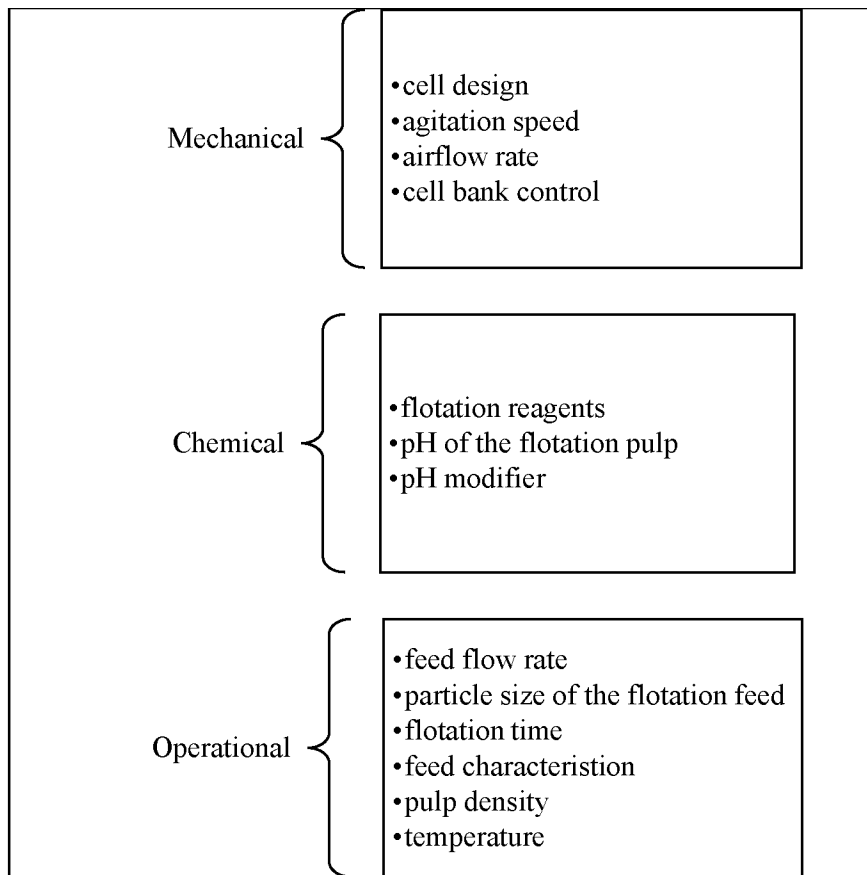


Figure 2.2 Different variables in froth flotation process.

To maximize the flotation efficiency (recovery and grade) of a specific mineral, the flotation process is usually undertaken in different stages [46]. As shown in Figure 2.3,

the first stage called rougher flotation, which produces products with coarse particle size and removes most of the valuable mineral to the next stage, the cleaning stage. The cleaning stage aims at producing as high a concentrate grade as possible. The final stage, the scavenging stage, is applied to recover the valuable minerals that were not collected during the first roughing stage [23], [47]–[49].

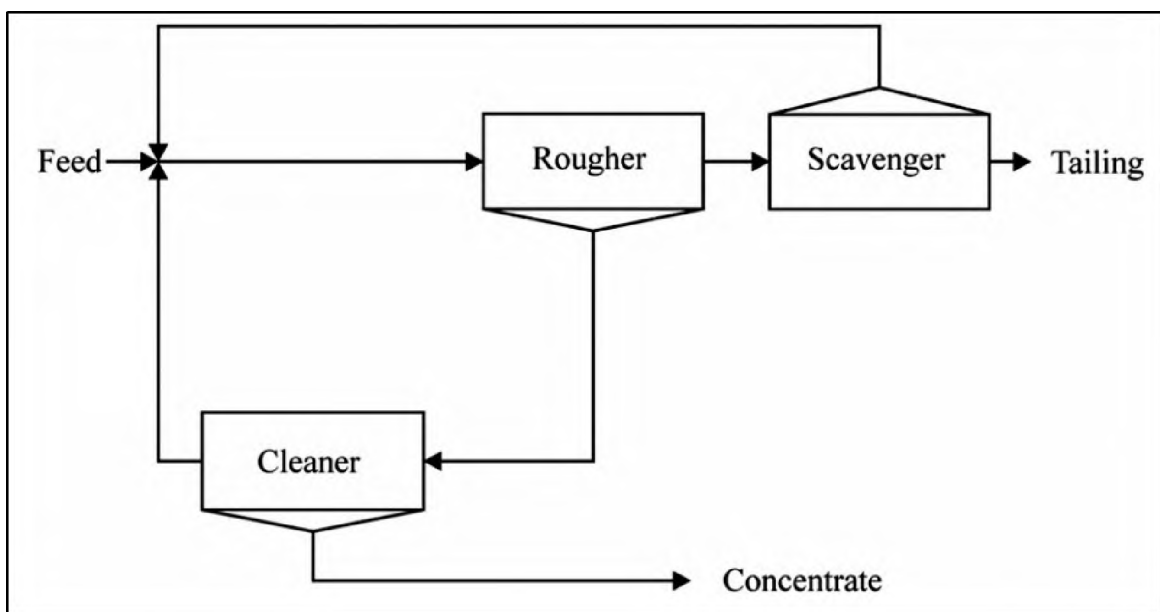


Figure 2.3 Simplified flowsheets of a typical flotation circuit [48].

2.2. PHOSPHATE FLOTATION PROCESS

In general, the separation of phosphate minerals from the associated gangue minerals by froth flotation is technically a challenging process due to the variability in ore composition and similar physicochemical properties of constituent minerals [2], [46], [50]–[52]. There are two main flotation practices adopted by the phosphate industry: the direct flotation process and the reverse flotation process.

2.2.1. Direct Flotation. The direct process is more preferred due to its high separation efficiency. It is generally used to separate the phosphate ores that contain significant amounts of silicates and dolomite within 20-25% and 4-6%, respectively [10], [53]. In this process, phosphate minerals are rendered hydrophobic, floated, and collected in the froth zone at ~ 75% - 80% recovery and 30% - 34% grade, while the gangue minerals are depressed [4]. Florida's phosphate mines have used direct froth flotation for a long time [4]. As shown in the flow diagram, Figure 2.4, the phosphate feed is conditioned by adding fatty acid as a collector of phosphate minerals and sodium silicate as a dispersant of silicate minerals at pH 9-9.5 and 70-75 wt.% of solid concentration. The flotation feed is then transferred to the rougher flotation circuit to float phosphate minerals and fine silicates while coarse silicates sink in the tailings zone [4].

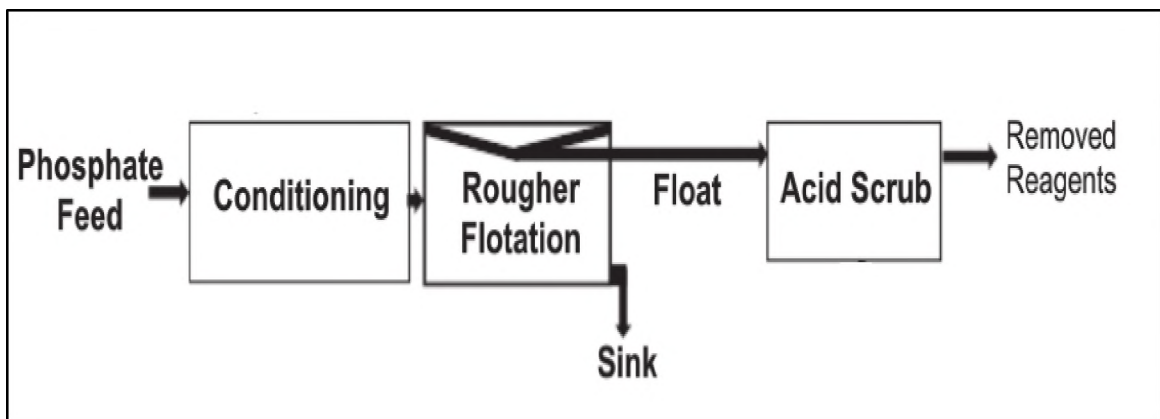


Figure 2.4 Flow diagram of the direct flotation process at Florida's phosphate mines [4].

2.2.2. Reverse Flotation. In the reverse flotation practice, gangue minerals are floated while the phosphate minerals are depressed or dispersed and collected in the

tailings [4], [10]. Reverse flotation is used to separate the phosphate ores that contain significant amounts of silicate minerals and more than 25% of carbonates [53].

As an example, Florida's phosphate mines also use the reverse froth flotation process[4]. As shown in the flow diagram, Figure 2.5, the phosphate feed is conditioned by adding amines as a collector of silicates and starch as a dispersant of phosphate minerals at pH 6.5-8 to float the fine silicates to tailings and sink the phosphates and coarse silicates to sink zone followed by dewatering. The dewatered phosphate sink is floated from coarse silicates by direct flotation process [4].

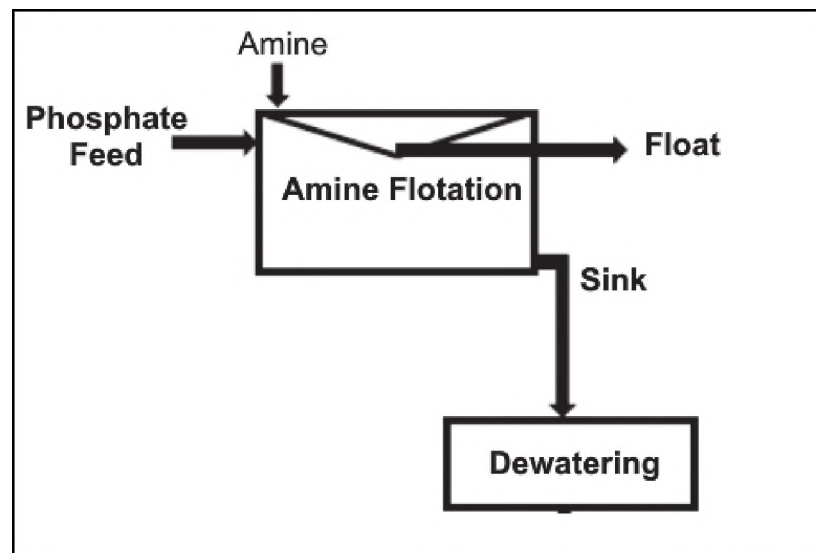


Figure 2.5 Flow diagram of reverse flotation process at Florida's phosphate mines [4].

2.3. VARIABLES AFFECTING FROTH FLOTATION EFFICIENCY

Froth flotation process utilized the difference in surface properties of minerals at water-solid-gas interfaces. Chemical reagents are added in the flotation cell in order to modify the surface properties of different minerals to allow selective separation.

Therefore, the types and dosages of different chemical reagents added to the flotation pulp can adversely affect the flotation process efficiency. The reagents can be classified into various types: collectors, depressants, dispersants, and frothers [9], [54]. For example, fatty acids anionic collectors are usually used as phosphate collectors in the direct phosphate flotation process for ore containing 20%-25% silicates minerals [11], [55]. Whereas cationic collectors, such as amines, are used in the reverse flotation process to float silicates and carbonate minerals [9]. Table 2.1 shows the most common collectors used in phosphate flotation operations.

Table 2.1 Common collectors used in phosphate flotation operations [9].

Floated mineral	Ionic property	Collector group	Flotation system
Phosphate	Anionic	Oleic acid Tall oil Disodium dodecyl phosphate	Direct Flotation
Silicates	Cationic	Amines Dodecylamine	Reverse Flotation
Carbonates	Anionic	Fatty acids Sulfonated fatty acids	Direct Flotation

On the other hand, the dispersants and depressants are usually used to suppress the flotation of gangue minerals in direct froth flotation [9], [54], [56]–[59]. Many types of depressants and dispersants are available. For the best results, the type of flotation system (direct or reverse) and collector type need to be determined [9]. Table 2.2 shows a list of common depressants used in phosphate flotation operations.

The mineral impurities in the phosphate ore present many challenges due to the similarity in most of their physical and chemical properties to those of phosphates. This makes the separation difficult, costly, and environmentally influential. For example, the ore at the

Kapuskasing Phosphate Operations (KPO) contains a significant amount of magnetite, which has similar surface properties to phosphate minerals. In this operation, the fatty acids used as collectors of phosphate minerals could also collect iron minerals [60], [61]. Similarly, the starch used as a depressant of iron minerals could depress phosphate minerals [60], [61]. Therefore, a magnetic separator is usually applied in such cases after the flotation process to remove magnetite. Figure 2.6 shows the process flowsheet. First, the ore is crushed and ground to minus 300 microns [62]. A flotation feed contains 55 wt.% of solids is conditioned with water and reagents. Starch is added first as a depressant of iron minerals, then tall oil “fatty acids” is used as phosphate collector at typical dosages of 1200 g/ton and 800 g/ton, respectively. The pH of the flotation pulp is kept between 10.5 to 11 using sodium hydroxide (NaOH). After that, the concentrate is sent to a two-stage wet magnetic separation circuit to remove magnetite minerals that floated with phosphate minerals. The final concentrate is thickened, filtered, and thermally dried. The P₂O₅ grade of the concentrate shall be at least 36%, and the equivalent contents of Fe₂O₃ and MgO should be less than 2.5% and 0.6%, respectively [62].

Table 2.2 Common depressants used in phosphate flotation operations [9].

Depressed mineral	Depressant	Flotation system	Collector for floated minerals
Phosphate	Aluminum sulfate Sodium carbonate Phosphoric acid Starch	Reverse Flotation	Amines Carboxyethyl- imidazoline
Silicates	Sodium silicates	Direct Flotation	Fatty acids
Carbonates	Sodium silicates Polysaccharides Hydrofluoric acid	Direct Flotation	Fatty acids

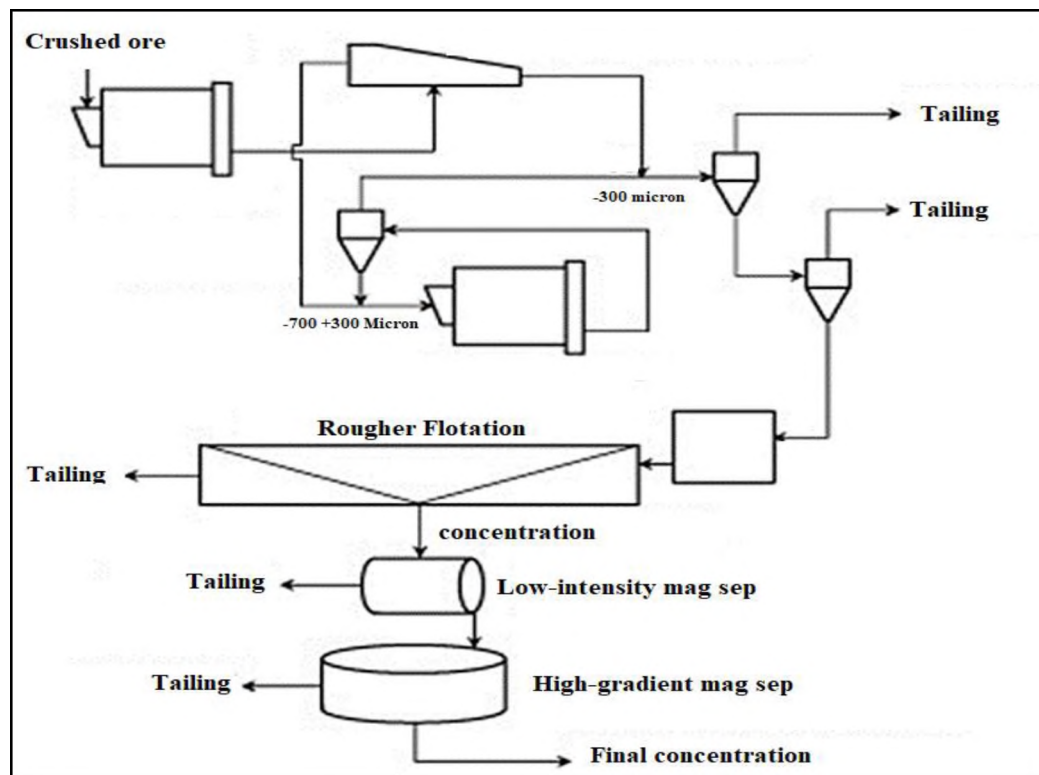


Figure 2.6 Flotation process flowsheet adopted at Agrium Inc.–Kapuskasing Phosphate Operations (KPO) [62].

The particle size of the feed plays a significant role in the phosphate flotation process. Research efforts have been made to figure out the optimum particle size range. As shown in Figure 2.7, the optimum particle size that gives the best flotation efficiency of phosphate minerals was found between +36 micron to -125 micron [16], [46], [63]–[65].

Moreover, in any flotation process, pH is a critical factor that can adversely impact the selectivity of reagent adsorption at mineral surfaces and thus the efficiency of minerals separation. In phosphate flotation, the optimum pH in the direct froth flotation process is between pH 9 and pH 11. It is usually modified by adding soda ash (sodium carbonate). However, in reverse froth flotation process wherein silicates or carbonates are floated, the optimum pH is between five and eight [46], [58], [66], [67].

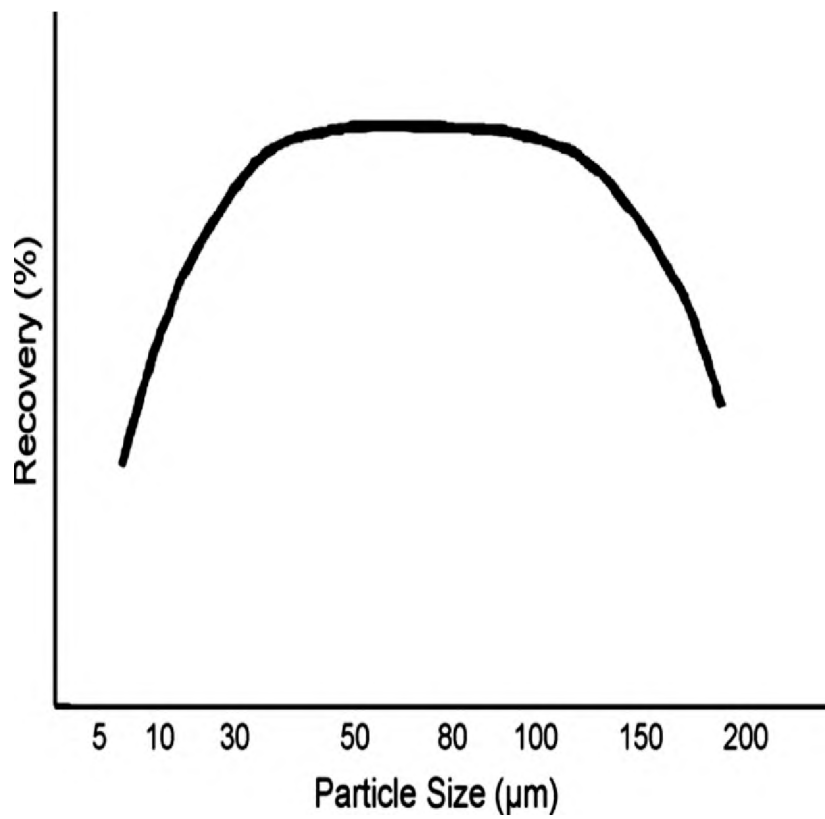


Figure 2.7 Flotation recovery of phosphate minerals as a function of particle size of flotation feed [16].

3. ENHANCED RECOVERY OF PHOSPHATE MINERALS FROM LOW-GRADE ORE USING DIRECT FROTH FLOTATION

3.1. BACKGROUND

Both synthetic and natural polymers have been extensively applied for decades in mineral flotation [37], [68], [69]. This is due to their tenability and the opportunity to enhance the flotation performance at lower costs [68], [69]. Chitosan has been successfully tested as a green depressant to replace sodium cyanide in complex sulfide ore flotation [37]. Polyacrylamide-based synthetic polymers are widely used in mineral flotation as multifunctional reagents. Depending on the integrated functional groups, polyacrylamides and their derivatives have been used as collectors, depressants, activators, or modifiers [37], [70]. Hybrid organic-inorganic polyacrylamide polymers (Hy-PAM) were successfully applied in fine coal flotation to enhance the combustible recovery and reduce the ash contents of coal concentrates [70].

Two different polymers were selected in this study: hybrid polyacrylamide-based polymers (Hy-PAM), as an example of functional synthetic polymers; and chitosan polymer as an example of sustainable, biodegradable natural polymers. Hy-PAM is an organic-inorganic hybrid polymer consisting of nano-size Al (OH)₃ inorganic particles grafted on polyacrylamide organic chains. Figure 3.1 shows the structure of the hybrid polyacrylamide polymer (Hy-PAM) used in this study.

Hy-PAM was anticipated to adsorb on the surface of slime-forming minerals in fine coal flotation process and depress their flotation and mechanical entrainment into the froth layer [70]. A previous study by Alagha et al. (2011) showed the capability of Hy-PAM

polymers to adsorb on the surface of ultrafine silica particles, flocculate them, and enhance their sedimentation in solid-liquid separation processes [71].

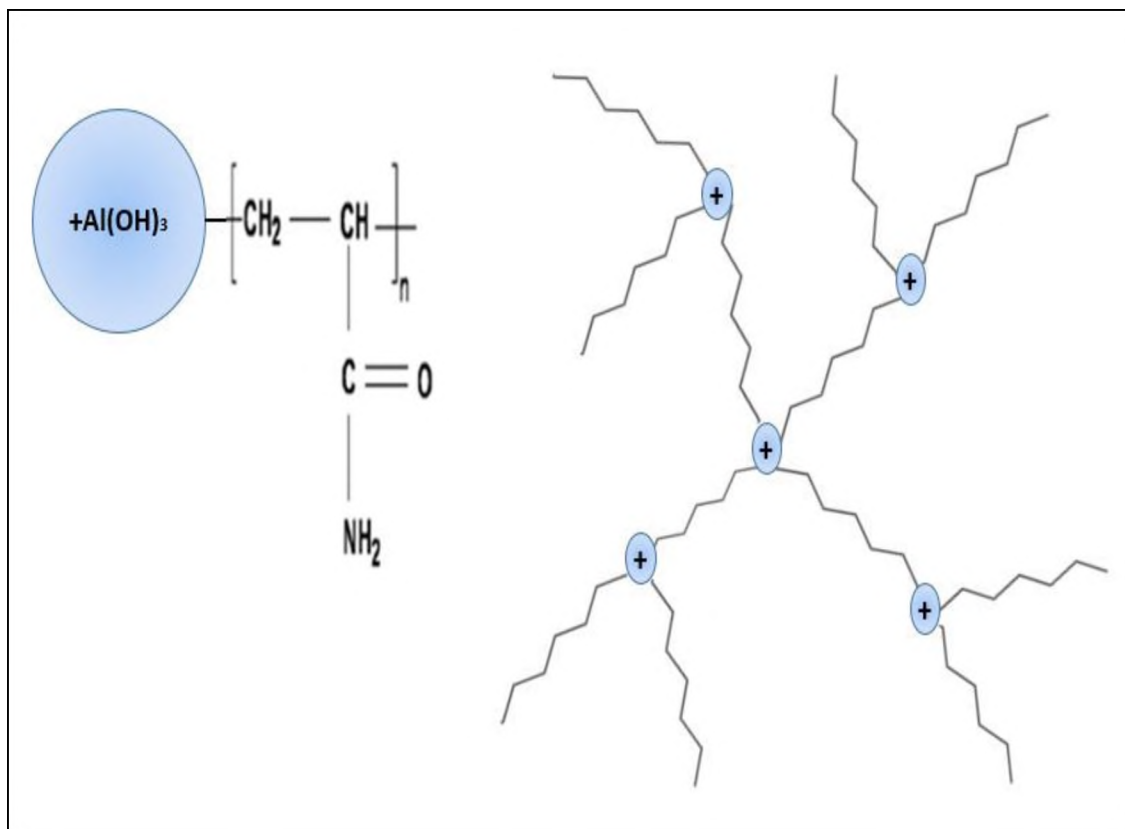


Figure 3.1 Structure of hybrid polyacrylamide polymer (Hy-PAM).

Natural polyaminosaccharide (chitosan) was utilized as a depressant of pyrite in the sulfide flotation process [37], [72]–[74]. The structure of the chitosan polymer is shown in Figure 3.2. It is anticipated that chitosan could potentially form metal complexes (chelates) on specific mineral surfaces — depending on the electron affinity of metal ions in the crystal lattice — and makes the surface hydrophilic, thus depressing their flotation. [37],[74]–[80].

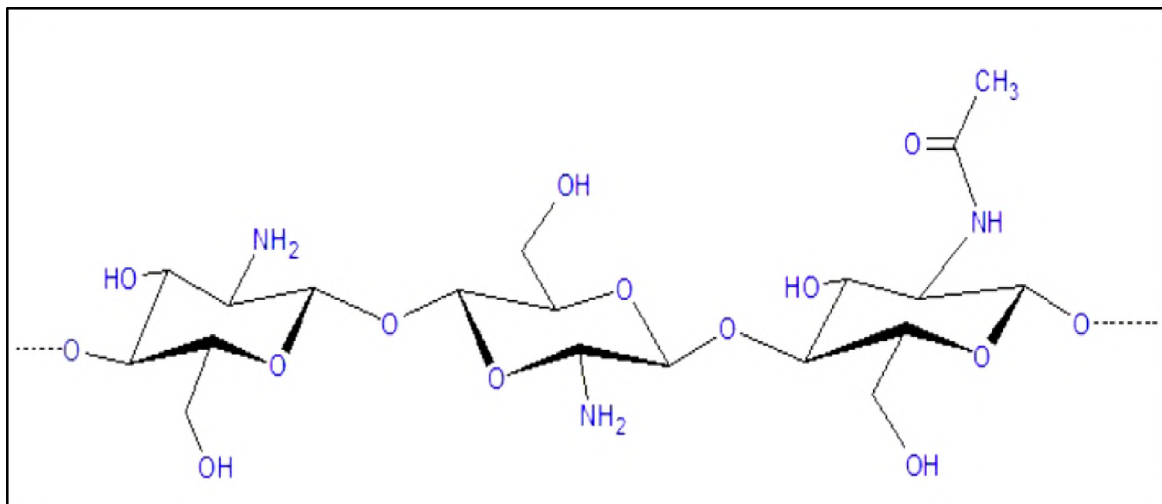


Figure 3.2 Structure of chitosan polymer [37].

The successful application of Hy-PAM and chitosan in the previously mentioned studies, along with their unique structural characteristics, have brought the motivation to use these polymers in this study as depressants of silicate minerals in the direct flotation process of low-grade phosphate ore.

3.2. METHODOLOGY AND MATERIALS

3.2.1. Mineral Samples and Flotation Reagents. Representative low-grade phosphate ore samples were provided from a phosphate plant located in the United States. All reagents used in the direct flotation tests, displayed in Table 3.1, were purchased from Fisher Scientific Company, USA. The chitosan polymer's molecular weight used in the flotation tests was 1526.464 g/mol, and the deacetylation degree was 85%. Hy-PAM was synthesized in-house according to a procedure described elsewhere [59], [71], [81]. The molecular weight of the synthesized Hy-PAM polymer was 6×10^6 Dalton and was determined using the Zetasizer Nano ZS instrument. Sodium carbonate (Na_2CO_3) and

hydrochloric acid (HCl) were used to adjust the pH of flotation pulp and mineral suspension used in zeta potential studies. Pure apatite and quartz were purchased from Ward's Science Company, USA.

Table 3.1 A list of reagents used throughout this study.

Reagent Type	Reagent Name	Target Mineral
Collector	Sodium Oleate	Apatite
Dispersant	Sodium silicate	Quartz
Depressant	Al(OH) ₃ -PAM (Hy-PAM)	Quartz
	Chitosan	Quartz
Frother	Methyl isobutyl carbinol (MIBC)	—

3.2.2. Characterization of the Flotation Feed. In order to understand the mineralogical and morphological properties of low-grade phosphate ore, a comprehensive characterization studies were employed by using X-ray Diffraction (XRD), X-ray Fluorescence (XRF), Scanning Electron Microscopy (SEM), and Mineral Liberation Analysis (MLA) on the low-grade phosphite ore and flotation feed.

3.2.2.1. Particle size distribution. Several screens with different size fractions were used for sieving. These screens were placed and shaken for a specific time, as determined by the ASTM C136-14 protocol. Figure 3.3 shows the particle size distribution of the flotation feed. The 80% passing size (P_{80}) of the flotation feed was approximately 100 microns.

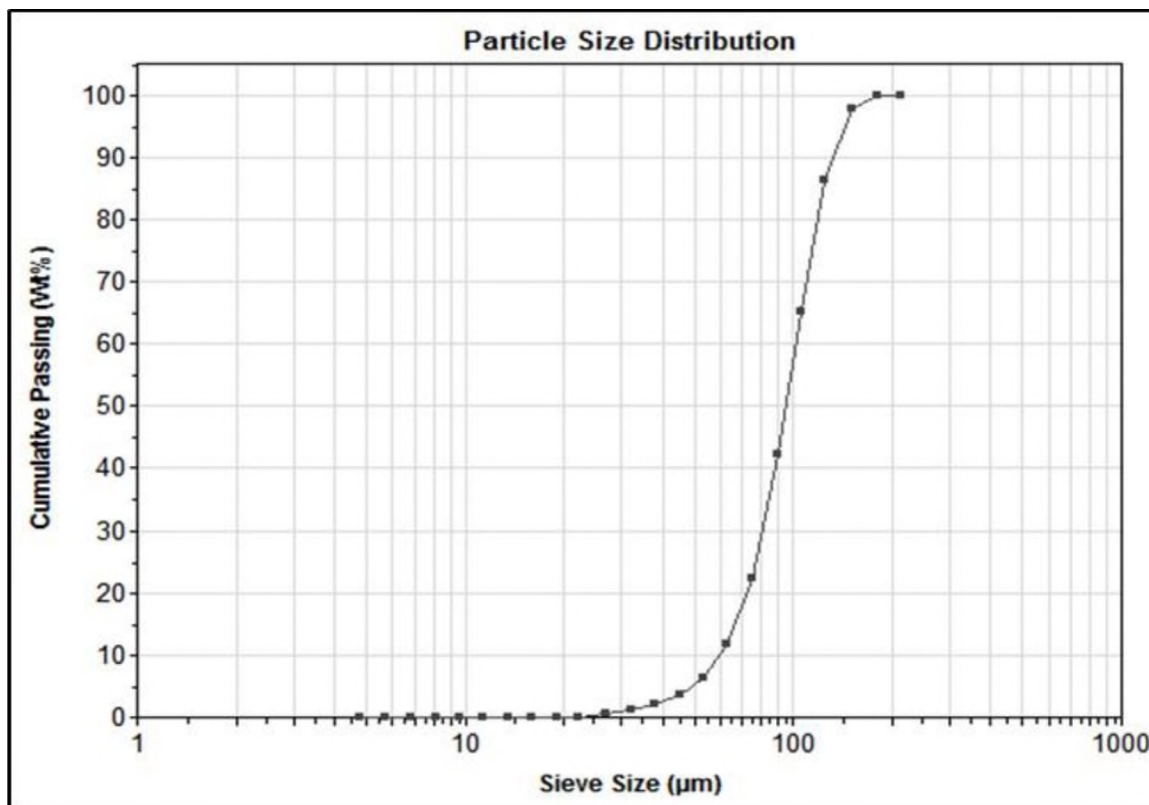


Figure 3.3 Particle size distribution of the flotation feed.

3.2.2.2. Mineral liberation analysis (MLA). Random particle mounts were created from the sieved material for MLA analysis. MLA data was obtained by the XBSE method, where the acquired backscattered electron (BSE) image is used to differentiate the mineral phases based on the gray level as the gray level intensity varies, dependent on the phase composition. The acquired X-ray spectrum obtained from each phase was compared to the X-ray mineral database to determine mineral phases qualitatively. The surface area data for each mineral was used for the quantitative determination of the minerals identified.

- **Modal mineralogy.** As shown in Figure 3.4.A, the flotation feed particles presented complex textures with many of the phases displaying variable chemistries. The primary phosphorus-containing phases were apatite and apatite-fluorite mix. Apatite and

mixed apatite phase (apatite-fluorite mix) were found in the flotation feed at 33.06% and 29.96, respectively. Quartz was found to be 17.81%, mica (K-Al silicate) was nearly 8.49%, fluorite was 4.95%, and K-Feldspar was 4.24%.

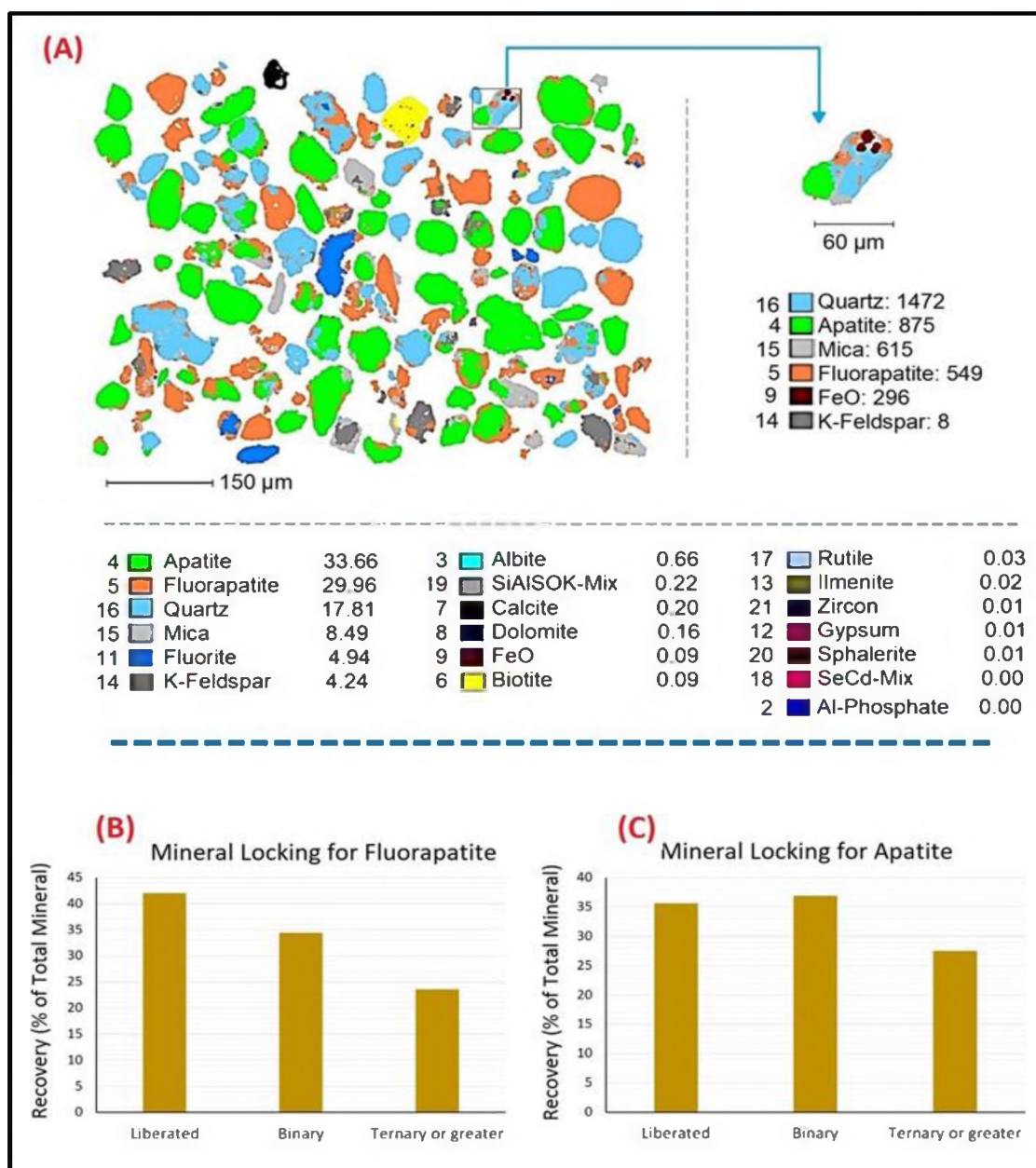


Figure 3.4 Model mineralogy (A) Classified MLA image of the flotation feed (Particle inset units are in pixels and concentration palette values are in area percentages); (B) Mineral locking of fluorapatite; (C) Mineral locking of apatite [59].

The distribution of the main minerals in the flotation feed is shown in Figure 3.4.B and C, which shows the percentages of the liberated and locked phosphate minerals in the flotation feed. As indicated, more than 50% of phosphate minerals in the feed were locked or associated with other gangue minerals (mainly quartz, mica, and feldspar). The grade of phosphate minerals (P_2O_5) in the flotation feed was 21.6%, as determined by MLA. MLA indicated that some interlocking of quartz, apatite, and fluorapatite occurred. Many particles were mostly-one mineral. This observation indicated that it might be possible to concentrate the phosphorus bearing minerals by flotation.

- **MLA-calculated composition.** The MLA-calculated bulk elemental content, presented in Figure 3.5, was derived from the MLA modal mineralogy and the assigned chemical formulas. Phosphorus was 12.4% in the sample according to MLA-based calculations.

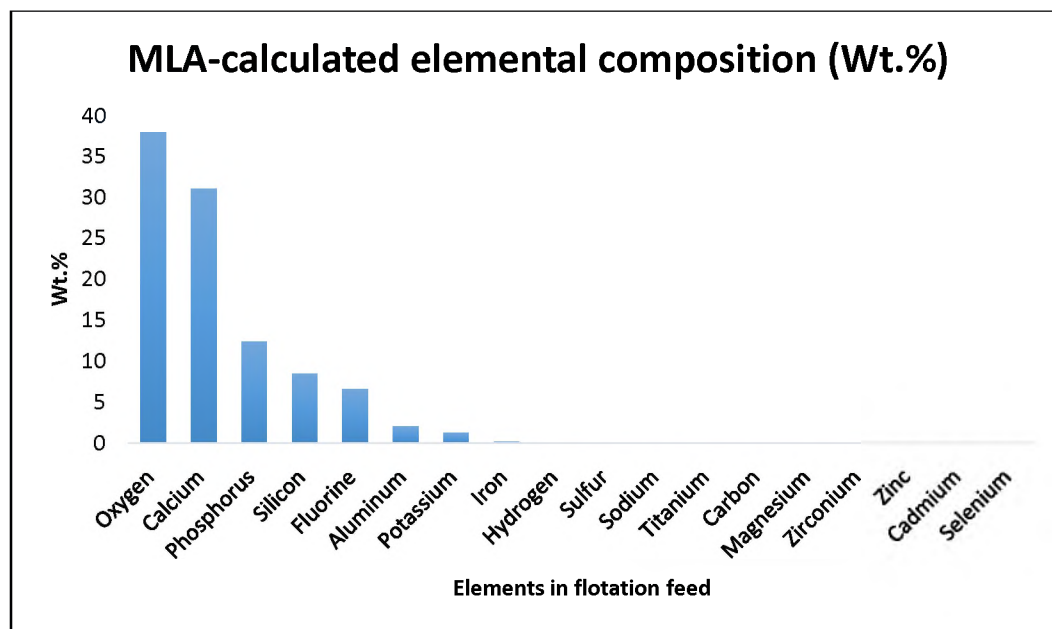


Figure 3.5 MLA-calculated elemental composition (Wt.%).

- **Elemental distribution.** Apatite was the primary phosphorus-containing phase, which accounted for 53.4% of the total phosphorus distribution by mineral, as seen in Table 3.2.

Table 3.2 Phosphorus distribution by mineral type.

Mineral	Flotation feed
Apatite	53.4
Apatite-Fluorite mix	46.6
Al-Phosphate	0.0
SeCd mix	0.0
Fe-Phosphate	0.0
Total	100

- **Grain size.** Figure 3.6 shows the grain size of apatite, mixed apatite/fluorite, and quartz. The apatite was grained larger than the mixed apatite/fluorite with a grain size distribution P_{80} of over 100 microns for apatite compared to 90 microns for mixed apatite/fluorite. Both apatite and apatite/fluorite phases were larger than quartz (65 microns).
- **Mineral liberation.** Apatite was slightly better liberated than the mixed apatite/fluorite phase and quartz, as shown in Figure 3.7. The liberation of apatite by sieve fraction showed decreasing liberation with decreasing particle size (Figure 3.8), which is unusual. However, observation of the MLA false-color image indicated that attached mixed phases were more prevalent as particle size decreased and likely caused this result. The liberation of the mixed apatite/fluorite phase was not clear, but also seemed to show better liberation for the coarser particles (Figure 3.9) vice versa in the liberation of quartz (Figure 3.10).

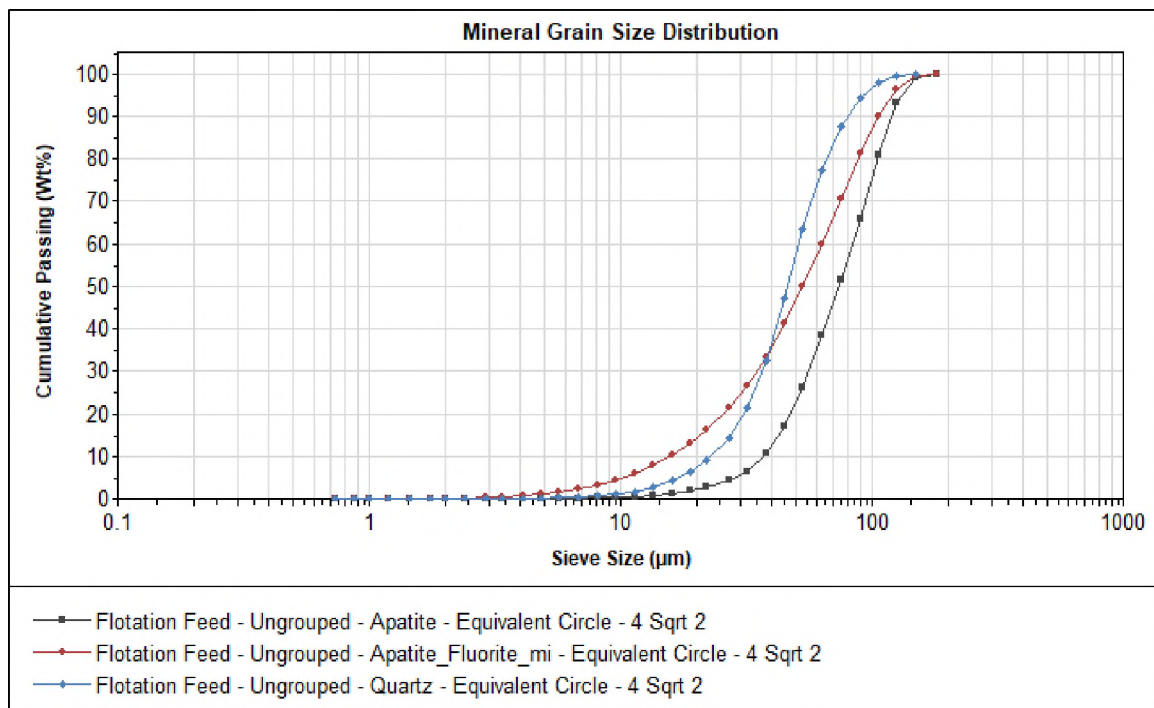


Figure 3.6 Mineral grain size distributions of apatite phases.

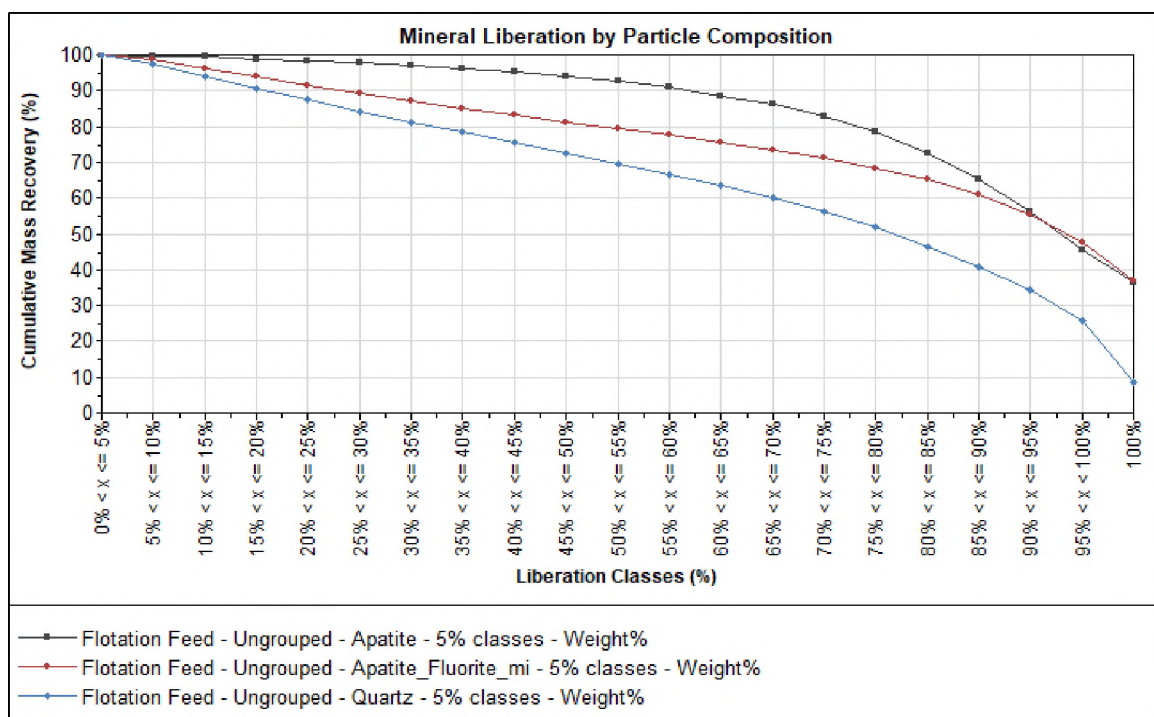


Figure 3.7 Composite mineral liberation by particle composition for the apatite, mixed apatite/fluorite, and quartz.

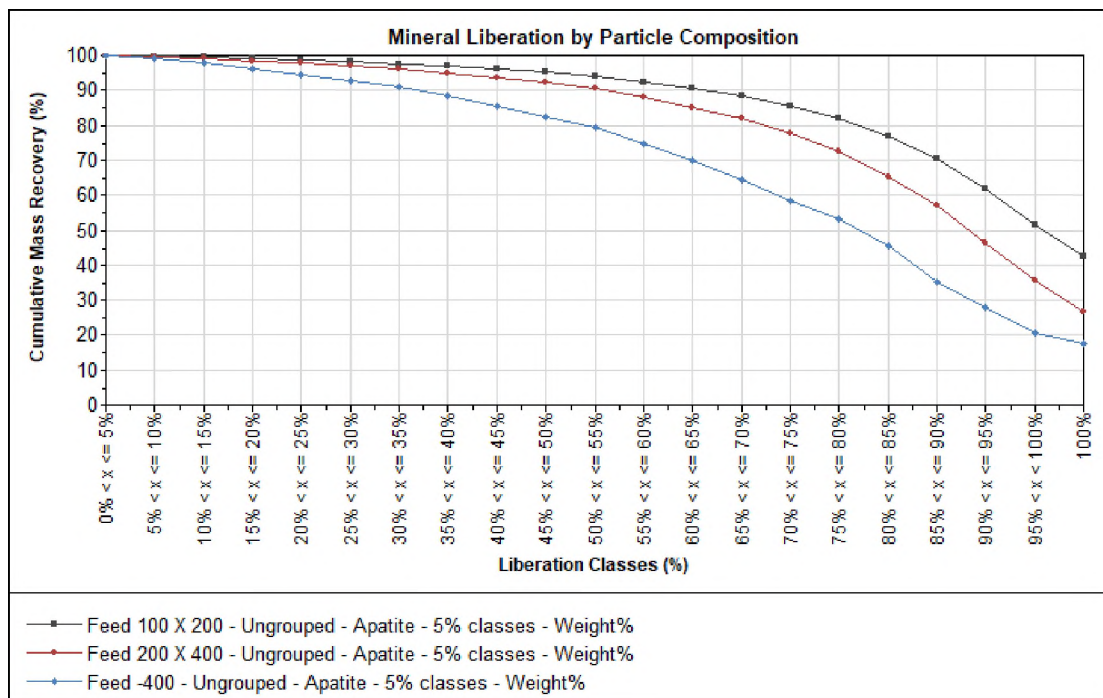


Figure 3.8 Mineral liberation of apatite phase by sieve fraction in the flotation feed.

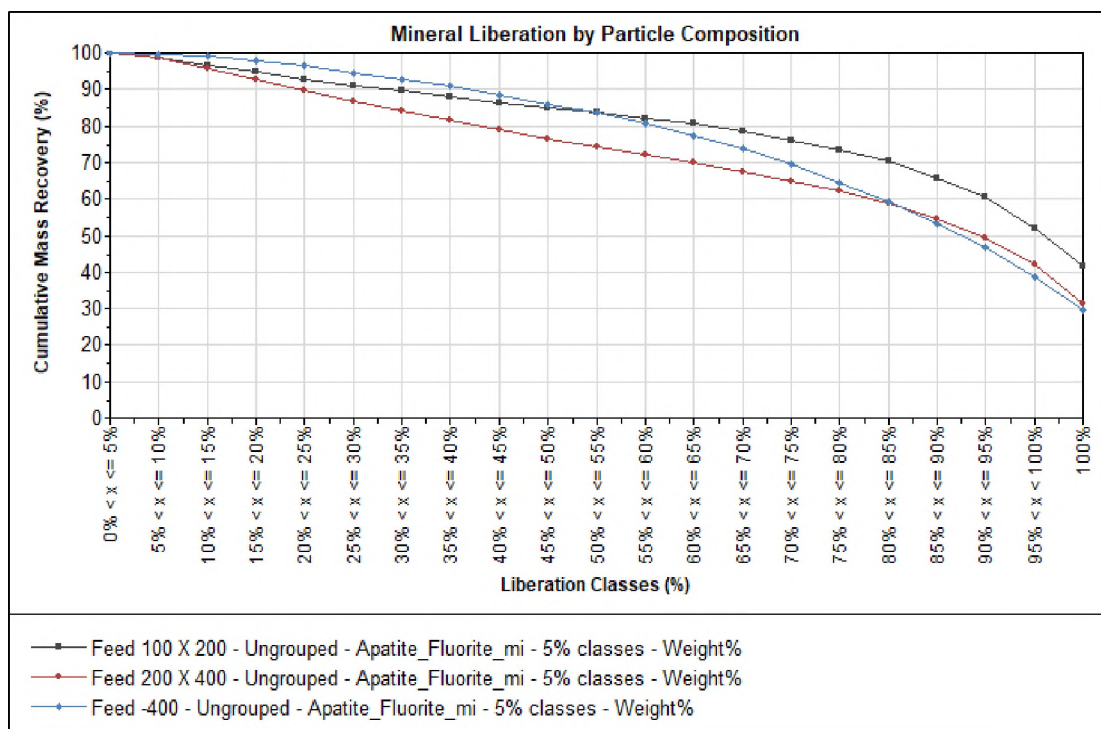


Figure 3.9 Mineral liberation of the mixed apatite phase by sieve fraction in the flotation feed.

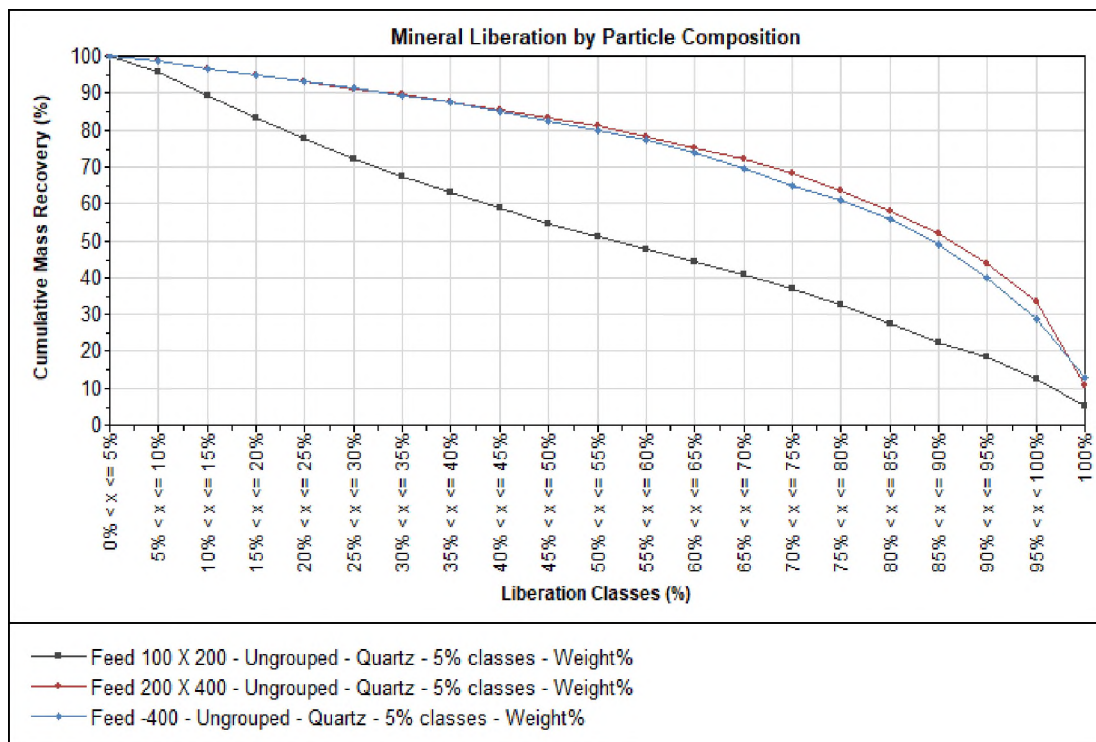


Figure 3.10 Mineral liberation of the quartz phase by sieve fraction in the flotation feed.

- Mineral associations.** As seen in Table 3.3, the apatite was associated with three phases: mixed apatite, quartz, mica, and K-Feldspar. Moreover, it was also shown as free surfaces. The mixed apatite-fluorite phase was most strongly associated with apatite than other associations.

Table 3.3 Phosphate mineral associations in the flotation feed.

Mineral	Apatite	Apatite/Fluorite Mix	Feldspar	Mica	Quartz	Free Surface
Al-Phosphate	0.8	5.2	3.7	9.4	10.4	70.5
Apatite		21.8	3.2	7.2	7.7	59.3

3.2.2.3. X-ray diffraction (XRD). XRD was conducted on the flotation feed to investigate the crystalline minerals phases associated with the phosphate minerals. As shown in Figure 3.11, two major minerals were detected: apatite and quartz.

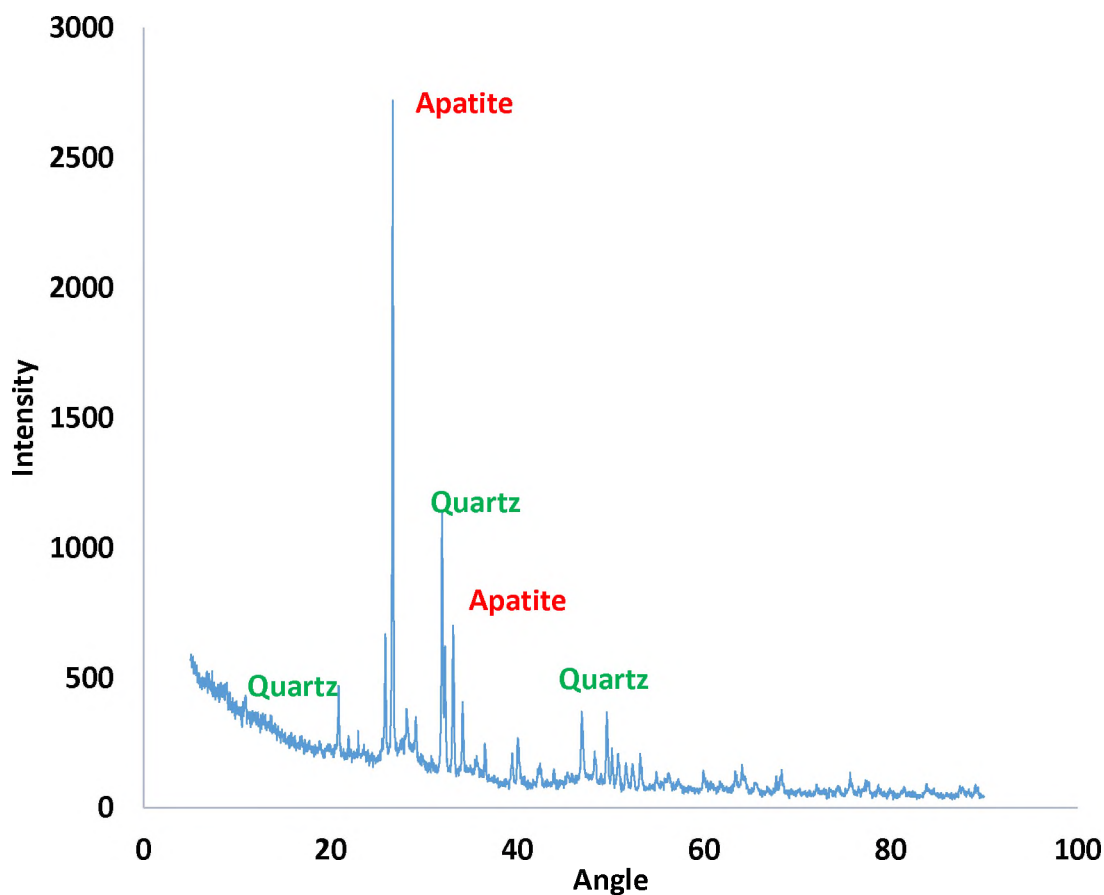


Figure 3.11 X-ray diffraction (XRD) patterns of the flotation feed.

3.2.2.4. Scanning electron microscope (SEM). Qualitative and semi-quantitative chemical analyses in the Energy Dispersive X-Ray Spectroscopy (EDS) mode were performed to detect the flotation feed's significant elements. EDS analysis in Table 3.4 revealed Oxygen (O), Fluorine (F), Calcium (Ca), Phosphorus (P), Silicon (Si), and Sodium

(Na) atoms in large amounts, which demonstrates that apatite and quartz are the dominant minerals in the sample.

Table 3.4 EDS analysis of flotation feed.

Element	Wt.%	At%	Element	Wt.%	At%
O	30.66	48.73	Cl	0.15	0.1
F	10.03	12.4	Cd	0.42	0.09
Na	4.85	4.95	K	1.14	0.68
Mg	1.43	1.38	Ca	18.73	10.98
As	0.36	0.11	Ti	0.2	0.1
Al	2.29	2.86	V	0.34	0.16
Si	9.53	8.24	Cr	0.36	0.16
P	10.63	5.16	Fe	1.9	0.8
Hg	0	0	Zn	5.37	1.93
S	1.61	1.18	Total	100	100

3.2.2.5. Zeta potential measurements. Zeta potential measurements were used to examine the electrical properties of mineral surfaces in the presence and absence of reagents (i.e., sodium oleate, sodium silicate, Hy-PAM, and chitosan) to understand the behavior of the flotation feed. Zeta potential measurements were performed using a Zetasizer Nano ZS (Malvern, Westborough, MA, USA) (Figure 3.12). A stock solution was prepared at 0.1 wt.% of pure mineral (apatite or quartz) in a 0.1M potassium chloride (KCl). Zeta potential measurements were obtained at different pH. Either hydrochloric acid (HCl) or sodium carbonate (Na₂CO₃) was used to adjust the pH in all zeta potential measurements.



Figure 3.12 A photograph of zetasizer nano ZS instrument used in this study.

3.2.3. Flotation Experiments. Flotation experiments were performed using a laboratory-scale Denver flotation machine, as shown in Figure 3.13. Baseline experiments using collector “sodium oleate” and frother” MIBC” without any dispersant or depressant were first conducted to define the base recovery and grade of P_2O_5 and to determine the optimum solid concentration. As mentioned in Table 3.1, both dispersant and depressants were tested at four different dosages: 150, 200, 250, and 300 g/ton. The pH of the flotation pulp and flotation time was varied, as shown in Table 3.5. The flotation feed was prepared and sieved based on the optimum size fraction between $+35\mu\text{m}$ and $-125\mu\text{m}$. In a typical flotation experiment, the pulp containing the ore sample in tap water was first agitated for

4 minutes, followed by the addition of Na_2CO_3 to adjust the pH as needed. Collector “sodium oleate” was then added, followed by dispersant “sodium silicate” or depressant “Hy-PAM or chitosan” at a predetermined dosage. The pulp was agitated for 4 min then frother “MIBC” was added. The concentrate products were collected at different flotation time, dried, and characterized. The flotation performance was examined based on the recovery and the grade of P_2O_5 in the concentrate product. P_2O_5 recovery was calculated using the dry weights of concentrates and tailing products using Equation 3.1, where C and T are dry weights of the concentrate and tailing products, respectively, and c and t are the percentages of P_2O_5 in concentrates and tailings, respectively [82].

$$\text{Recovery} = Cc / (Cc + Tt) * 100\% \quad (3.1)$$



Figure 3.13 A photograph of denver flotation cell used in this study.

Table 3.5 Different conditions and parameters used in this study.

Experiment	Variable conditions	Reagents' dosages			Fixed conditions
		Collector (g/ton)	Frother (g/ton)		
Baseline experiments (Collector and Frother)	Effect of the solid content	20 wt.%	200	63.5	Flotation time: 10 min pH ~9
		40 wt.%			
		60 wt.%			
	Effect of the pulp pH	Natural pH (6.87)	200	63.5	Flotation time: 10 min Solid content: 60 wt.%
		pH 9			
	Effect of the flotation time	10 min 4 min	200	63.5	Solid content: 60 wt. % pH ~ 9
Flotation experiments with sodium silicate	Effect of the dispersant dosage	150 g/ton	200	63.5	Solid content: 60 wt. %
		200 g/ton			
		250 g/ton 300 g/ton			
	Effect of the pulp pH	Natural pH (6.87) pH 9	200	63.5	Solid content: 60 wt. %
	Effect of residence time	10 min 4 min	200	63.5	Solid content: 60 wt. %
Flotation experiments with Hy-PAM	Effect of the Hy-PAM dosage	150 g/ton	200	63.5	Solid content: 60 wt. %
		200 g/ton			
		250 g/ton 300 g/ton			
	Effect of the pulp pH	Natural pH (6.87) pH 9	200	63.5	Solid content: 60 wt. %
	Effect of residence time	10 min 4 min	200	63.5	Solid content: 60 wt. %
Flotation experiments with chitosan	Effect of the Hy-PAM dosage	150 g/ton	200	63.5	Solid content: 60 wt. %
		200 g/ton			
		250 g/ton 300 g/ton			
	Effect of the pulp pH	Natural pH (6.87) pH 9	200	63.5	Solid content: 60 wt. %
	Effect of residence time	10 min 4 min	200	63.5	Solid content: 60 wt. %

3.3. RESULTS AND DISCUSSIONS

3.3.1. Zeta Potential Measurement. Zeta potential measurements were performed on pure mineral samples (apatite and quartz) before and after mixing with reagents at different pH. As mentioned earlier, zeta potential measurements were performed using a Zetasizer Nano ZS instrument (Malvern Instruments, Inc., Westborough, MA, USA). Figure 3.14 shows the change of the surface charge of apatite and quartz dispersions over the pH range of 2-12 without any reagent addition. As shown in Figure 3.14, at the natural pH of the flotation feed (pH ~ 7), the measured zeta potential values of apatite and quartz were -7.4 and -20.3 mV, respectively. The optimum pH in direct phosphate flotation reported in the literature is 9–11 [83].

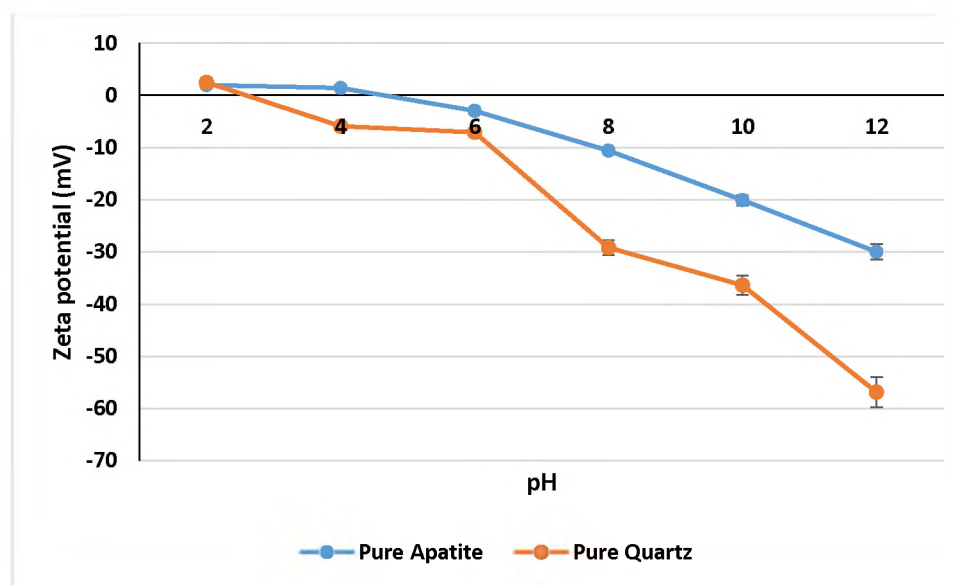


Figure 3.14 Zeta potential measurements of apatite and quartz at different pH.

At that pH range, the average zeta potential values of apatite and quartz were between -17 mV to -25 mV and between -34 mV to -50 mV, respectively. This difference

in the electrical characteristics at natural and basic pH makes it possible to selectively alter the surface properties of either mineral through the addition of an appropriate reagent. For example, a negatively charged reagent will preferentially adsorb on the surface of apatite particles since they are less negative. In contrast, a positively charged reagent will preferentially adsorb on the surface of quartz particles due to attractive electrostatic forces that will lead to partial charge neutralization.

On the other hand, Figures 3.15 A and B show the change in zeta potential values of quartz and apatite suspensions after mixing with different reagents (i.e., sodium oleate, sodium silicate, Hy-PAM, and chitosan) at natural pH of ~ 7 and pH 9, respectively. As indicated by the change in the magnitude of zeta values ($\Delta\zeta$) after reagent adsorption, the interaction of quartz with Hy-PAM was stronger in comparison with apatite. For example, at pH 9, quartz's zeta value increased by +18 (from -34mV to -16 mV) after mixing with Hy-PAM. In apatite, the zeta value increased by +6 mV when mixed with Hy-PAM polymer at the same pH.

Also, Figure 3.15 shows the zeta potential of apatite and quartz after mixing with chitosan. As indicated, the change in the magnitude of zeta potential after chitosan's addition was more significant for quartz at both pH values tested. For example, at pH 9, the magnitude of zeta potential change ($\Delta\zeta$) after the addition of 250 ppm of chitosan polymer was +30.2 mV compared to +0.3 mV in the case of apatite. This difference in the electrical characteristics at pH 9 makes it possible to selectively alter the surface properties of quartz through the addition of chitosan to suppress the flotation of silicate minerals and thus enhance the flotation efficiency of apatite.

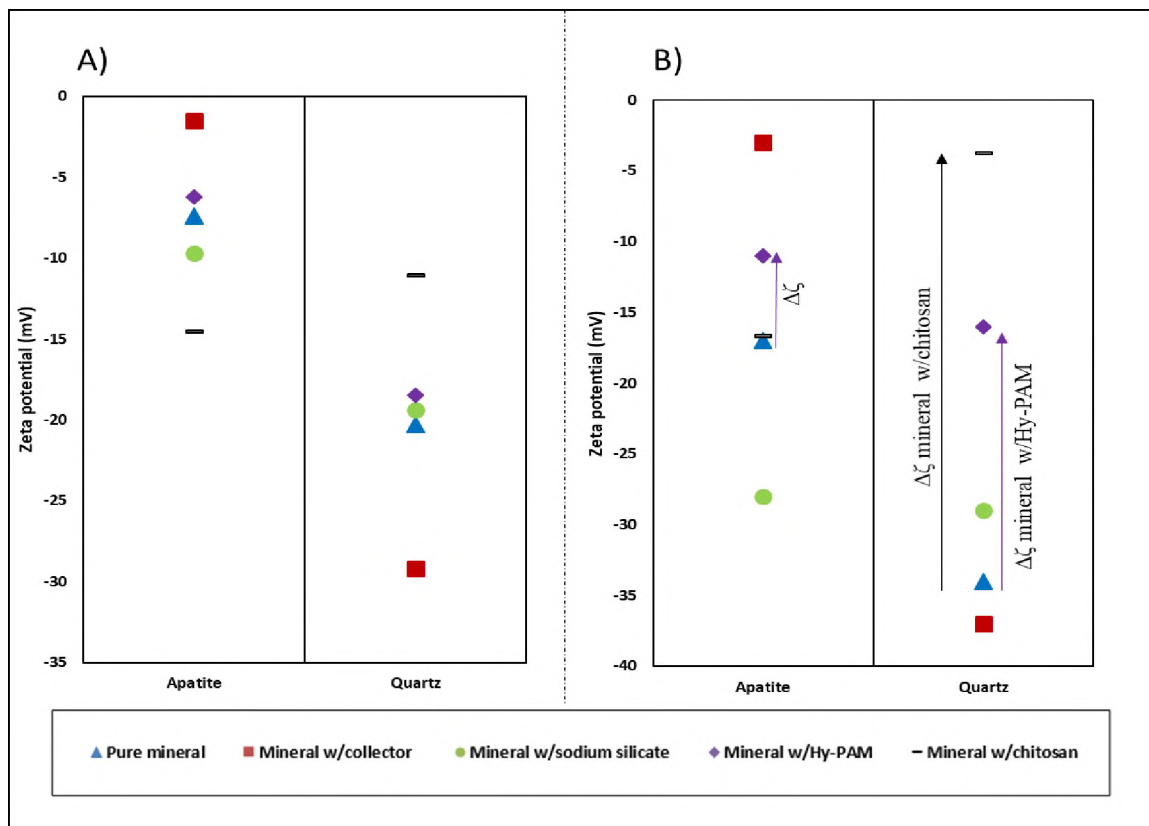


Figure 3.15 Zeta potential measurements of apatite and quartz after mixing with different reagents at natural pH (A) and pH 9 (B).

3.3.2. Investigations on the Potential of Polymers to Aid Silicate Depression in Phosphate's Flotation Process. Baseline experiments, flotation experiments with sodium silicate, flotation experiments with Hy-PAM, and flotation experiments with chitosan were conducted using a laboratory-scale Denver cell. The flotation process outcomes were studied as a function of various process variables including pulp's pH, flotation time, reagent type, and reagent dosages.

3.3.2.1. Baseline experiments. The baseline experiments were performed periodically at different conditions, including a solid percentage in the flotation pulp, flotation time, and pulp's pH. These experiments were conducted to define base recovery

and ensure the reproducibility of the results and congruity of the experimental parameters. As shown in Figure 3.16, the best P_2O_5 recovery was obtained at 60 wt. % of solid. The flotation performance at pH 9 was better as compared to the performance at natural pH, whether the flotation time was short (4 min) or long (10 min). The recovery of P_2O_5 at pH 9 was slightly better when the flotation time was at 10 min. For example, at 10 min of flotation time, the average recovery of P_2O_5 was 77% and 76% at pH 9 and natural pH, respectively. At the same flotation time, the P_2O_5 grade of the concentrate products was 23.4% at pH 9 and 24.1% at natural pH.

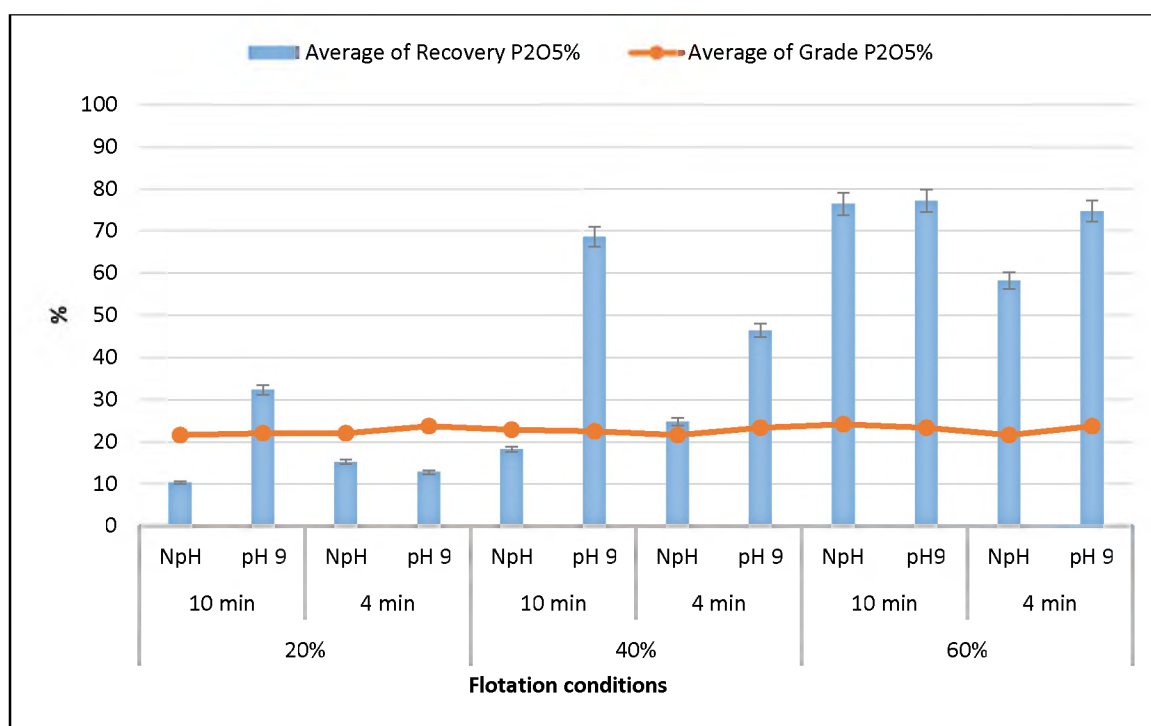


Figure 3.16 Baseline flotation experiments at different flotation conditions.

3.3.2.2. Flotation experiments in the presence of sodium silicate dispersant. In

this set of experiments, sodium silicate was chosen as a dispersant since it is considered

one of the most effective inorganic dispersants for silicate minerals. It is widely used in industrial operations. Different influencing parameters such as flotation time, pH, and dispersant's dosage were examined to optimize the flotation process in the presence of sodium silicate dispersant. As shown in Figures 3.17 and 3.18, the highest recovery and grade were obtained at 4 min flotation time, 250 g/ton sodium silicate dosage, and pH 9.

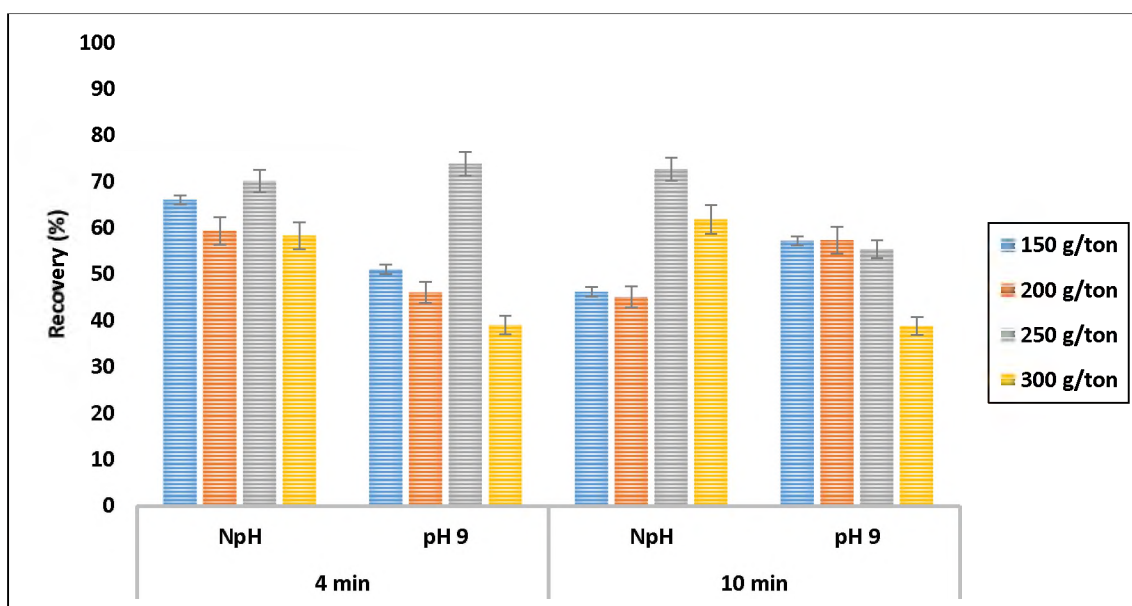


Figure 3.17 Flotation recovery of P₂O₅ in the presence of sodium silicate at different flotation conditions.

Sodium silicate dispersant helped significantly to improve the flotation outcomes at shorter flotation time, which is critical at an industrial scale where energy consumption is a determinant factor in assessing the economic feasibility of flotation processes. At a shorter flotation time of 4 min, the addition of sodium silicate at pH 9 increased the grade of concentrates to 28.4% compared to 23.4% in the baseline experiment without affecting

the recovery. As indicated, the recoveries of P_2O_5 in concentrate products were 74% in the baseline experiment compared to and 73.88% when sodium silicate was used.

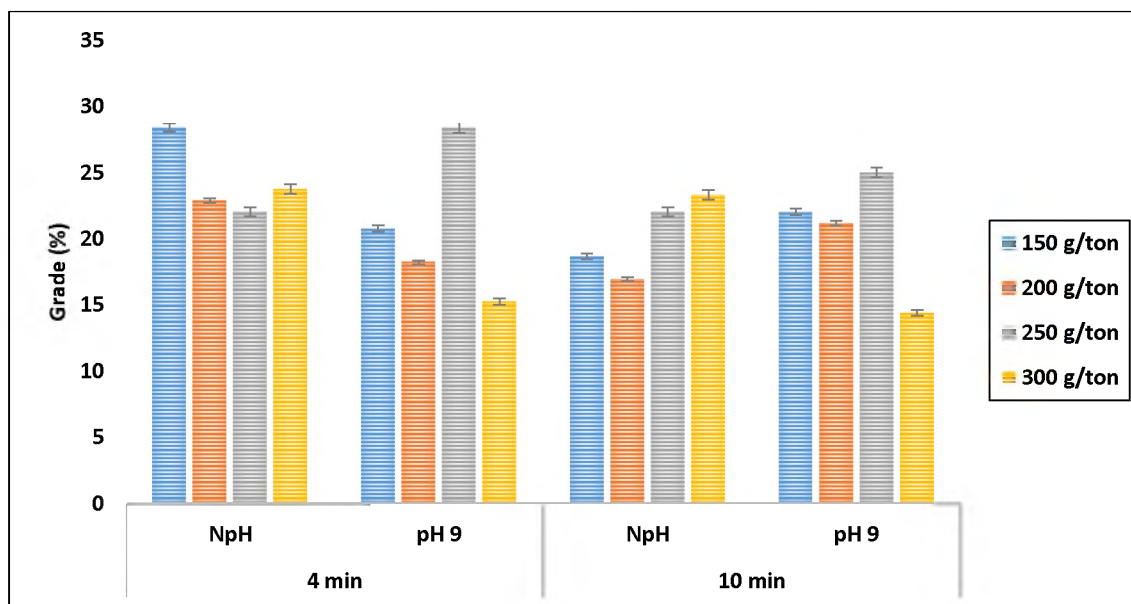


Figure 3.18 Concentrate grade of P_2O_5 in the presence of sodium silicate at different flotation conditions.

3.3.2.3. Flotation experiments in the presence of Hy-PAM depressant. Flotation experiments in the presence of Hy-PAM were conducted at 60 wt. % feed solids. In this set of experiments, the influence of polymer dosage and froth collection time was examined at different pH values (Figures 3.19 and 3.20). As shown, in the presence of 250 g/ton of Hy-PAM, the recovery of phosphates minerals significantly improved when the flotation was performed at natural pH compared to alkaline pH at both shorter and longer flotation time. At natural pH and flotation time of 4 min, the P_2O_5 grade increased to 28.6% compared to ~27% at alkaline pH.

Moreover, when the flotation time increased to 10 min, the grade of the concentrate products marginally changed at both natural and alkaline pH. At natural pH and in the presence of 250 g/ton Hy-PAM polymer, the recovery of phosphates minerals at 10 min of flotation increased to 84.8% compared to 80.5% at 4 min of flotation time while the grade marginally decreased by ~0.2%. However, from the economic point of view, only a 4% increase in recovery with more than double increase in time makes it less expensive and more valuable to run the process at a shorter time as there is no improvement in the grade. Under these conditions, the average recovery of P_2O_5 was 80.5%, and the grade of P_2O_5 increased from 21.6% in the feed to 28.6% in the concentrate products.

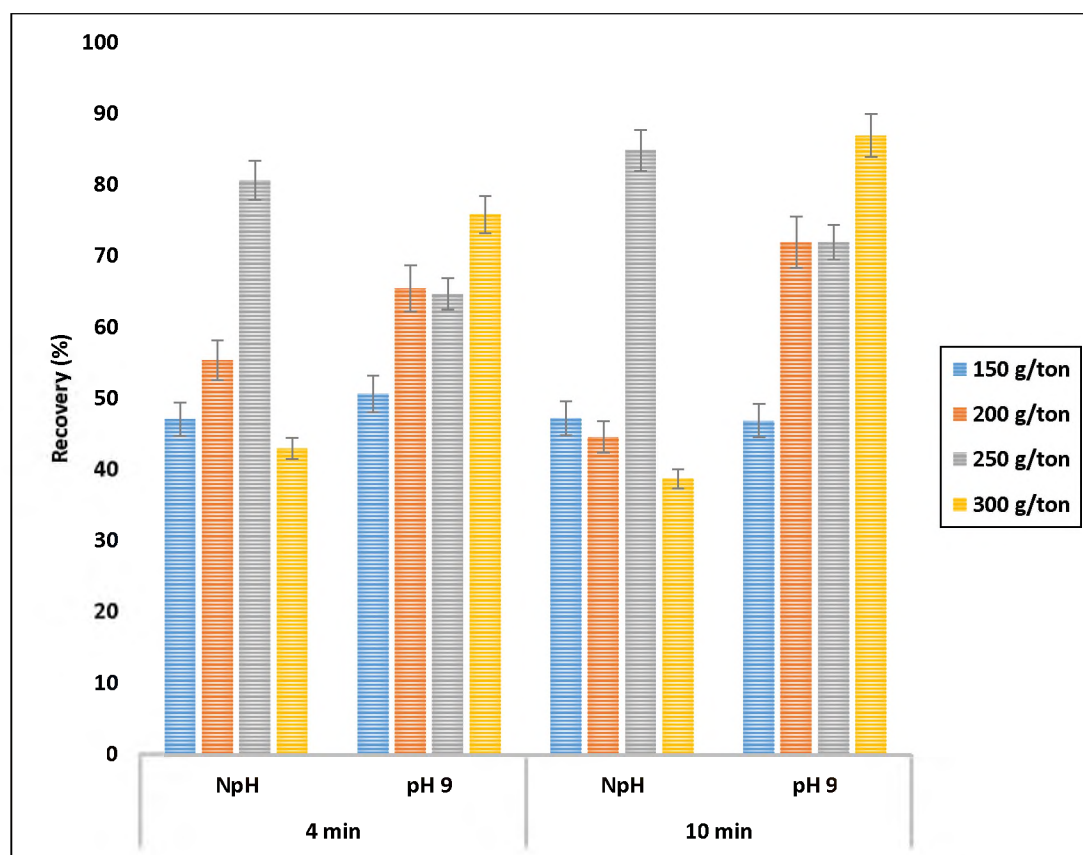


Figure 3.19 Flotation recovery of P_2O_5 in the presence of Hy-PAM at different flotation conditions.

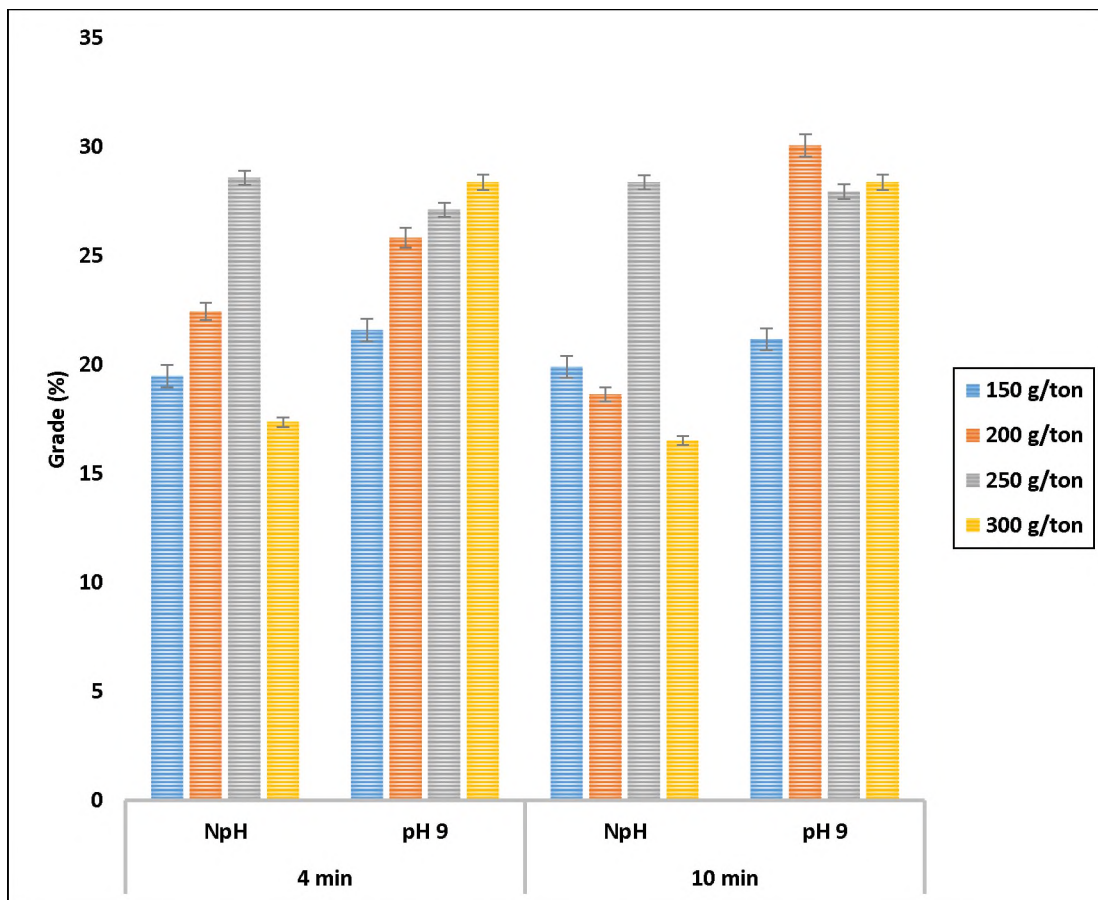


Figure 3.20 Concentrate grade of P₂O₅ in the presence of Hy-PAM at different flotation conditions.

Figure 3.21 shows a comparison between the flotation performance of P₂O₅ in the presence of 300 g/ton of sodium silicate and Hy-PAM at pH 9. At the shorter time (4 min), both P₂O₅ recovery and grade were higher when the Hy-PAM was used compared to the sodium silicate. The average recovery and grade of P₂O₅ was 75% and 28.4% in the presence of Hy-PAM. Compared to 39% P₂O₅ recovery and 15% P₂O₅ grade in the presence of the sodium silicate.

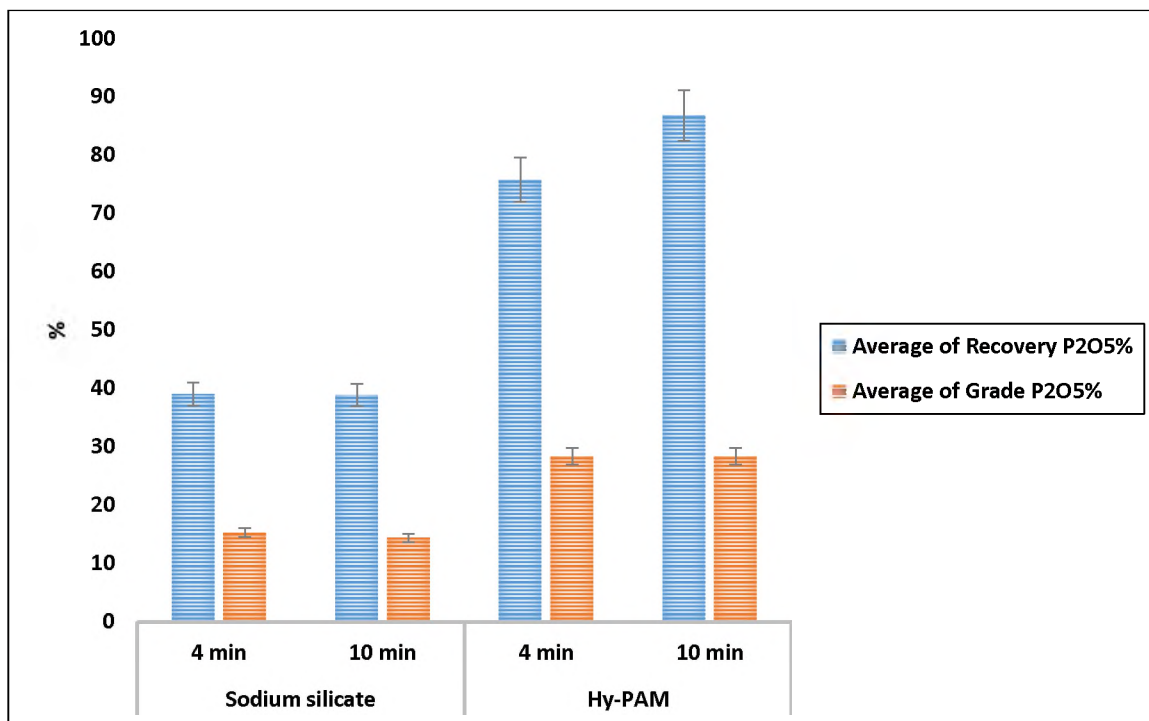


Figure 3.21 Comparisons of flotation performance of P₂O₅ in the presence of sodium silicate and Hy-PAM at pH 9.

3.3.2.4. Flotation experiments in the presence of chitosan depressant. Flotation experiments in the presence of chitosan were conducted at a solid concentration of 60 wt.%. In this set of experiments, the influence of chitosan dosage and froth collection time was examined at different pH levels. As shown in Figures 3.22 and 3.23, the highest recovery was obtained at 10 min flotation time, pH 9, and 300g /ton of chitosan. Figures 3.22 and 3.23 also show the average recovery and grade of P₂O₅ collected after 4 minutes and 10 minutes at natural pH (pH~7) and pH 9. As indicated, increasing flotation time had a positive impact on the flotation performance of phosphate minerals. The maximum recovery and grade of P₂O₅ collected after 10 minutes were 66% and 25%, respectively,

compared to recovery and grade values of 55% and 23%, respectively, after 4 minutes of flotation time.

Results showed that the flotation recovery of P_2O_5 was enhanced when pulp's pH increased to 9 at both 4 and 10 minutes of flotation time. For example, the recovery and grade of P_2O_5 at pH 9 and 10 minutes of flotation time were 67% and 25%, respectively, compared to 54.1% and 21.6% at natural pH. These results support the zeta potential measurements, which indicated stronger interactions between quartz and chitosan at higher pH. In addition, results showed that the flotation recovery of P_2O_5 slightly increased by increasing the dosage of chitosan at both pH values tested regardless of the flotation time. For example, in the presence of 300 g/ton of chitosan polymer, the recovery of P_2O_5 was 68% compared to 62% at 250 g/ton.

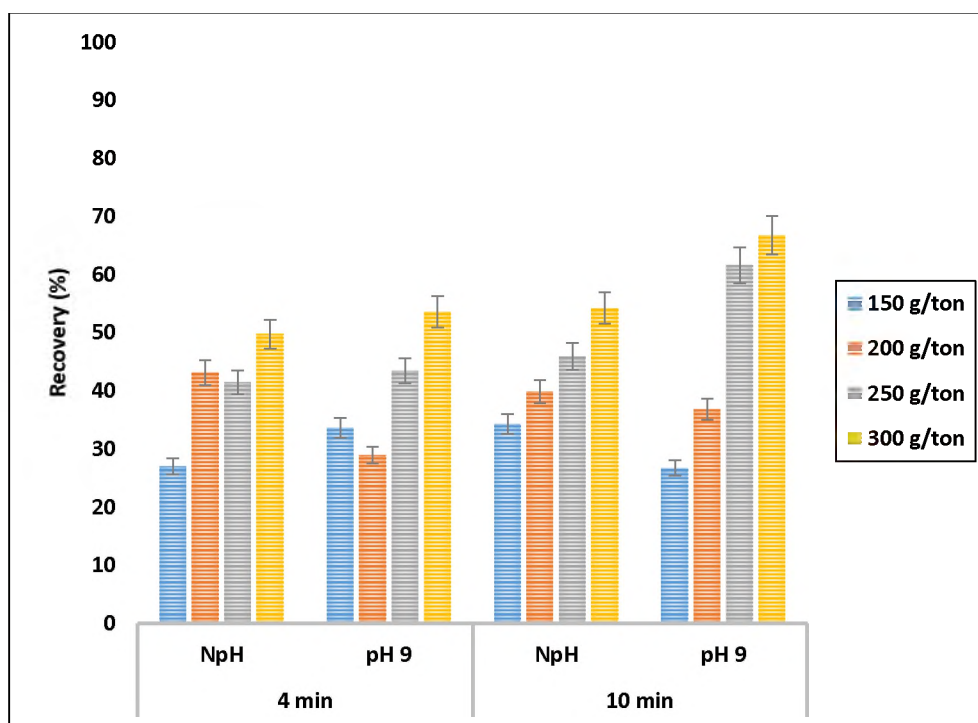


Figure 3.22 Flotation recovery of P_2O_5 in the presence of chitosan at different flotation conditions.

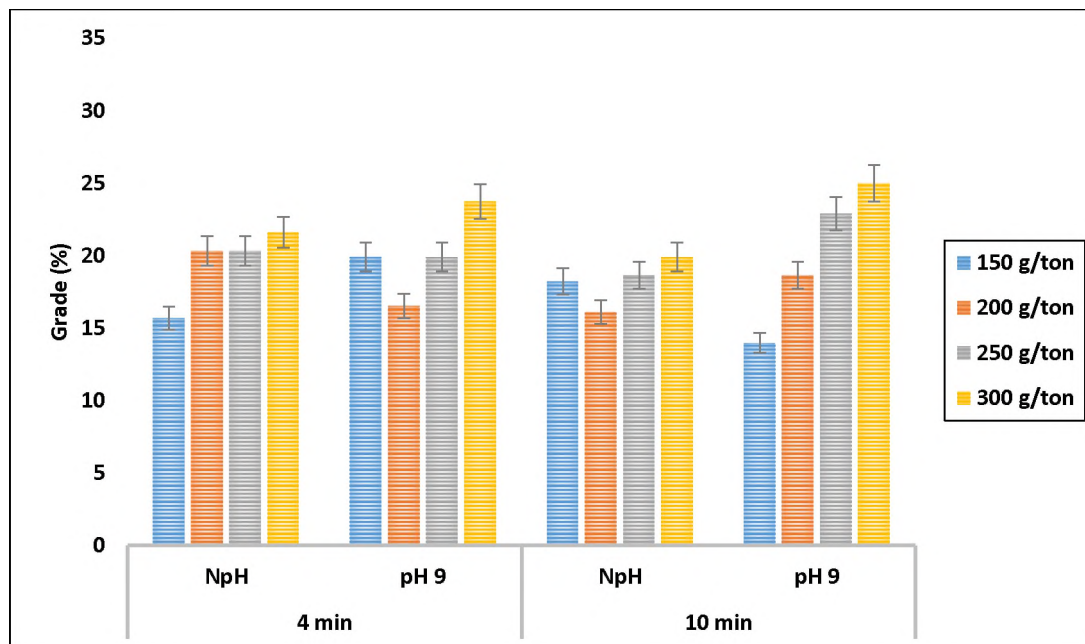


Figure 3.23 Concentrate grade of P₂O₅ in the presence of chitosan at different flotation conditions.

Overall, the results indicated that the optimum conditions of phosphate flotation, and simultaneous depression of silicates, in the presence of chitosan polymer are: 300 g/ton of chitosan, pH 9, and 10 minutes of flotation time. At these optimum conditions, the overall recovery of P₂O₅ was ~ 70% compare to ~40% in the presence of commercially applied silicate dispersants, as shown in Figure 3.24.

Figure 3.25 shows a comparison between the flotation performance of phosphate minerals presented at % recovery of P₂O₅ in the presence of 300 g/ton of commercially dispersant sodium silicate, Hy-PAM, and chitosan at pH 9. The results showed that at 10 min flotation, the highest recovery of P₂O₅ (86.82%) was observed when the Hy-PAM was used. The second highest recovery obtained was 66.7% when chitosan polymer was used. Both polymers were more selective than sodium silicate. Also, the highest grade of P₂O₅ (28.4%) was obtained when H-PAM was used.

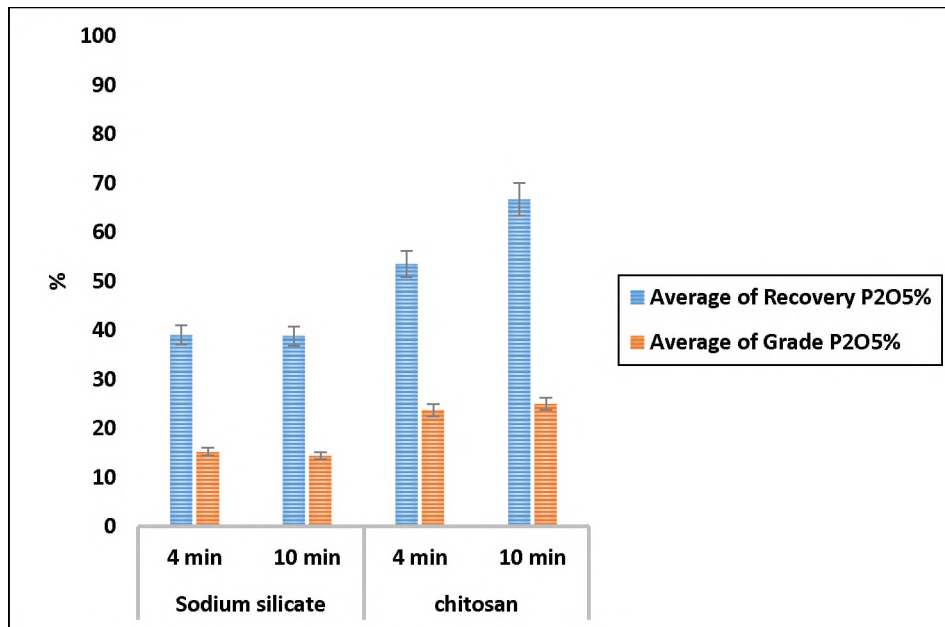


Figure 3.24 Comparisons of flotation performance of P₂O₅ in the presence of sodium silicate and chitosan at pH 9.

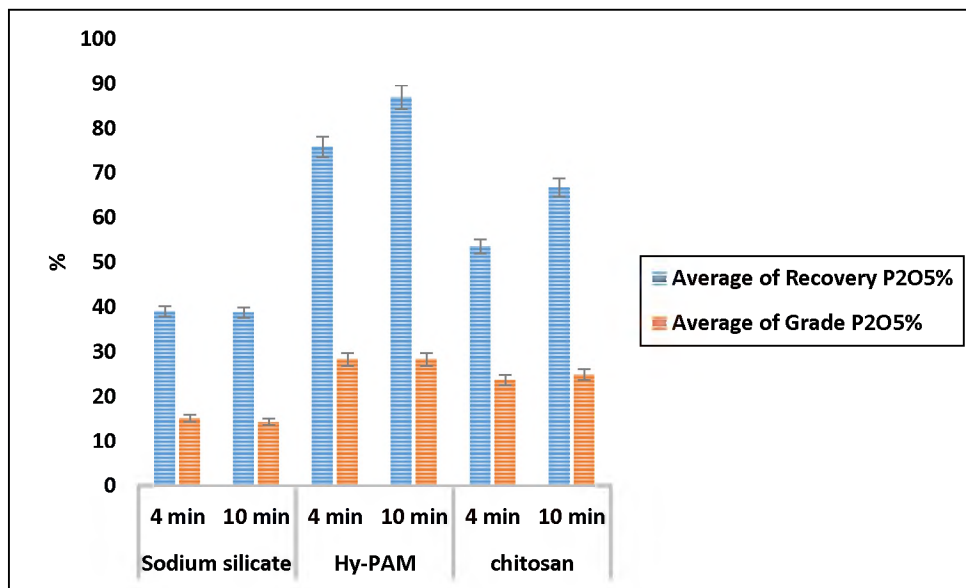


Figure 3.25 A comparison between the flotation performance of P₂O₅ in the presence of commercial dispersant sodium silicate, Hy-PAM, and chitosan at pH 9.

4. RECOVERY OF PHOSPHATE MINERALS USING IONIC LIQUIDS IN REVERSE FLOTATION PROCESS

4.1. BACKGROUND

Ionic liquids (ILs) are molten salts with melting temperatures below 100C°. They have gained considerable attention due to their unique structural properties [75], [76]. Among these properties are non-flammability and negligible vapor pressure. Moreover, It is possible to tailor their structures by changing the cation or anion parts to target a specific metal ion [77]–[80].

Due to their unique structural properties and physiochemical flexibility, ILs have been widely used in separation techniques such as froth flotation, leaching, solvent extraction, and ion exchange [75], [76], [81]–[83]. In the froth flotation process, ILs were first introduced by Sahoo et al. The authors studied trioctylmethylammonium salicylate (TOMAS) as a novel collector of quartz in iron ore flotation. In the study, iron minerals were upgraded from 38% to 67%, which was better than the grade obtained using conventional collectors such as Amines [84]. A mixture of an imidazolium ionic liquid was used to develop a new type of coal slime collector, tested in coal slime flotation, and compered with n-dodecane [85]. The flotation experiments showed that the new collector could be applied to recover the clean coal without the need for a frother, and it could be yielded the same performance as that in n-dodecane. A comprehensive study was also performed to examine the adsorption behavior of different ILs on quartz in iron ore [86]. FTIR, XPS, and molecular modeling were used to investigate the adsorption mechanism. The results showed stronger adsorption of IL's onto the quartz surfaces compared to the iron oxide surfaces [86]. Azizi et al. used tetrabutylammonium bis (2-Ethylhexyl)-

phosphate as a collector of model monazite and bastnaesite minerals. Results indicated that IL was a better collector as compared to hydroxamic acid collectors that are commonly used in the flotation of Rare-Earth Elements (REE) [87]. In addition to their high selectivity, another advantage to use ILs in froth flotation is their dual functionality (i.e., collectors and frothers)[84], [86]–[89].

To the best of the authors' knowledge, the application of ILs in phosphate processing has not been explored yet. Therefore, in this work, micro-flotation tests and fundamental studies have been conducted to investigate the potential of ILs to serve as selective collectors of silicates in reverse flotation of phosphate minerals. As shown in Figure 4.1, two ILs were chosen: Tetrahexylammonium iodide ($\text{CH}_3(\text{CH}_2)_{54}\text{N}(\text{I})$), and 1-Hexyl-3-methylimidazoli hexafluorophosphate ($\text{C}_{10}\text{H}_{19}\text{F}_6\text{N}_2\text{P}$). These ionic liquids have been selected because they possess the quaternary nitrogen atom that is anticipated to preferentially adsorb on the negatively charged fine and ultrafine silicate particles [83], [89]. The long alkyl chain in the IL structures facilitates the attachment of silicates to air bubbles and enhances floatability [89].

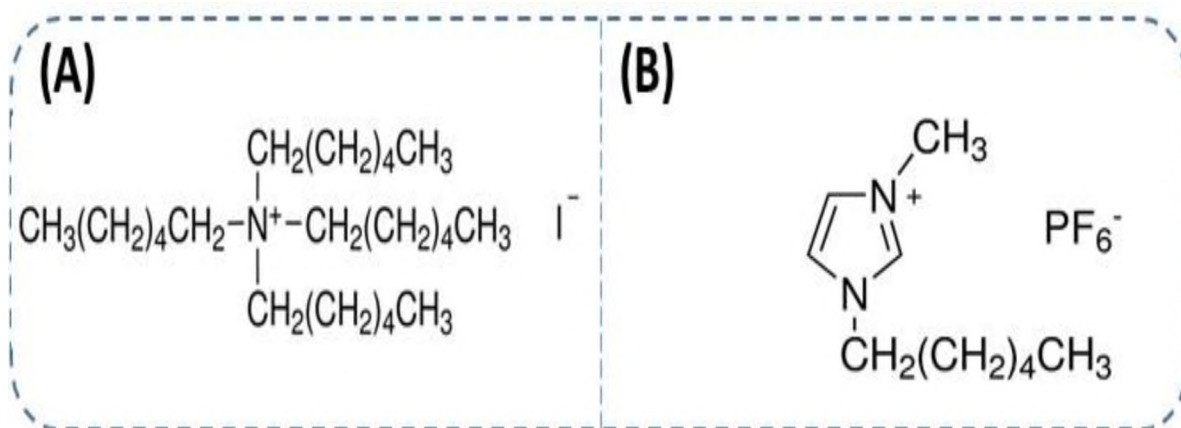


Figure 4.1 Chemical structure of A) Tetrahexylammonium iodide (THAI), and B) 1-Hexyl-3-methylimidazoli hexafluorophosphate (HMLHF).

4.2. METHODOLOGY AND MATERIALS

4.2.1. Materials. Chemical reagents and pH modifiers used in this study were purchased from Fisher Scientific (Hampton, NH, USA). These included dodecylamine (DA) conventional collector of silicate minerals; Tetrahexylammonium iodide (THAI), and 1-hexyl-3methylimidazoli hexafluorophosphate (HMLHF) — the proposed alternative collectors of silicates minerals. Both hydrochloric (HCl) and sodium carbonate (Na_2CO_3) were used as pH modifiers to adjust the pH in both flotation and adsorption experiments. Pure apatite and pure quartz were purchased from Ward's Science Company, USA.

4.2.2. Zeta Potential Measurement. Zeta potential of mineral suspensions was measured using the Zetasizer Nano ZS instrument (Malvern Instruments, Inc., Westborough, MA, USA). Zeta potential measurements of apatite and quartz surfaces were conducted in the presence and absence of the ILs at a pH range between 3-to-11. A stock solution was prepared at 0.1 wt. % of pure mineral in a 0.1M KCl. Either HCl or NaOH was used to adjust the pH of mineral suspensions. The prepared mineral suspension was agitated using an IKA RW20 mechanical stirrer for 30 min at a constant agitation rate of 250 rpm. The suspensions were allowed to settle overnight. The supernatant liquid was considered for all the zeta potential measurements.

4.2.3. Adsorption Studies. Both X-ray Photoelectron Spectroscopy (XPS) and Fourier-transform infrared spectroscopy (FTIR) were used to detect the change in bonding characteristics and binding energy after the adsorption of ILs on mineral surfaces (i.e., apatite and quartz). The XPS and FTIR studies were carried out using the KRATOS AXIS 165 XPS and Thermo Scientific™ Nicolet™ iS50 FTIR Spectrometer at 32 scans with a resolution of 4cm^{-1} , respectively. All the ILs-treated quartz and apatite samples were

prepared by adding 1×10^{-3} M of IL to mineral suspensions of either quartz or apatite (10 wt. %). The suspensions were agitated for 30 min, filtered, thoroughly rinsed with distilled water, and dried at room temperature. In XPS studies, the instrument was first calibrated by running broad surveys of clean Ag sample at 80 and 160 pass energy (PE), focusing on Ag3d range, running pre-adjustments spectra, and maximizing the single-noise ratio for each channel spectroscopic detector, then re-running all broad surveys. Internal standards were used to calibrate the curve fitting and high-resolution spectra of quartz and apatite samples. Calibration process were done by using the C 1s component at (Binding Energy “BE” = 28.4.8 eV), Si 2p component (BE = 102.0 eV), and P 2p component (BE = 132.5 eV). All XPS spectra were processed by using CasaXPS software.

4.2.4. Micro-flotation Experiments. A Hallimond micro-flotation tube, shown in Figure 4.2, was utilized in this study with 150 mL internal volume. Micro-flotation tests of a single mineral system (apatite or quartz) and binary mineral system (equal masses of apatite and quartz) were conducted at room temperature to explore the potential of ILs to serve as selective quartz collectors. Nitrogen was used as a gas phase at a rate of 40 cm³/min, and the pressure was kept at 10 psi. One gram of either apatite or quartz was used in each flotation experiment in single mineral flotation tests. In binary mineral flotation tests, 0.5 grams of apatite and 0.5 grams of quartz were used in each test. The particle size of minerals was between +75 μ m to -150 μ m obtained by grinding and sieving. The pulp was conditioned for 3 min before any reagent addition. Na₂CO₃ was used to adjust the pH to 7, 9, or 11 as needed. IL dosages were added at 50, 100, and 150 g/ton. The pulp was then pumped into the Hallimond tube. In single flotation tests, apatite and quartz's recoveries were calculated using the net dry weight of concentrates, assuming the grade of

minerals was 100%. Since the grade of apatite and quartz in the concentrates were variable in a binary mineral system, XRD was applied to determine the grade and calculate the recovery. For comparison, the flotation performance of minerals in the presence of dodecylamine (DA) — a conventional collector of silicate minerals was tested. Flotation experiments using DA were conducted at optimum conditions as determined from single and binary micro-flotation tests using. Table 4.1 shows the different experimental conditions used to investigate the flotation efficiency of apatite and quartz in the reverse flotation process.



Figure 4.2 A photograph of hallimond micro-flotation tube used in this study.

Table 4.1 Experimental conditions used to investigate the flotation efficiency of apatite and quartz in the reverse flotation process.

Minerals	Reagents	pH	Dosage (g/ton)	Time (min)
Quartz	HMLHF	7, 9, and 11	50, 100, and 150	1, 2, and 3
	THAI	7, 9, and 11	50, 100, and 150	1, 2, and 3
	DA	Optimum pH*	Optimum dosage**	1, 2, and 3
Apatite	HMLHF	7, 9, and 11	50, 100, and 150	1, 2, and 3
	THAI	7, 9, and 11	50, 100, and 150	1, 2, and 3
	DA	Optimum pH*	Optimum dosage**	1, 2, and 3
Binary mineral system	HMLHF	Optimum pH*	Optimum dosage**	1, 2, and 3
	THAI	Optimum pH*	Optimum dosage**	1, 2, and 3
	DA	Optimum pH*	Optimum dosage**	1, 2, and 3
* The optimum pH was at 9 and 11.				
** The optimum dosage was at 150 g/ton				

4.3. RESULTS AND DISCUSSIONS

4.3.1. Adsorption Studies. FTIR spectra of pure minerals before and after mixing with ILs are shown in Figures 4.3 and 4.4 (1 and 2). Spectra 1-B and 2-B show apatite/THAI (A-THAI) and quartz/THAI (Q-THAI), respectively. In the case of quartz, the spectra (2-B) displayed a new primary amine peak (N-H stretching) at $\sim 2950 \text{ cm}^{-1}$ and alkane peak (C-H stretching) at 2850 cm^{-1} , while no new peaks were detected for apatite when treated with A-THAI (1-B). Results showed preferential adsorption of THAI on quartz surfaces through the N-H functionality in THAI's structure. Spectra 1-C and 2-C show the FTIR spectra of apatite and quartz after being treated with HMLHF, respectively.

A new primary amine group peak (N-H stretching) and alkane group (C-H stretching) were detected for both apatite (spectra.1-C) and quartz (spectra.2-C). These results indicated that HMLHF has the ability to adsorb on both minerals.

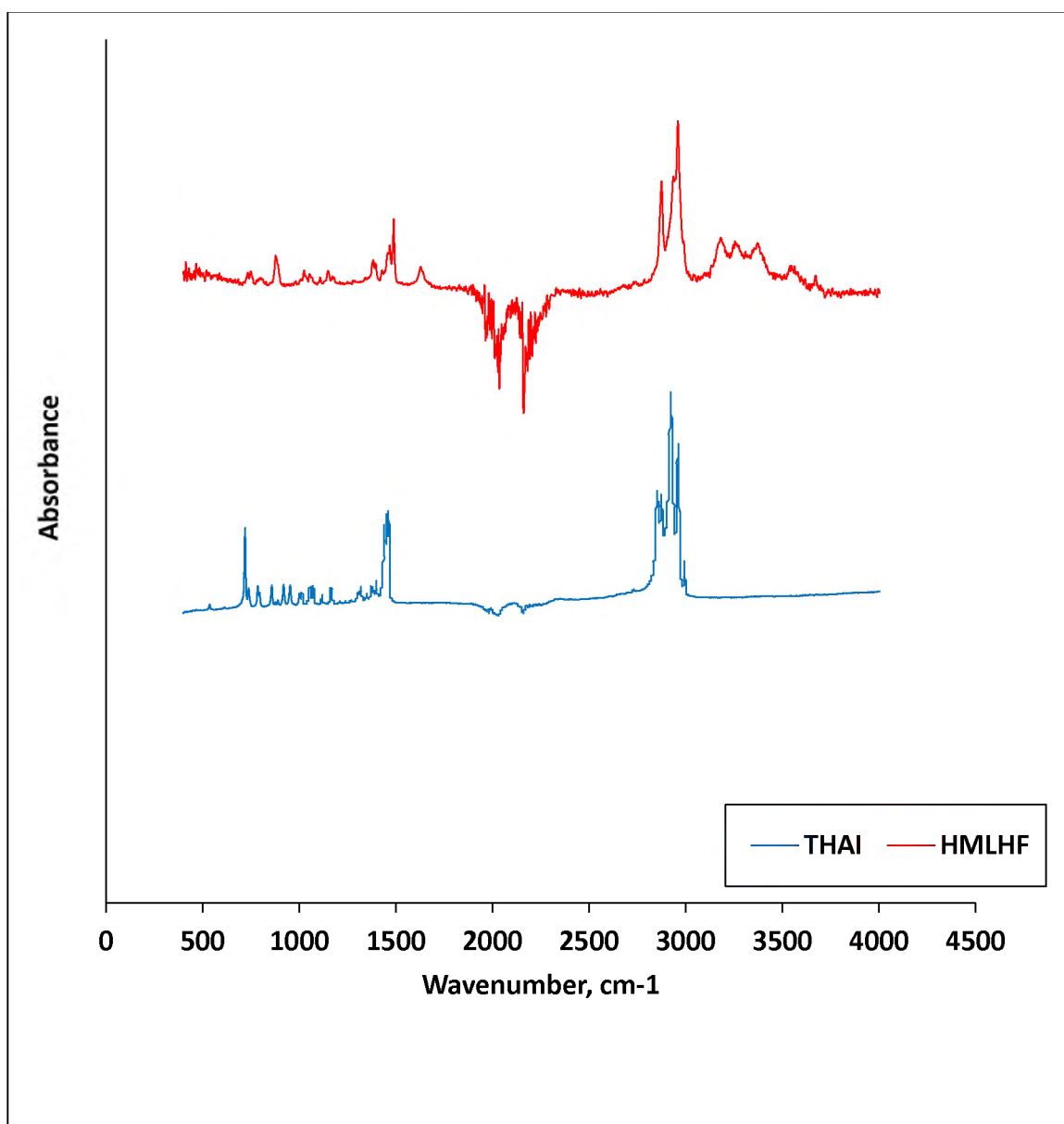


Figure 4.3 FTIR spectra of pure THAI and HMLHF.

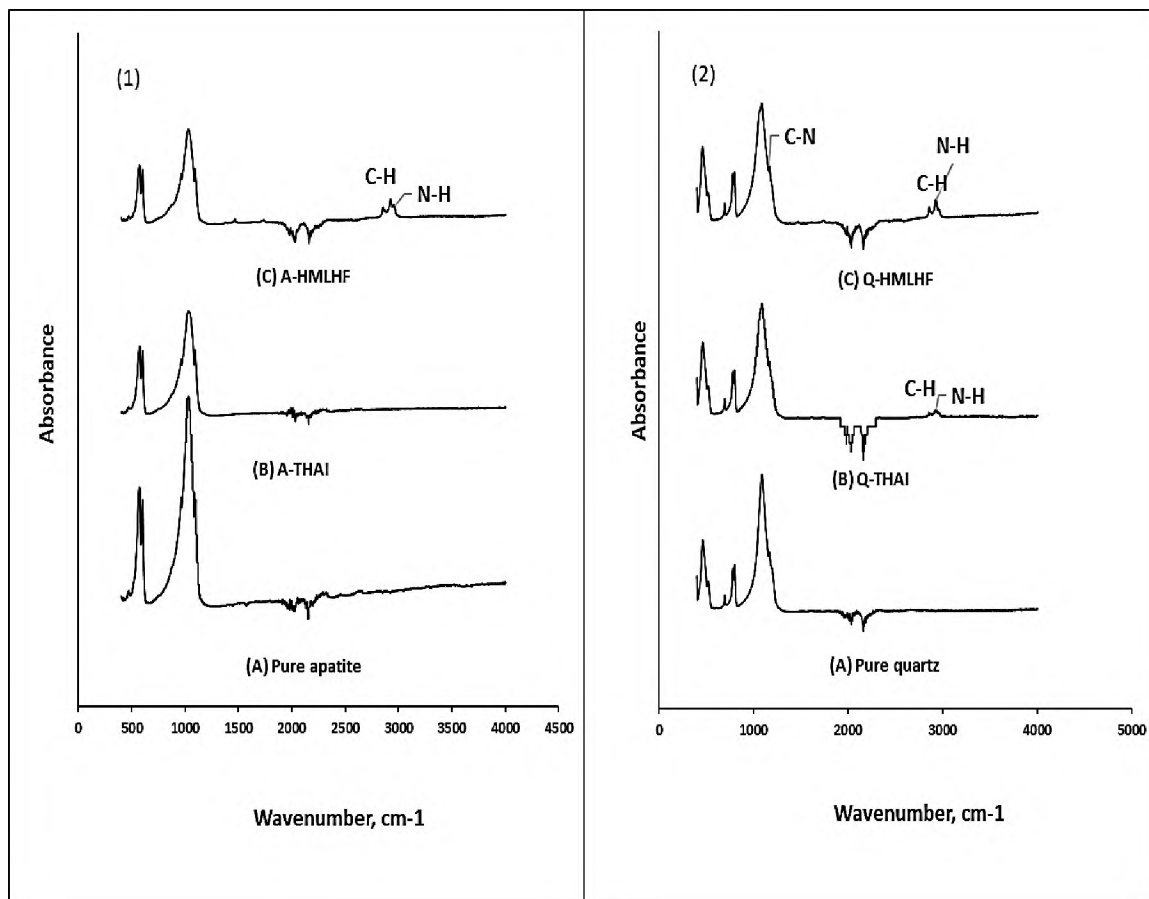


Figure 4.4 FTIR spectra of pure apatite(1-A), A-THAI (1-B), A-HMLHF (1-C), pure quartz(2-A), Q- THAI (2-B), and Q-HMLHF (2-C).

The XPS spectra were obtained from apatite and quartz single minerals that were treated with HMLHF and THAI. As charging occurred in the measurement, the Si 2p component (BE = 102.0 eV) and P 2p component (BE = 132.5 eV) were used as internal standards to calibrate the entire XPS spectra of quartz and apatite samples. The XPS spectra of THAI and HMLHF were obtained as references. Figures 4.5 (A and C) show the XPS spectra for ILs in a pure state. As seen, the presence of carbon and nitrogen peaks was confirmed according to the chemical formula of both ILs. The high-resolution spectra of N 1s electron were acquired for both ILs. As shown in Figure 4.5-B, the N 1s of THAI spectra

consist of a single binding energy peak at 401.5 mV. This peak corresponds to a primary amine s group (N-H stretching). N 1s of HMLHF spectra (Figure 4.5-D) consists of two binding energy peaks; the first peak was detected at 397.9 mV and the second peak at 401.0 mV. These two peaks correspond to the two nitrogen atoms in HMLHF.

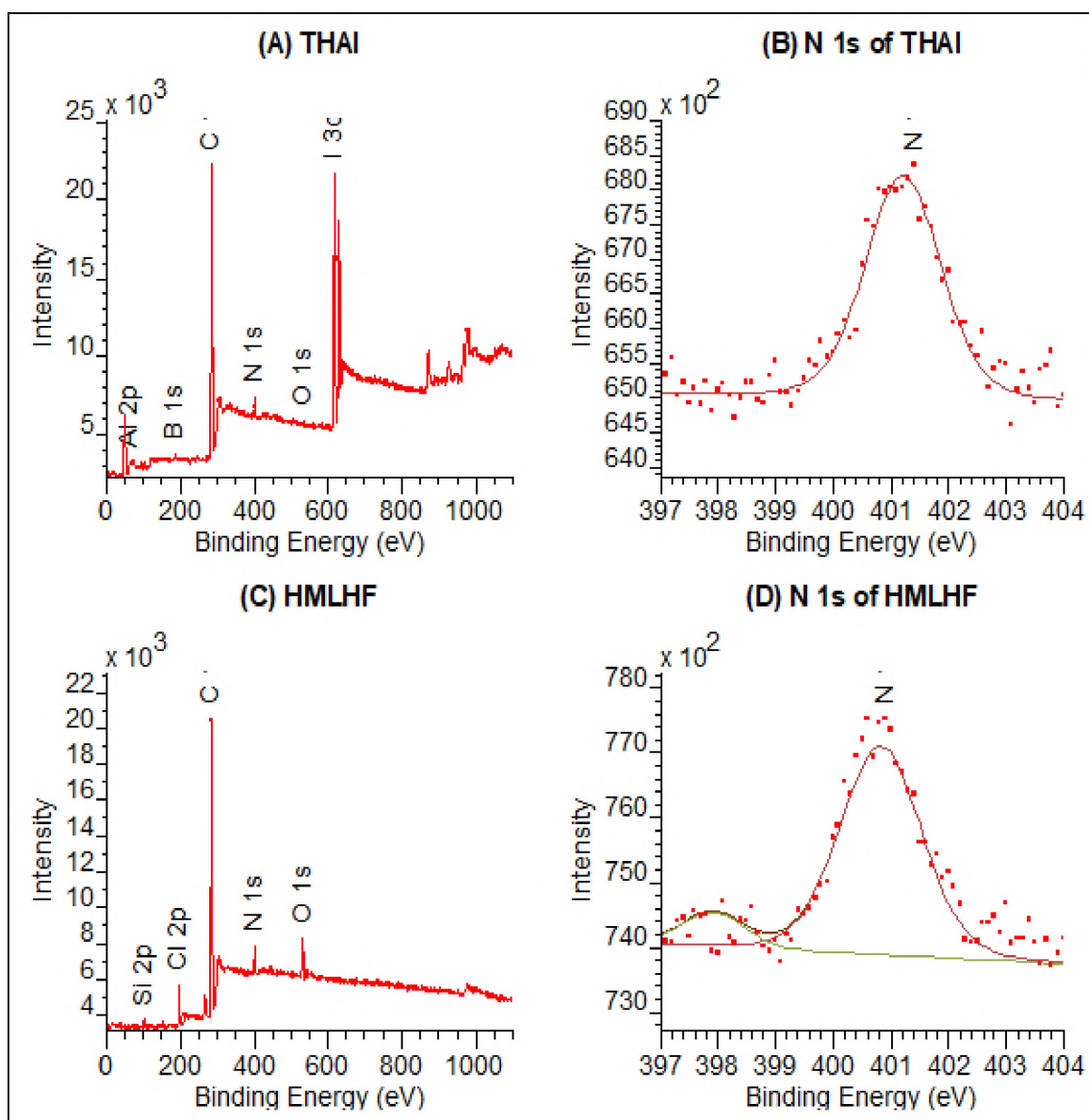


Figure 4.5 XPS spectra for (A) THAI, (B) N 1s of THAI, (C) HMLHF, and (D) N 1s of HMLHF.

The high-resolution spectra of N 1s were examined on quartz and apatite before and after ILs adsorption. As shown in Figures 4.6 A and B, no N 1s peaks were observed on the high-resolution spectra of pure quartz or pure apatite (before ILs treatment).

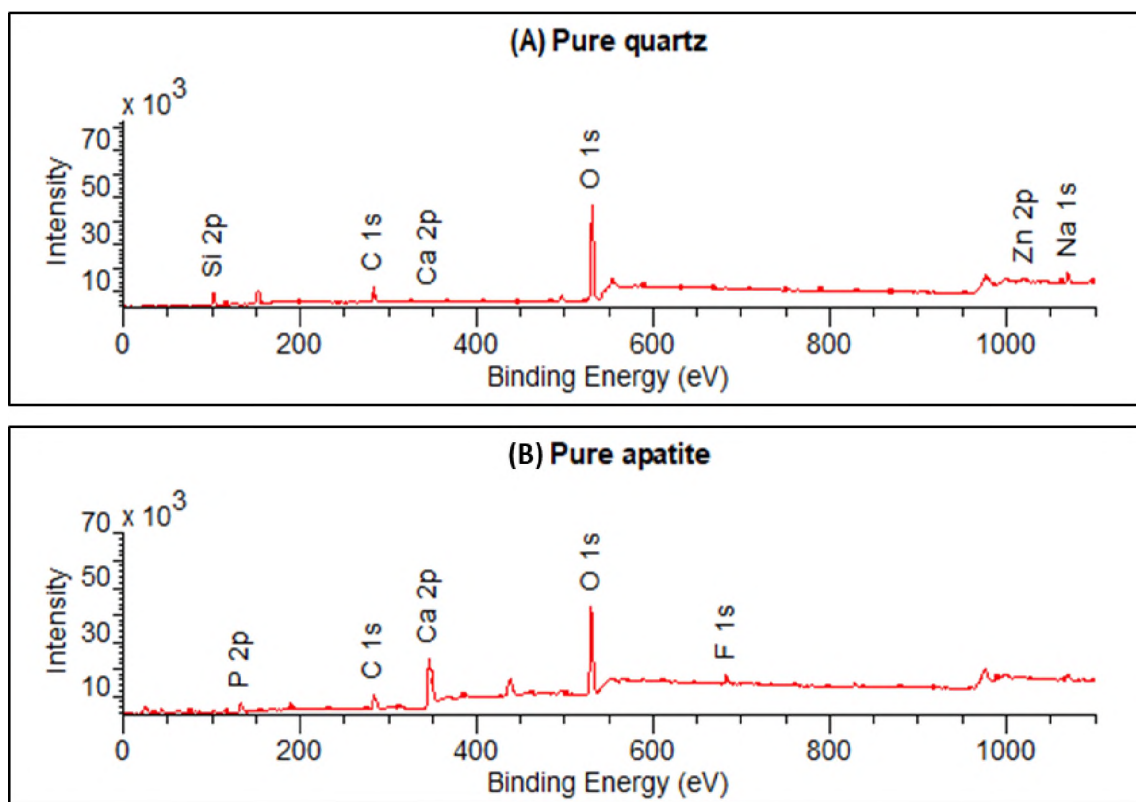


Figure 4.6 XPS spectra for (A) pure quartz and (B) pure apatite.

The N 1s high-resolution spectra of quartz-treated THAI (Q-THAI) in Figure 4.7 were deconvoluted into a single component at 401.1 eV from nitrogen atoms. This new peak in the XPS spectra Q-THAI suggested that THAI may get adsorbed on quartz surface. Compared to the N 1s spectrum of apatite-treated THAI (A-THAI), no peak corresponding to amine was detected, which suggested that there was no adsorption of THAI on apatite surface.

The N 1s high-resolution spectra of quartz-treated HMLHF (Q-HMLHF) is shown in Figure 4.7. The spectra showed two peaks at 399.8 eV, and 401.1 eV originated from the two nitrogen atoms in the HMLHF structure. The N 1s spectrum of apatite-treated HMLHF (A-HMLHF) also showed 2 peaks at 399.7eV and 400.8 eV (Figure 4.7). Table 4.2 showed the magnitude shifting of the binding energies of N 1s after adsorption on mineral surfaces. The result suggested that HMLHF could adsorb on both apatite and quartz with a larger binding energy shift in the case of quartz. There was no observed shift of N 1S in the case of Q-THAI which suggested that the adsorption of THAI on quartz is physisorption rather than chemisorption.

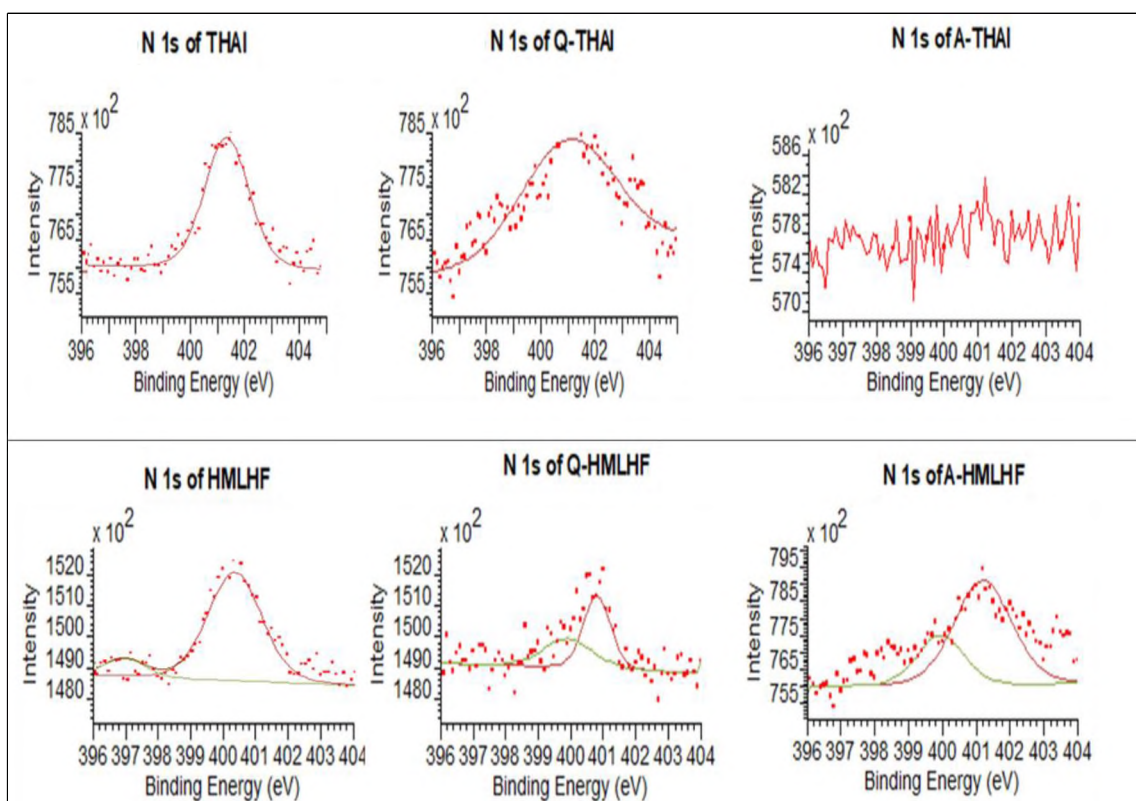


Figure 4.7 XPS spectra of N 1s of pure IL and IL treated quartz and apatite.

Table 4.2 Binding Energy Shifts of the N 1s of ILs before and after adsorption on apatite and quartz.

<i>Pure sample name</i>	<i>Initial N (1s)</i>	<i>Treated sample name</i>	<i>Final N (1s)</i>
Pure THAI	N1: 401.5	A-THAI	N1: 0
		Q-THAI	N1: 401.1
Pure HMLHF	N1: 401 N2: 397.9	A-HMLHF	N1: 400.8
			N2: 399.7
		Q-HMLHF	N1: 401.1
			N2: 399.8

According to the previous observations, two nitrogen atom peaks were observed in both Q-HMLHF and A-HMLHF spectrum, which indicates that HMLHF can adsorb both mineral surfaces. Figure 4.8 shows the intensity of N 1s spectra pure minerals before and after being treated with HMLHF. As shown, a higher intensity value was observed for Q-HMLHF compared to A-HMLHF. The change in intensity value between pure quartz and Q-HMLHF was more significant than the changing intensity value between pure apatite and A-HMLHF. The direct relationship between the binding energy and intensity suggested that adsorption between HMLHF and quartz is stronger than HMLHF and apatite [84], [89]. Also, the results indicated that HMLHF has abilities to adsorb the quartz surfaces better than THAI due to the shifting of two nitrogen atoms into the quartz surface instead of one nitrogen atom. But also, it can adsorb into the apatite surfaces as mentioned previously which is anticipated to preferentially adsorb on the negatively charged quartz surfaces [83], [89]. Results from the XPS studies suggested that both THAI and HMLHF have the potential to serve as selective collectors of silicates in reverse flotation of phosphate minerals.

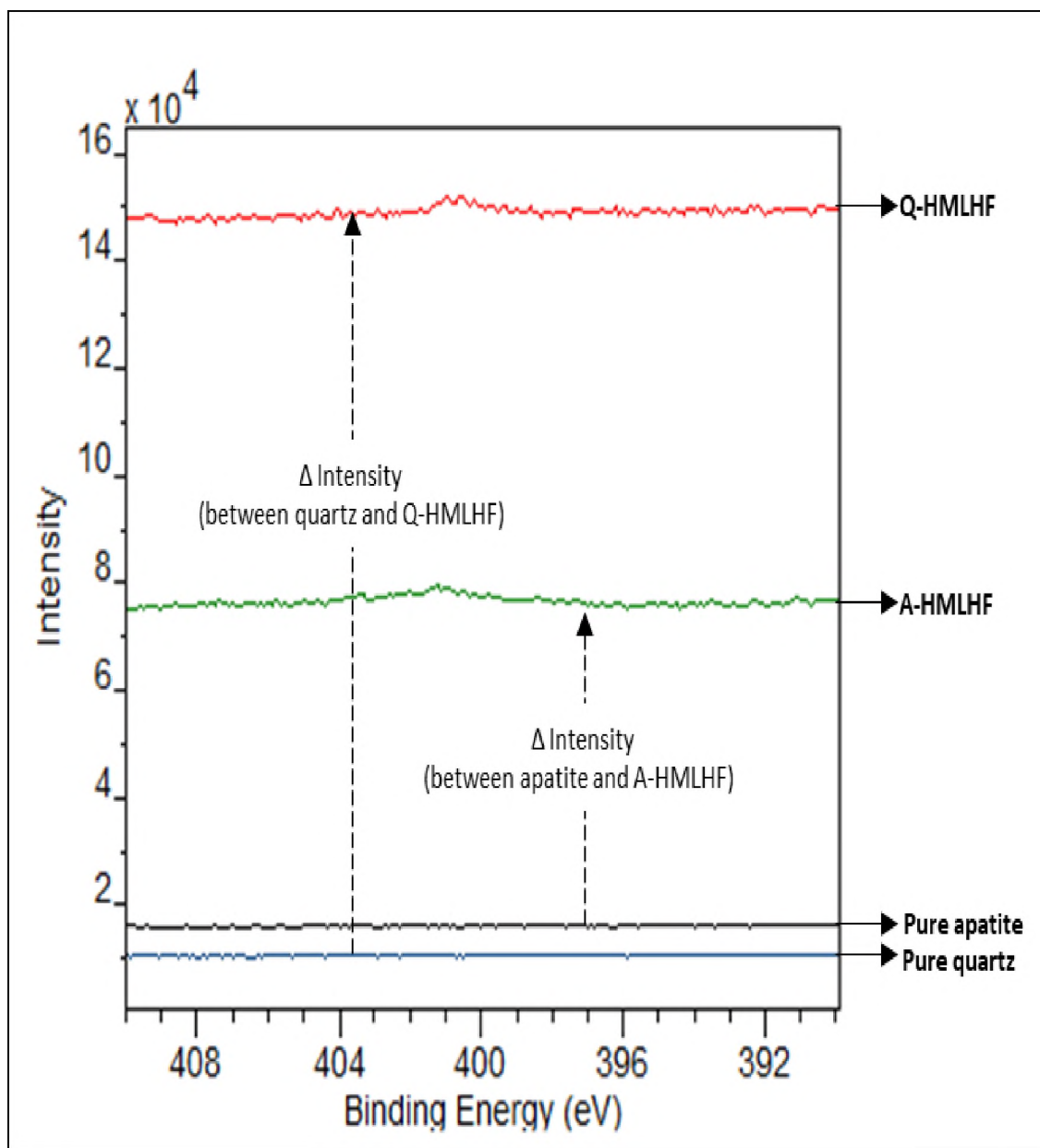


Figure 4.8 the XPS curve fitting of N (1S) of pure minerals and HMLHF treated quartz and apatite.

4.3.2. Zeta Potential Measurements. Zeta potential was used to investigate the electrical characteristics at mineral/water interfaces before and after the adsorption of ILs at different pH and stock concentrations. As indicated, the zeta values of pure apatite and

quartz in Figure 3.9 (section 3.0) regularly decreased with increasing the pH. It was also noticed that the magnitude of zeta potential of pure quartz is more negative compared to apatite at pH 9 and pH 11 (most of the phosphate flotation plants carry out flotation of phosphate ores at this pH range [21], [46]). The average zeta potential values of apatite and quartz were -17mV and -34mV , respectively, at pH 9 and -25 and -42 mV at pH 11. This difference in the electrical characteristics at each pH makes it possible to selectively alter the surface properties of either mineral by adding an appropriate reagent.

Figures 4.9 show quartz and apatite's zeta values before and after treatment with THAI and HMLHF at pH 7, pH 9, and pH 11. At pH 7, the zeta potential value of apatite after treatment with THAI was -10.55 mV compared to -7.4 mV for pure apatite. The zeta potential value of quartz increased from -20.3 mV to -16.09 mV after treatment with THAI. At pH 9 and 11, the results indicated a stronger interaction between ILs, and quartz surfaces compared to apatite surfaces. The changes in the magnitude of zeta potential values of apatite after treatment with THAI were smaller compared to quartz at both pH. Also, at the same range of pH, the shift of zeta potential ($\Delta\zeta$) of quartz after treatment with HMLHF was higher compared to quartz with THAI. For example, at pH 9, the shift of zeta potential ($\Delta\zeta$) of quartz after treatment with THAI was $+12.22\text{ mV}$ compared to the shift of zeta potential ($\Delta\zeta$) of quartz after treatment with HMLHF ($+21.95\text{ mV}$). These results supported the XPS studies obtained in the previous section that indicated the HMLHF has better adsorption in quartz surfaces compared to THAI.

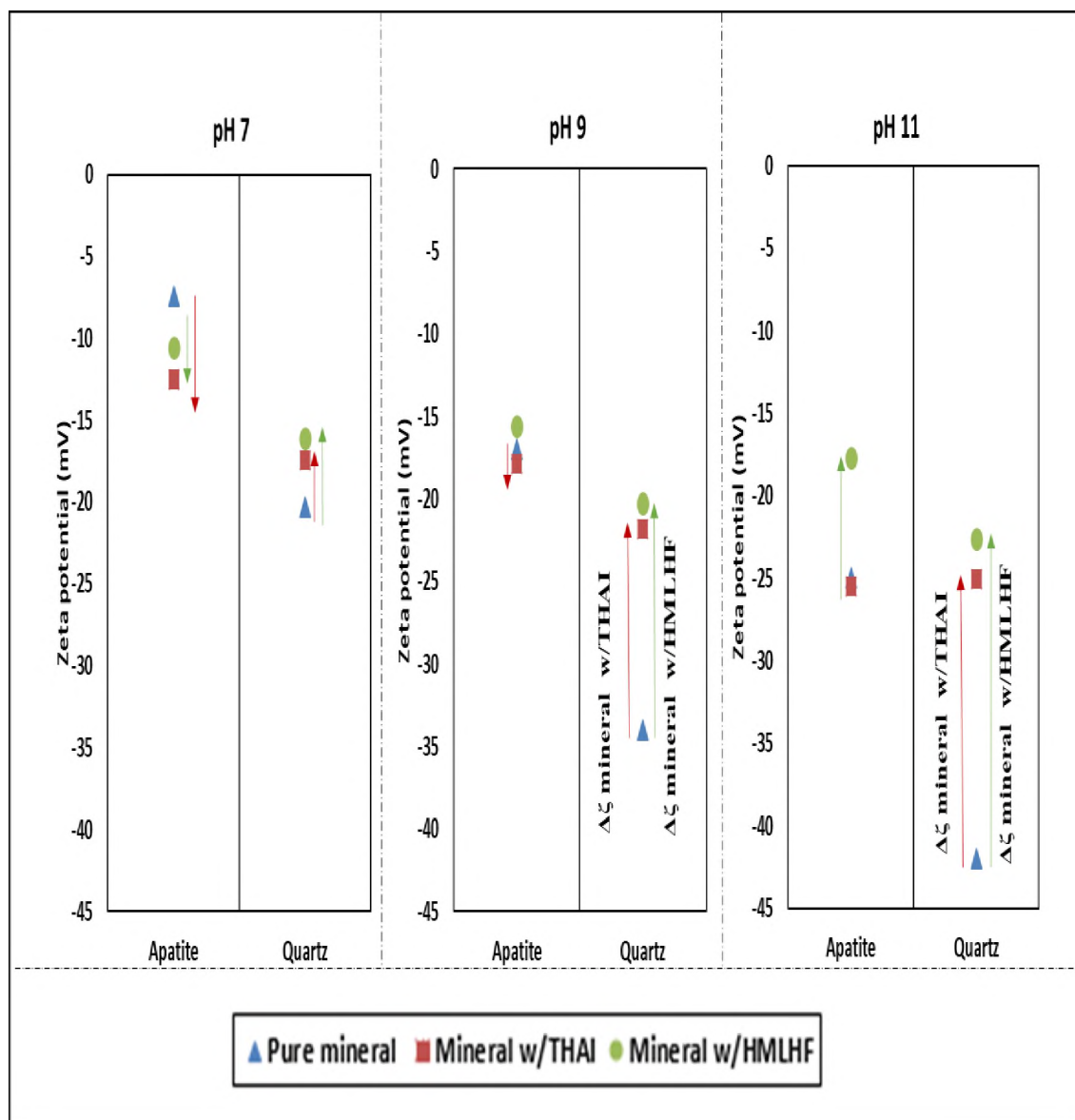


Figure 4.9 Zeta potential measurements of mineral suspensions before and after adsorption of ILs.

4.3.3. Micro-flotation Experiments. Micro-flotation tests were conducted using a Hallimond tube to understand the effect of ILs on the flotation of apatite and quartz without external factors such as mechanical parameters; thus, it is an excellent tool to assess the suitability of a particular reagent in the froth flotation process.

4.3.3.1. Single mineral flotation experiments in the presence of tetrahexyl-ammonium iodide (THAI) collector. Micro-flotation experiments using THAI were performed for single minerals (i.e., either apatite or quartz) at different experimental conditions, as shown in Table 4.1. In these experiments, the pulp pH, collector dosage, and flotation time were varied. The concentrate products were collected at different time intervals. Figure 4.10 shows the recovery of apatite and quartz in the presence of THAI. The overall flotation recovery of quartz was better than the flotation recovery of apatite. The quartz's recoveries at pH 11 were 90%, 86%, and 68% at 150, 100, and 50 g/ton, respectively, which were slightly better than the recoveries at pH 9 under the same conditions. The recovery of quartz increased with increasing THAI dosage and pH. The highest recovery of quartz (90%) was obtained at 150 g/ton of THAI and pH 11, while apatite recovery was 38% under the same condition. These results indicated that THAI could be used as a selective collector of silicate minerals in phosphates' reverse flotation.

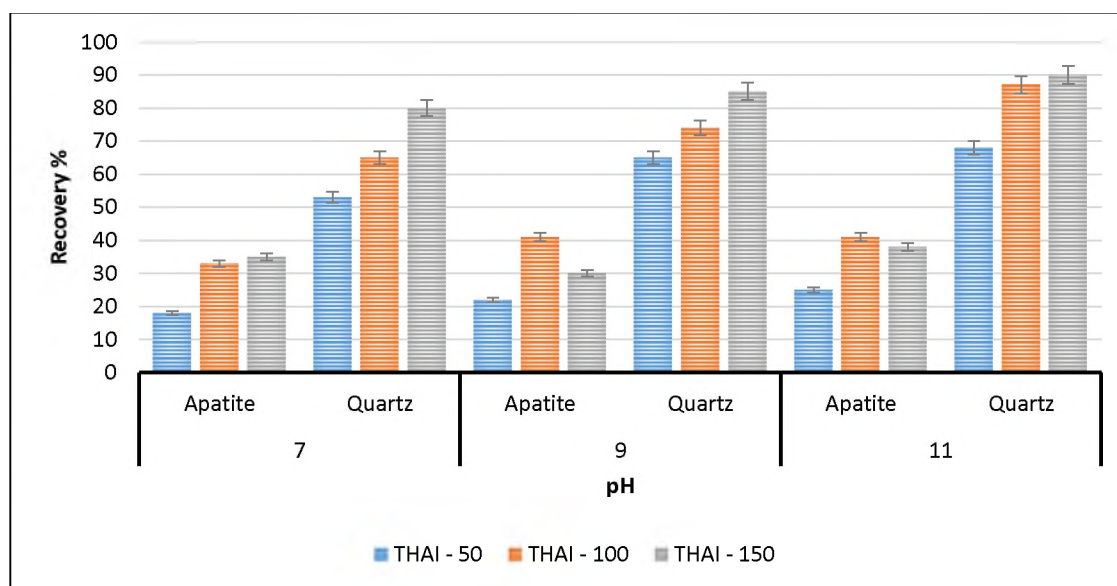


Figure 4.10 Recovery of apatite and quartz at different flotation conditions with THAI.

4.3.3.2. Single mineral flotation experiments in the presence of 1-hexyl-3-methylimidazoli hexafluorophosphate (HMLHF) collector. Micro-flotation experiments for single minerals with HMLHF were performed under conditions shown in Table 4.1. The concentrate products were collected at different time intervals. As shown in Figure 4.11, quartz recovery at different flotation conditions with HMLHF was better than apatite's flotation recovery. The recovery of quartz at 150 g/ton of HMLHF was 80%, 85%, and 90% at pH 7, 9, and 11, respectively. While at 50 g/ton of HMLHF, the recovery of quartz was 40%, 51%, and 67% at pH 7, 9, and 11, respectively. At 100 g/ton of IL and pH 11, quartz's flotation recovery was 84%, compared to 32% apatite.

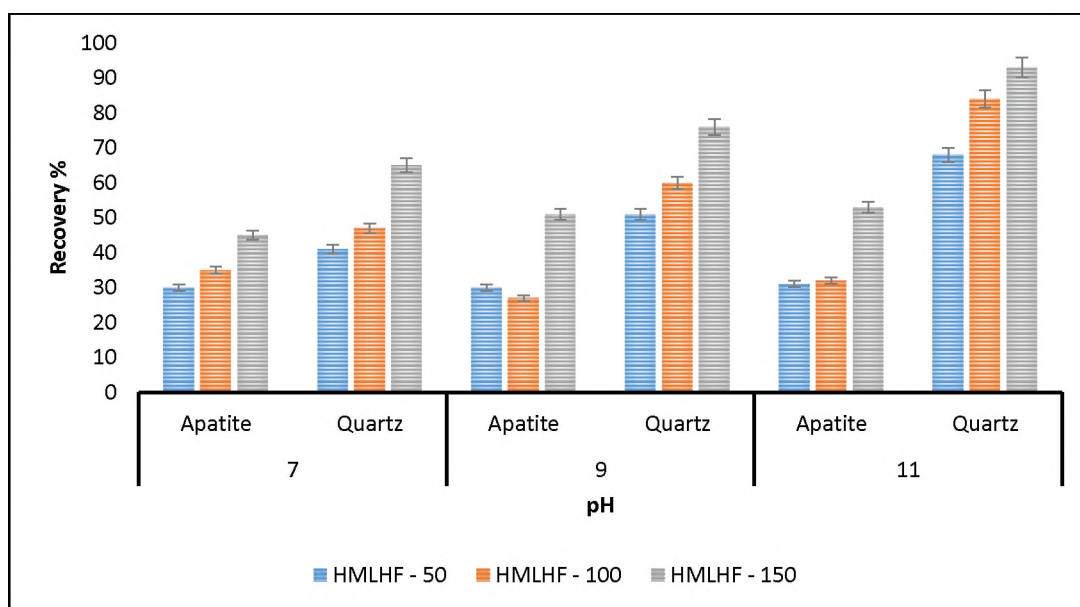


Figure 4.11 Recovery of apatite and quartz at different flotation conditions with HMLHF.

4.3.3.3. Comparison of single mineral flotation performance of apatite and quartz in the presence of ionic liquid collectors and commercially used dodecylamine collectors. Flotation performance of apatite and quartz in the presence of ionic liquid (ILs)

collectors and commercially Dodecylamine collectors were compared to explore the potential of ILs to serve as alternatives to DA. Based on the previous tasks, pH 9 and pH 11, and IL's dosage of 150 g/ton was the optimum conditions that gave the best recoveries of quartz in micro-flotation tests. Therefore, micro-flotation tests using Dodecylamine (DA) were conducted at DA dosage of 150 g/t and pH 9 and 11 to allow comparison of performance in both cases (i.e., IL and DA). Figure 4.12 shows the recoveries of quartz and apatite minerals in single mineral flotation using DA and ILs. The highest quartz recoveries were obtained at pH 11 and 150 g/ton of DA, HMLHF, and THAI (90%, 93%, and 90%), respectively. Under the same conditions, apatite recovery was significantly low (38%) when THAI was used compared to DA (47%). These results indicated that THAI and HMLHF could be more selectivity than DA at that the pH range studied.

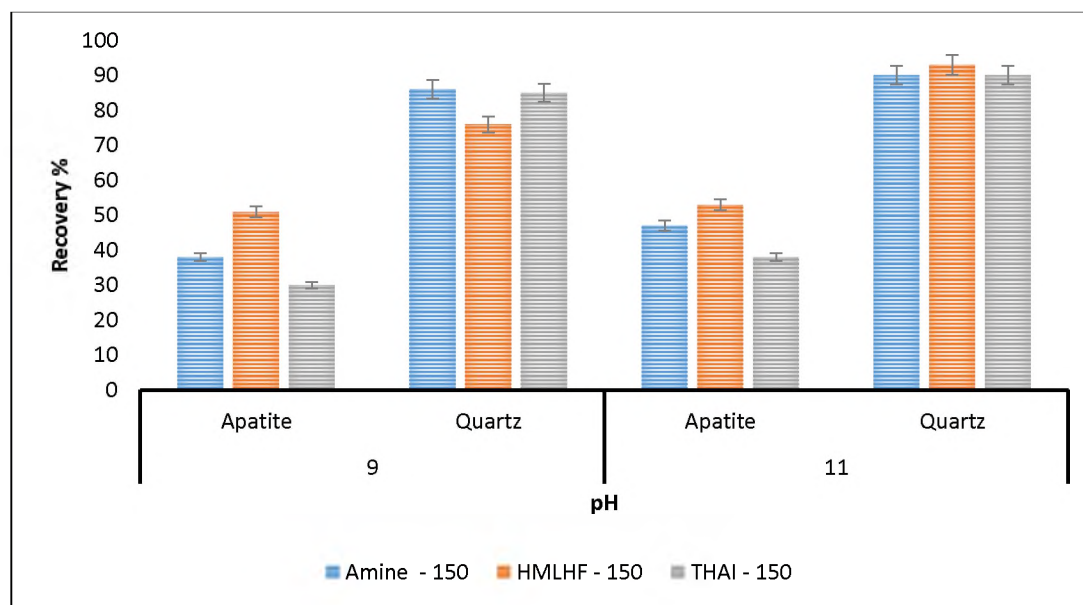


Figure 4.12 Recovery of apatite and quartz at optimum flotation conditions (pH 9 and 11, and 150 g/ton collector dosage).

4.3.3.4. Comparison of flotation performance of binary mineral system in the presence of ionic liquid collectors and commercially used dodecylamine collectors.

Micro-flotation tests of binary mineral systems were conducted to explore the selectivity of ILs as silicate collectors when mixed minerals exist. A binary minerals system was prepared by mixing pure apatite and pure quartz at an equal ratio (1:1). Micro-flotation tests of binary minerals systems were set up based on the optimum condition of identified from previous tasks (micro-flotation of single minerals). Figure 4.13 shows the recovery and grade of quartz minerals in concentrate products. As shown, when HMLHF was used, the recovery of quartz at pH 11 was the highest (recovery~90%), with low grade (~64%) as compared to THAI and Dodecylamine. Both THAI and Dodecylamine resulted in high recovery and grade at pH 9. For example, around 82% recovery of quartz at ~70% grade was obtained when Dodecylamine was used. While around 82% recovery at ~74% grade was obtained when THAI was used at the same pH. These observations are consistent with the results obtained from the adsorption studies in the previous section. HMLHF is anticipated to adsorb at both minerals (e.g., apatite and quartz); thus, it is less selective than THAI and DA. Results shown in Figure 4.14 indicated that a higher grade apatite's concentrate was obtained when HMLHF was used compared to THAI and Dodecylamine.

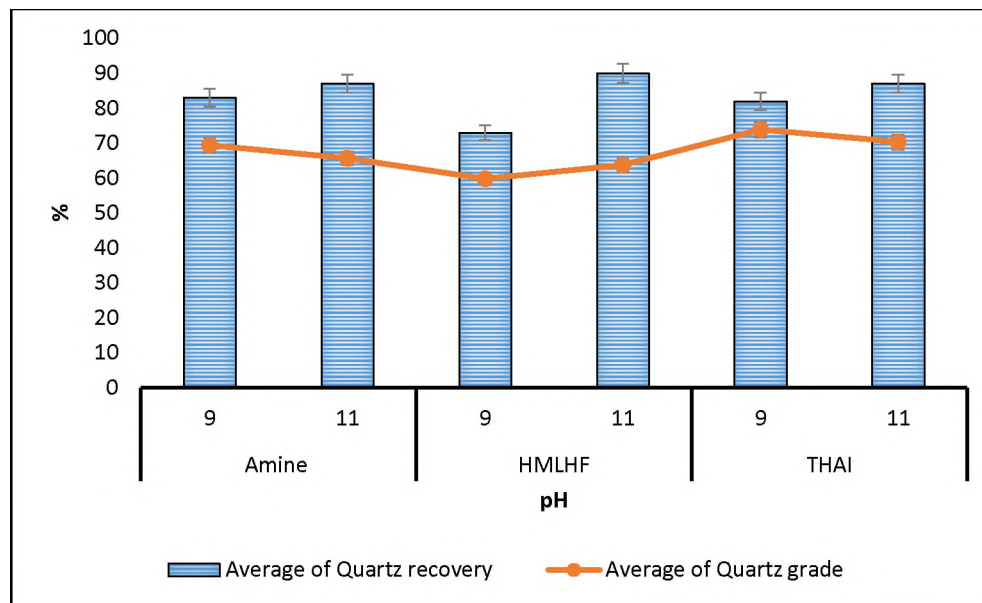


Figure 4.13 The recovery and grade of quartz in the presence of ionic liquids and Dodecylamine collectors.

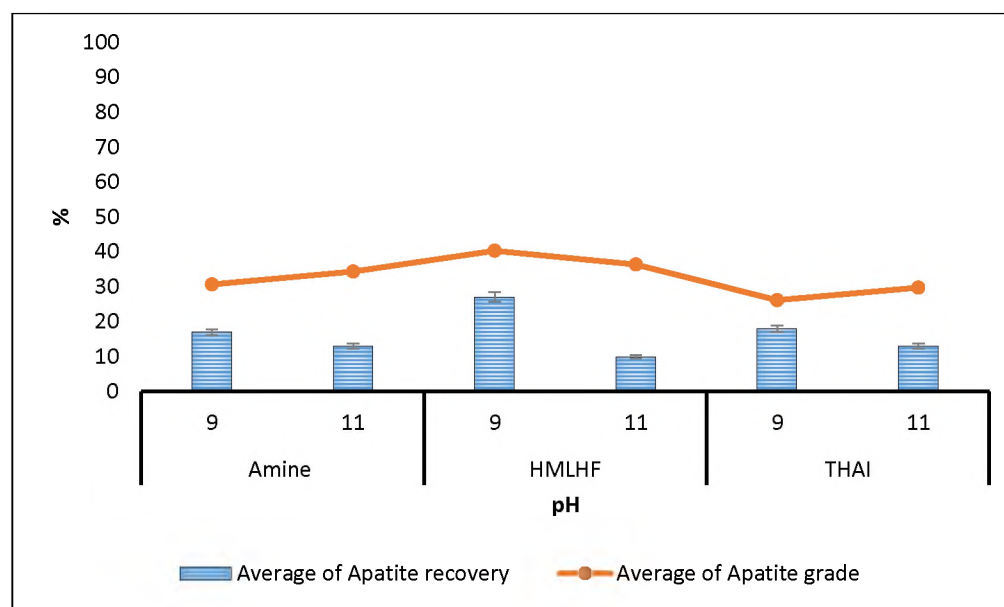


Figure 4.14 The recovery and grade of apatite in the presence of ionic liquids and Dodecylamine collectors.

5. APPLICATIONS OF ARTIFICIAL NEURAL NETWORK MODELING TO PREDICT THE FLOTATION PERFORMANCE OF PHOSPHATE-SILICATE ORES

5.1. BACKGROUND

The flotation efficiency of phosphate minerals is influenced by several key process variables [e.g., water chemistry, reagents chemistry, feed characteristics, cell type, and aeration rate]. Although each of these parameters influences the flotation process outcomes (recovery and grade) independently, their interdependence makes the process control very difficult.

Reliable prediction of process outcomes based on standard approaches is infeasible. Conventional modeling tools (e.g., semi-empirical mathematical functions and unconstrained/unsupervised statistical approaches) suffer from a number of limitations, including lack of applicability in complex systems (or systems that are different from the ones used for the model's calibration), requirement of extensive model validation, and poor prediction capabilities. Furthermore, the prediction performance of conventional modeling tools is further aggravated due to the intrinsically nonlinear cause-effect relations in such systems, wherein a large number of influential variables exist and interact, thereby giving rise to prodigiously large degrees of freedom and complex input-output correlations. Therefore, there is an urgent need to develop and employ adaptive intelligent control tools that take into account the diversity of these variables and their mutual interaction to ensure process stability and desired outcomes.

Machine learning (ML) models, in particular artificial neural networks (ANNs), have been used recently to predict the metallurgical performance of the flotation process in various applications [33]–[37]. Multi-layered ANN and random forests (RF) models were used to estimate concentrate grade in platinum flotation based on froth image analysis [98]. Labidi used ANN with 100 neurons to study the effect of various process variables on the flotation kinetics during paper de-inking [99]. Jorjani used ANN for predicting sulfur reduction in coal flotation (both organic and inorganic) using mixed culture microorganisms [100]. Multi-layered ANN was successfully employed to predict clayey coal's flotation behavior in the presence of $\text{Al}(\text{OH})_3$ -PAM polymer, which served as ash depressant [56]. In their work, a cascade-forward NN with the back-propagation (BP) algorithm was applied to predict the impact of five operational parameters on flotation performance and recovery of coal and ash. Ali et al. used five different machine learning models: ANN, RF, adaptive neuro-fuzzy inference system, Mamdani fuzzy logic, and hybrid neural fuzzy inference system to predict the froth ash and combustible recovery of fine high-ash coal [101].

In this study, experimental datasets produced from direct flotation processes in section 3.0 were assimilated within the progressive-and-adaptive framework of machine learning (ML) using artificial neural networks (ANNs) model. The ANN platform was trained, validated, and employed to predict the flotation outcomes in relation to the pulp and reagents characteristics, which in turn were used to determine the optimum process variables in the presence of the proposed reagents.

5.2. DATASETS DEVELOPMENT

Data generated from laboratory tests (described in section 3) were compiled into a database and used to train the ANN model and test its prediction performance. The database consists of 60 distinct data-records, featuring key process parameters (as shown in Figure 5.1) in the direct froth flotation experiments and their respective efficiencies (i.e., grades and recovery of P_2O_5). The variables were sodium silicate dosage (commercial dispersant), Hy-PAM dosage (novel depressant), Chitosan dosage (green depressant), pH (natural pH and pH 9), and flotation time (4 minutes and 10 minutes).

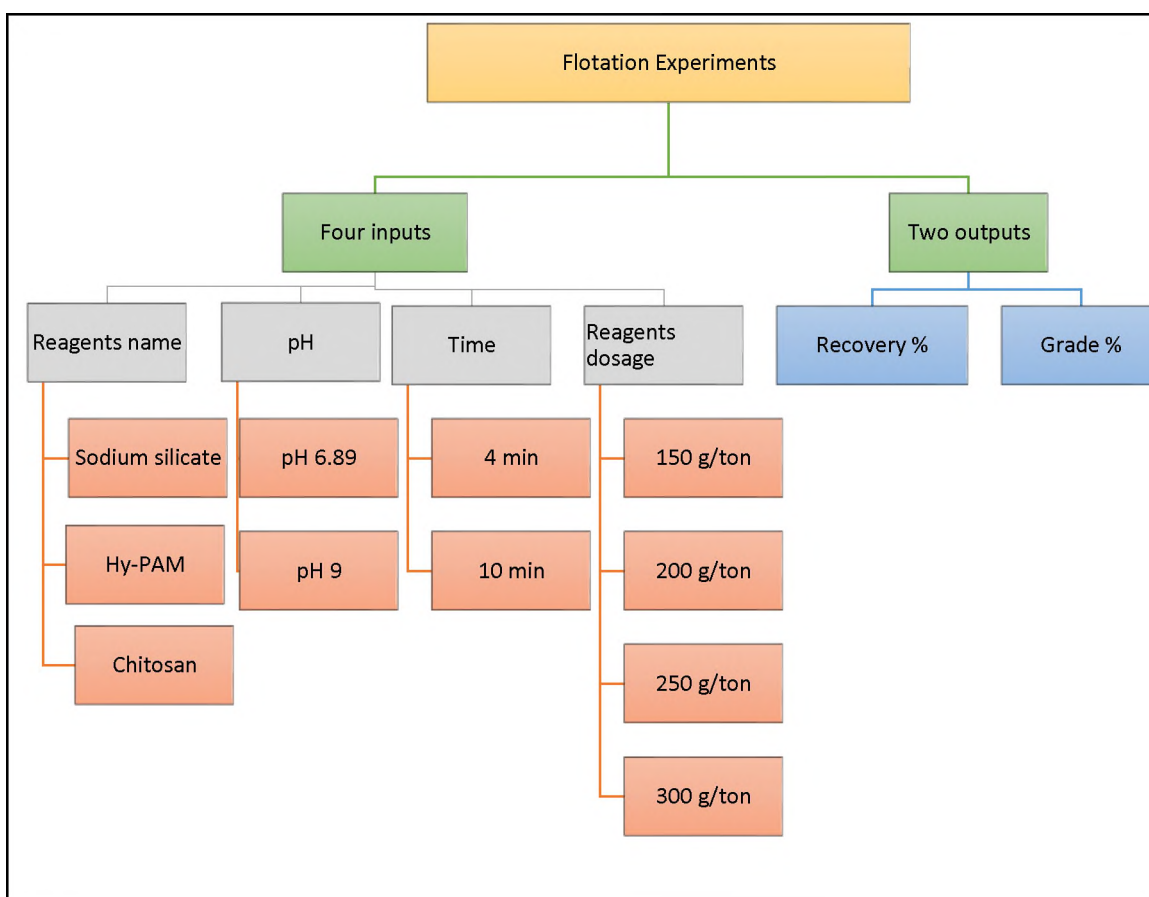


Figure 5.1 Datasets developed from laboratory scale batch flotation experiments of phosphate ore.

5.3. NEURAL NETWORK DESIGN

The artificial neural networks (ANNs) model was applied to predict and optimize phosphate minerals' flotation in the direct flotation process. Figure 5.2 shows the flowchart of the machine learning strategy applied in this study. Python was used to code the ANN model.

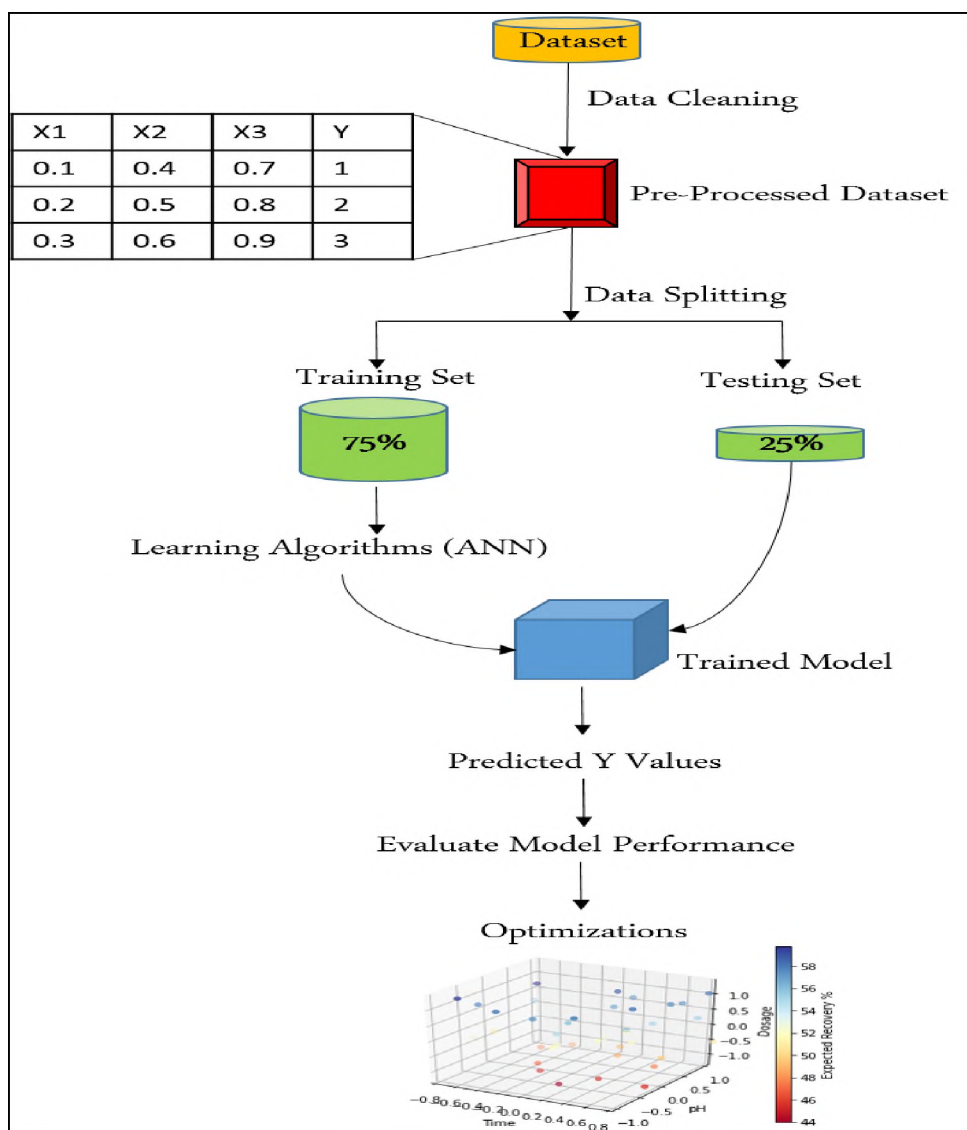


Figure 5.2 Flowchart of the machine learning strategy applied in this study.

To create a reliable dataset and improve the model's performance, data cleaning was performed to remove the errors and duplicate data from the dataset. Then, the dataset was split into 75% training and 25% testing to evaluate the model. The model was trained and validated in three different hidden layers at different nodes.

In order to evaluate the performance of the ANN model, Mean Absolute Error (MAE), Coefficients of Determination (R^2), and Root Mean Square Errors (RMSE) were used as performance indicators (Equations 5-1, 5-2, and 5-3). A good performance of the models was evaluated by defending the higher value of R^2 and the lower value of MAE and RMSE [101], [102]. The best-hidden layers were used to predict the flotation outcomes and optimize the floatation inputs.

$$MAE = \frac{[\sum_{i=1}^n (P_i - A_i)]}{n} \quad (5-1)$$

$$R^2 = \frac{[\sum_{i=1}^n (P_i - \bar{P})(A_i - \bar{A})]^2}{[\sum_{i=1}^n (P_i - \bar{P})^2 (A_i - \bar{A})^2]} \quad (5-2)$$

$$RMSE = \sqrt{\frac{\sum_{i=1}^n (P_i - A_i)^2}{n}} \quad (5-3)$$

where,

n = Total number of observations in the data being used

P_i = Predicted value by the model

A_i = Actual value in data

\bar{P} = Mean of all the predicted values

\bar{A} = Mean of all the actual value

For the optimization process, a 100 random input of flotation time, pH, and reagent dosage were generated for each set (sodium silicate, Hy-PAM, and chitosan). All the

random values were in the range of the trained data; for example, the range of flotation time was between 4 min and 10 min, the range of pH was between 7 and 11, and the range of reagent dosage was between 150g/ton to 300 g/ton. The model has predicted the flotation outputs based on the random inputs. After that, three-dimensional plots were established to optimize the flotation process.

5.4. RESULTS AND DISCUSSION

Table 5.1 shows the statistical analysis of training and testing data featuring four process variables: flotation time, pH, reagent type, and reagent dosage. 75% of the dataset was randomly selected as training data and 25% as testing data. As noted, the dataset contained three numerical features: time (4 min and 10 min), pH (pH 6.89 and pH 9), and reagent dosage (150, 200, 250, 300 g/ton), and one categorical variable (reagent type). The reagent type (sodium silicate, Hy-PAM, and chitosan) was converted into numerical data using One-Hot-Encoder. Data normalization was applied to capture the ANN model's accurate information. Table 5.2 shows the normalized data for both training and testing data.

Figures 5.3 and 5.4 show the real versus the predicted values of the ANN model's training and testing phases in three different hidden layers (one-hidden layer, two-hidden layer, and three-hidden layer) for both recovery and grade. Mean Absolute Error (MAE), Coefficient of determination (R²), and Root Mean Square Errors (RMSE) were used to evaluate the performance of the ANN model. These results indicated that three-hidden layers was given excellent performance compared to other hidden layers (Figure 5.3 E and F) and (Figure 5.4 E and F). It had MAE = 2.14, R² = 97.83% and RMSE = 4.03% in

training phosphate recovery, and MAE = 0.32%, R2 = 98.72% and RMSE = 0.42% for training phosphate grade. Table 5.3 presented the MAE, R2, and RMSE values for training and testing data for all the three hidden layers. These results showed a good performance in the three-hidden layer compared to other hidden layers; based on that, it was used to predict the flotation performance and for optimization study.

Table 5.1 Statistical analysis of trained and tested data.

Training data								
	count	mean	std	min	25%	50%	75%	max
Time	45.0	6.66	3.02	4.0	4.0	4.00	10.0	10.0
pH	45.0	7.95	1.06	6.89	6.89	7.95	9.0	9.0
Dosage	45.0	225.00	59.16	150.0	150.0	225.00	300.0	300.0
Sodium silicate	45.0	0.355	0.48	0.00	0.00	0.00	1.00	1.00
Hy-PAM	45.0	0.266	0.44	0.00	0.00	0.00	1.00	1.00
Chitosan	45.5	0.377	0.49	0.00	0.00	0.00	1.00	1.00
Testing data								
	count	mean	std	min	25%	50%	75%	max
Time	15.0	8.00	2.95	4.00	4.00	10.00	10.0	10.0
pH	15.0	7.95	1.096	6.90	6.90	7.95	9.0	9.0
Dosage	15.0	225.00	50.00	150.0	200.0	225.00	250.0	300.0
Sodium silicate	15.0	0.200	0.439	0.00	0.00	0.00	0.00	1.0
Hy-PAM	15.0	0.533	0.516	0.00	0.00	1.00	1.00	1.0
Chitosan	15.0	0.266	0.457	0.00	0.00	0.00	0.50	1.0

Table 5.2 Statistical analysis of normalized trained and tested data.

Normalized training data								
	count	mean	std	min	25%	50%	75%	max
Time	45.0	0.444	0.50	0.00	0.0	0.00	1.00	1.00
pH	45.0	0.511	0.50	0.00	0.0	1.00	1.00	1.00
Dosage	45.0	0.600	0.34	0.00	0.5	0.60	0.83	1.00
Sodium silicate	45.0	0.355	0.48	0.00	0.0	0.00	1.00	1.00
Hy-PAM	45.0	0.266	0.44	0.00	0.0	0.00	1.00	1.00
Chitosan	45.5	0.377	0.49	0.00	0.0	0.00	1.00	1.00
Normalized testing data								
	count	mean	std	min	25%	50%	75%	max
Time	15.0	0.666	0.485	0.00	0.00	1.000	1.00	1.00
pH	15.0	0.500	0.514	0.00	0.00	0.500	1.00	1.00
Dosage	15.0	0.629	0.331	0.00	0.50	0.667	0.83	1.00
Sodium silicate	15.0	0.200	0.439	0.00	0.00	0.00	0.00	1.00
Hy-PAM	15.0	0.533	0.516	0.00	0.00	1.00	1.00	1.00
Chitosan	15.0	0.266	0.457	0.00	0.00	0.00	0.50	1.00

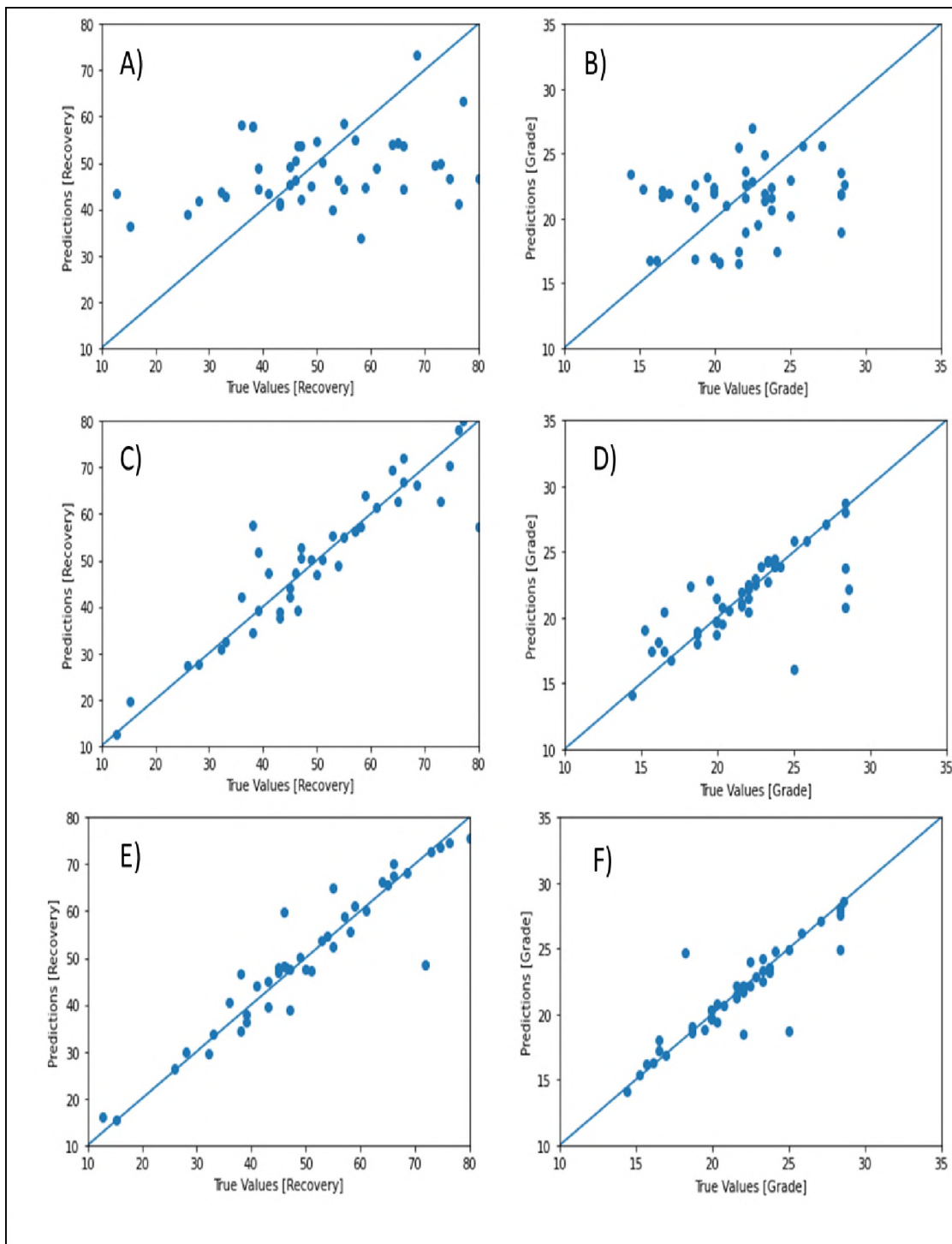


Figure 5.3 Real vs. predicted values of the training phase of the ANN model for both of recovery and grade (A) one-hidden layer recovery (%), (B) one-hidden layer grade (%), (C) Two-hidden layer recovery (%), (D) Two-hidden layer grade (%), (E) Three-hidden layer recovery %, and (F) Three-hidden layer grade (%).

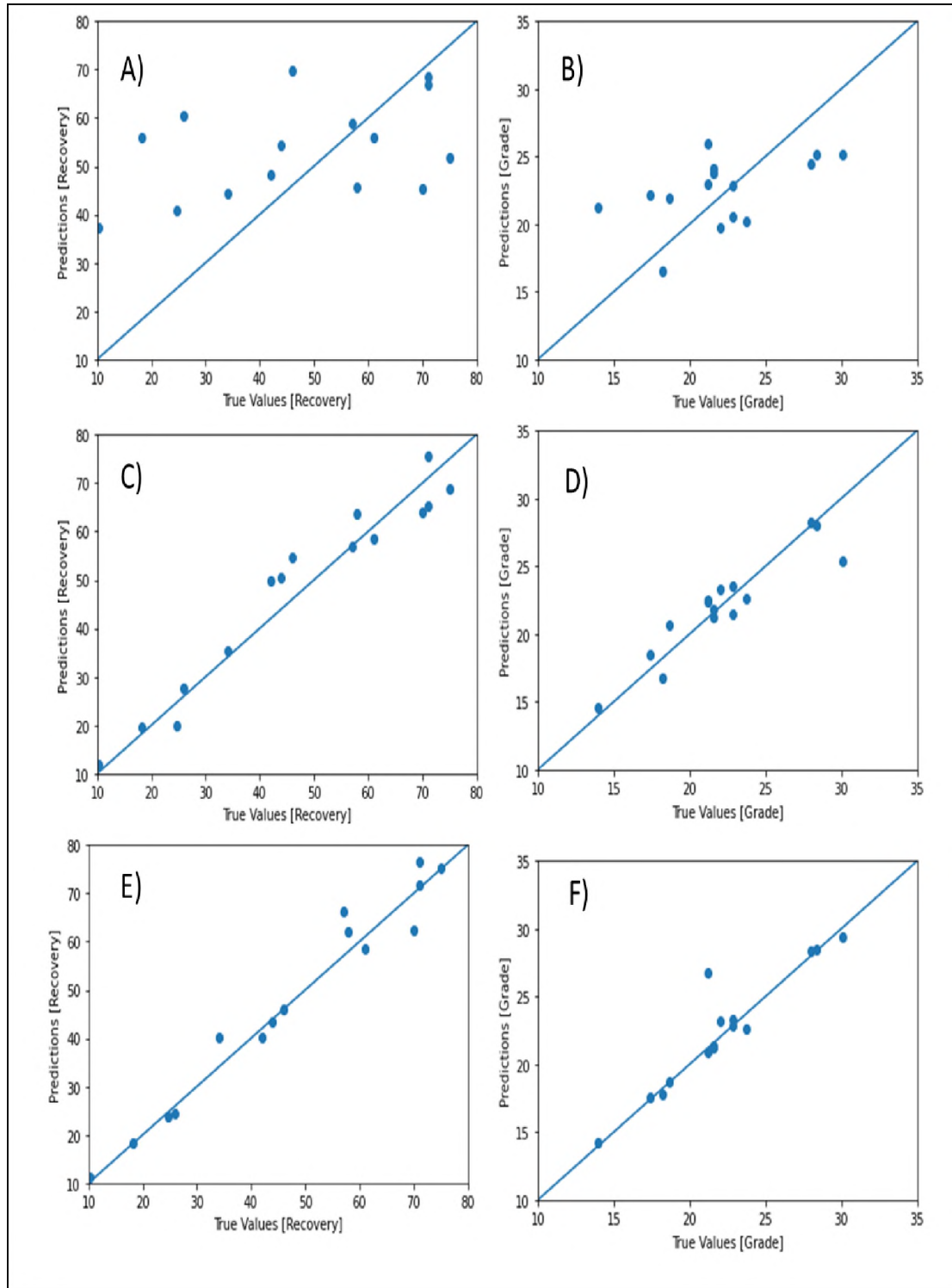


Figure 5.4 Real vs. predicted values of the testing phase of the ANN model for both of recovery and grade (A) one-hidden layer recovery (%), (B) one-hidden layer grade (%), (C) Two-hidden layer recovery (%), (D) Two-hidden layer grade (%), (E) Three-hidden layer recovery %, and (F) Three-hidden layer grade (%).

Table 5.3 Model evaluation of the three hidden layers.

ANN hidden layer	Flotation performance	MAE%		R ² %		RMSE%	
		Training	Testing	Training	Testing	Training	Testing
One-hidden layer	Recovery:	12.9	15.96	12.49	7.14	15.99	19.58
	Grade:	3.46	3.19	25.62	24.53	4.17	3.61
Two-hidden layer	Recovery:	4.79	4.30	84.16	93.88	6.84	5.02
	Grade:	1.53	1.20	59.74	85.01	2.36	1.6
Three-hidden layer	Recovery:	2.14	2.83	97.83	96.05	2.51	4.03
	Grade:	0.32	0.75	98.72	86.67	0.42	1.51

Figures 5.5 and 5.6 show a comparison between the predicted and the experimental values of P₂O₅ recovery and grade when three-hidden layer ANN model was employed. Results showed a good consistency. As indicated, optimal flotation inputs were observed in experiment number 10, 37, and 40 at 4 min of flotation time, 250-300 g/ton of reagents' dosages, and pH 9.

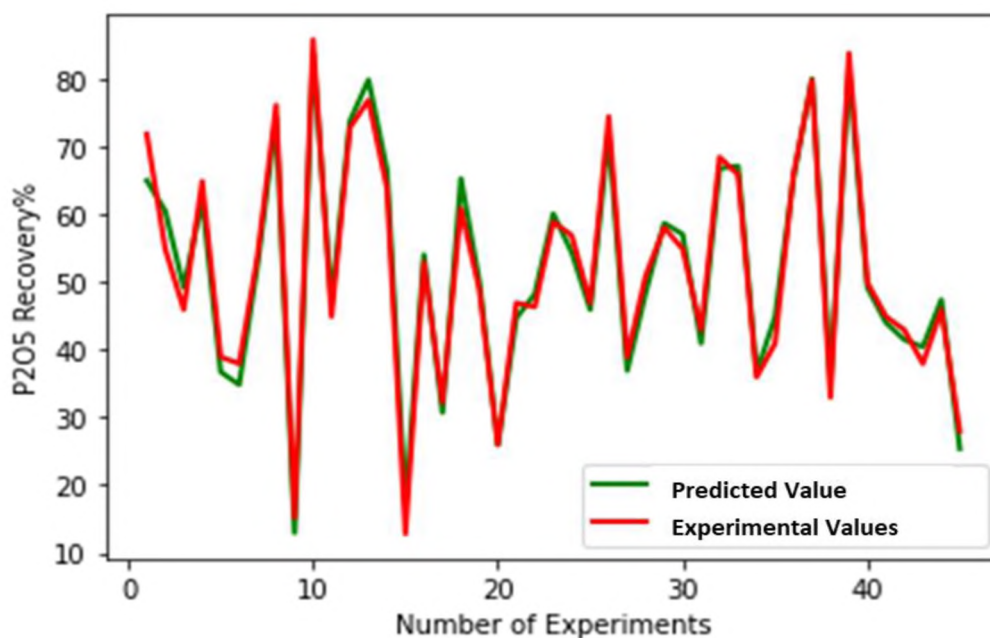


Figure 5.5 Predicted and experimental values of P₂O₅ recovery using three-hidden layer ANN.

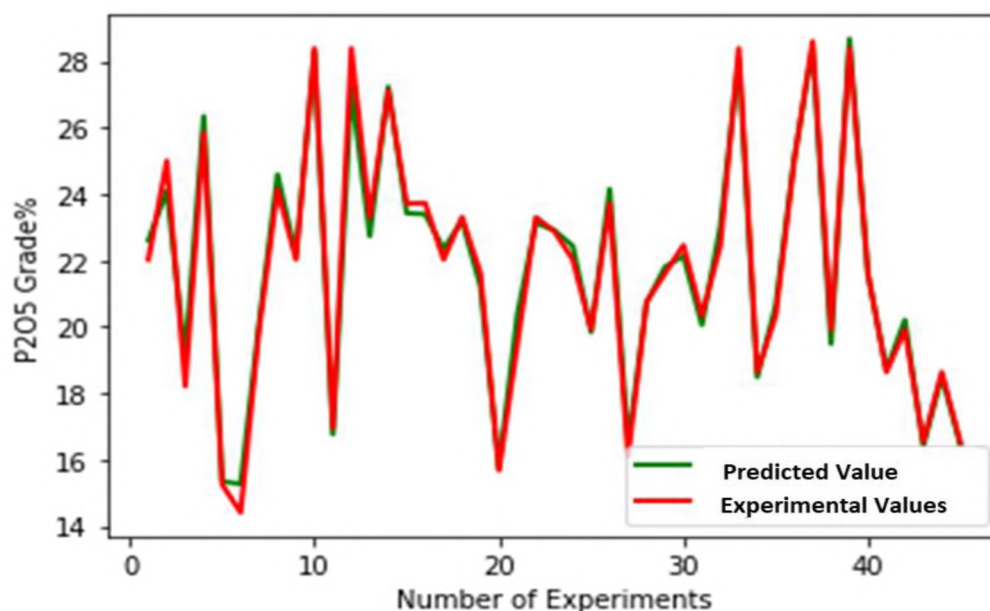


Figure 5.6 Predicted and experimental values of P_2O_5 grade using three-hidden layer ANN.

One hundred random flotation inputs, the flotation time, pH, and reagent dosage for each reagent type, were generated to optimize flotation efficiency of low-grade phosphate ore. The optimum values were selected based on the highest recovery and highest grade from the expected outputs. Figures 5.7 and 5.8 show the expected recovery and grade of phosphate minerals in the presence of sodium silicate. A three-dimensional scatter plot was used to present the relationship between the flotation inputs and flotation outputs. The random flotation inputs (time, pH, and reagent dosage) were customized on the three axes (x, y, and z), respectively. The expected flotation outputs were represented as scatter points and scaled by a color bar range. The base recovery and grade of P_2O_5 obtained in Section 3.3.2.1 were used as a minimum value for the purpose of the optimizations process.

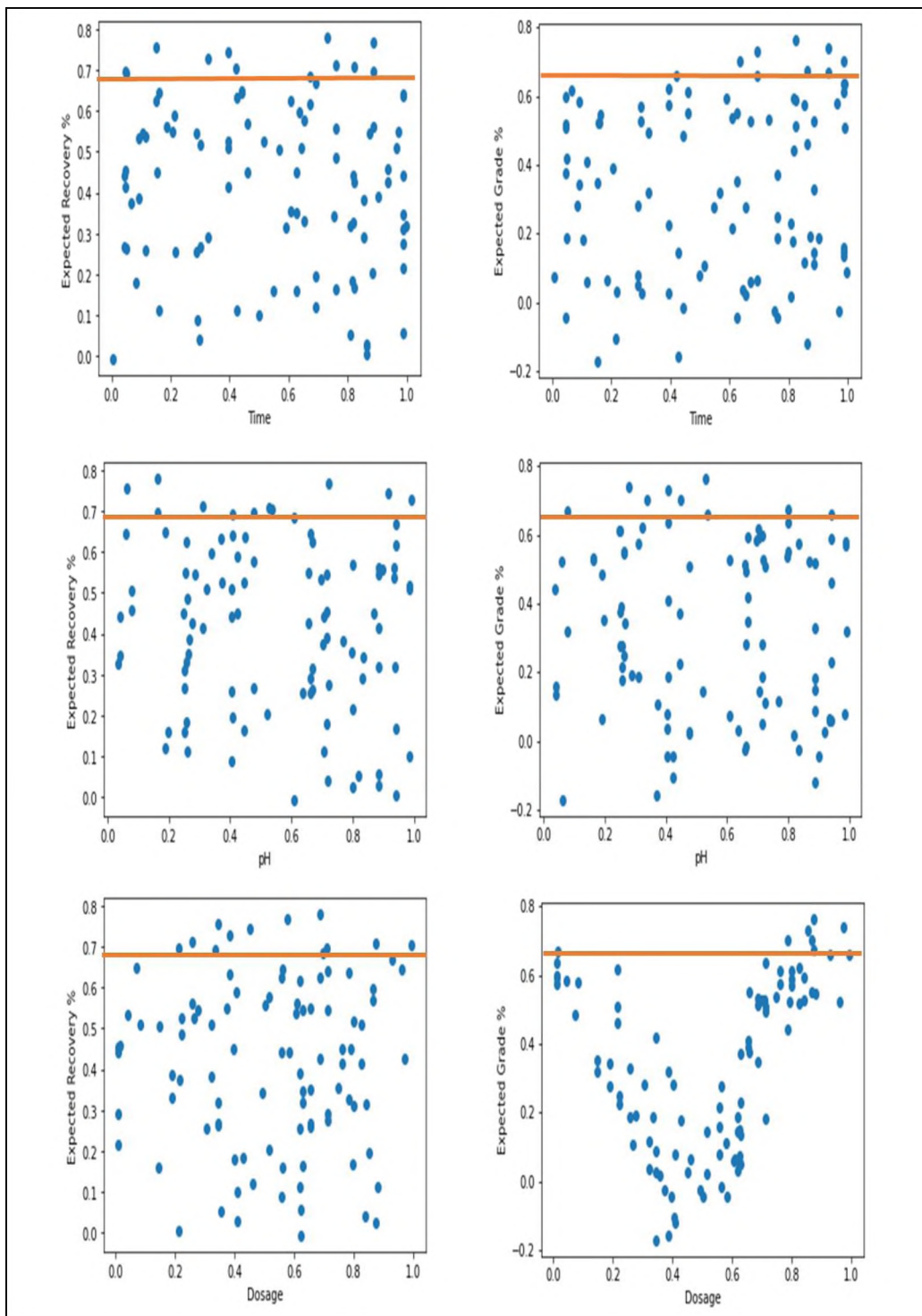


Figure 5.7 Predicted recovery and grade vs the random normalized input data in the presence of sodium silicate.

As seen, when the time is short, there was a possibility to obtain high recovery, but at the expense of grade at all range of other variables. While high recovery and high grade were expected at long flotation time. In the case of pH, high recovery and high grade were expected at low pH.

High recovery and high grade were also expected at a high dosage of sodium silicates. Results indicated that the optimum flotation performance in the presence of sodium silicate depressant could be obtained at long flotation time, low to medium pH, and high dosage. This means no real experiments are needed at a short time, high pH, and low dosages.

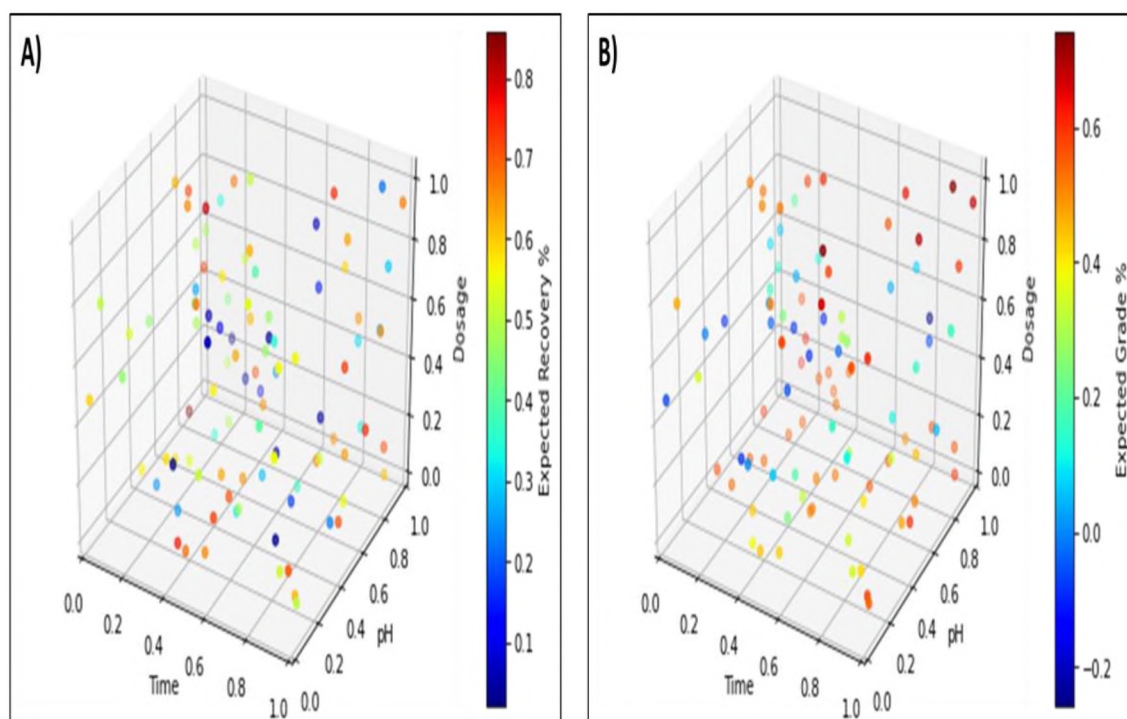


Figure 5.8 The relationship between the flotation inputs and expected flotation outputs in the presence of sodium silicate, recovery (A) and grade (B).

Figures 5.9 and 5.10 show the expected recovery and grade of phosphate minerals in the presence of Hy-PAM. High recovery and high grade were predicted at the all range of flotation time, low and high pH, and medium to high reagent dosage. Results indicated that the optimum flotation performance in the presence of Hy-PAM could be obtained at short flotation time, low pH, and high dosage. This means no real experiments are needed at a long time, high pH, and low dosages. While in the presence of chitosan, as shown in Figures 5.11 and 5.12, long flotation time, high pH, and high dosage were needed to obtain high recovery and high grade.

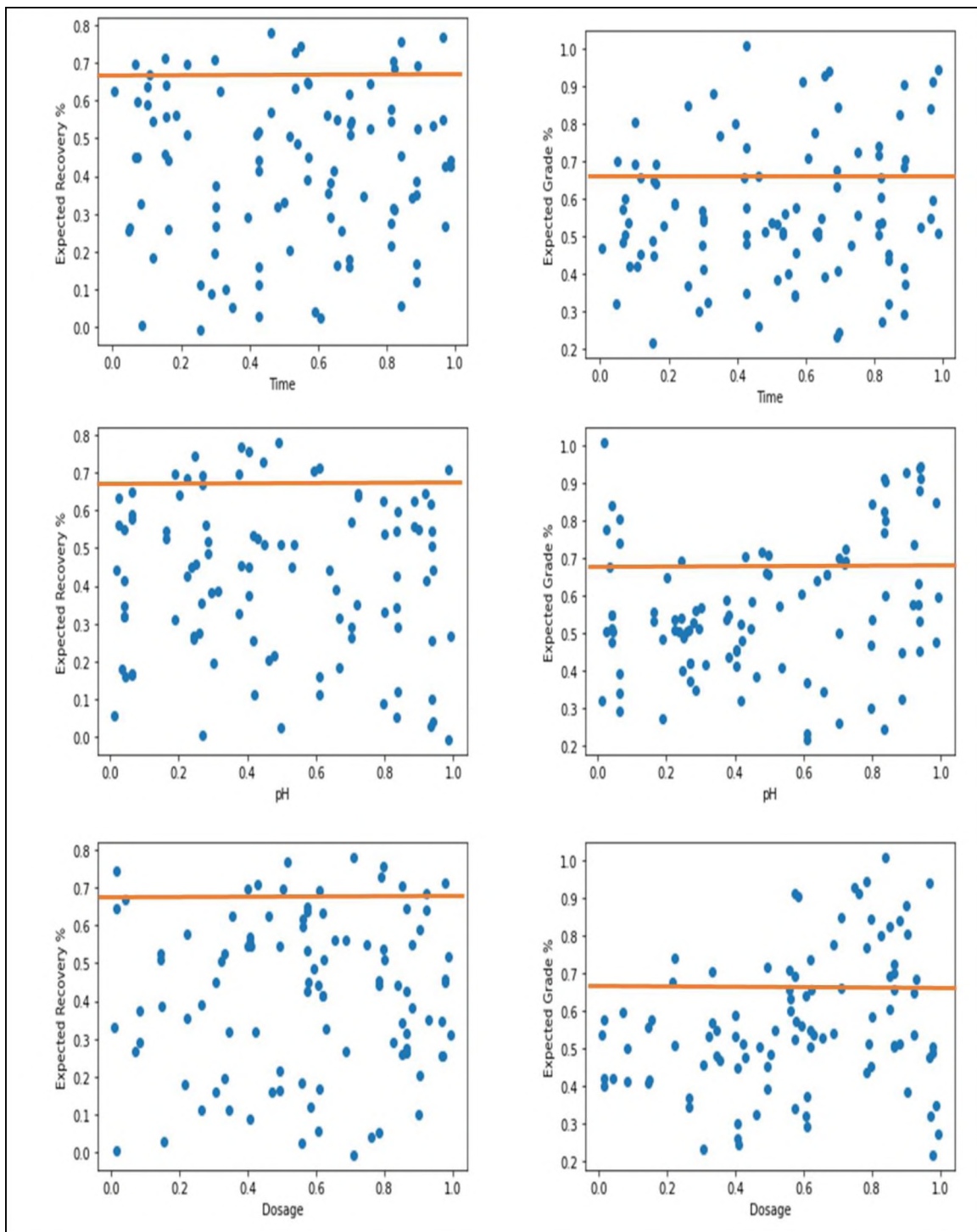


Figure 5.9 Predicted recovery and grade vs a random normalized input data in the presence of Hy-PAM.

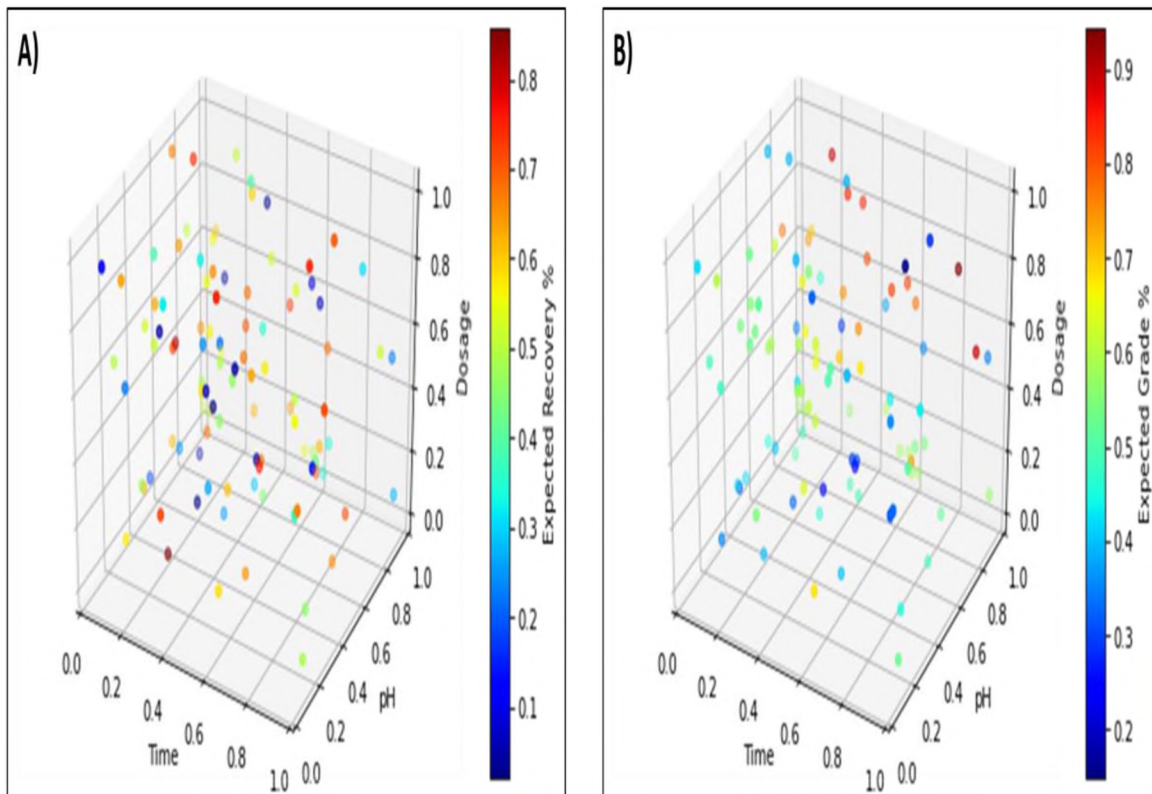


Figure 5.10 The relationship between the flotation inputs and expected flotation outputs in the presence of Hy-PAM, recovery (A), and grade (B).

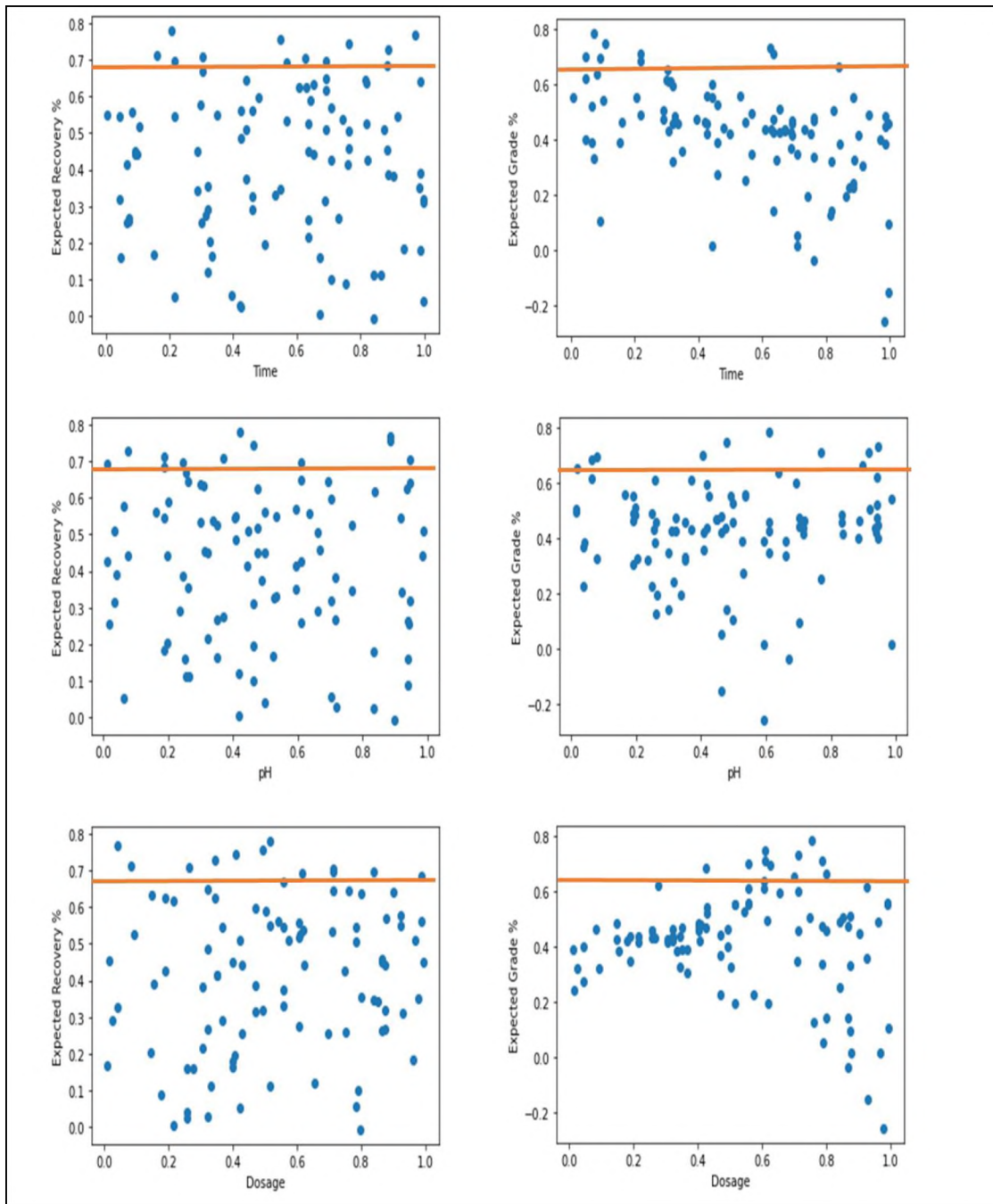


Figure 5.11 Predicted recovery and grade vs a random normalized input data in the presence of chitosan.

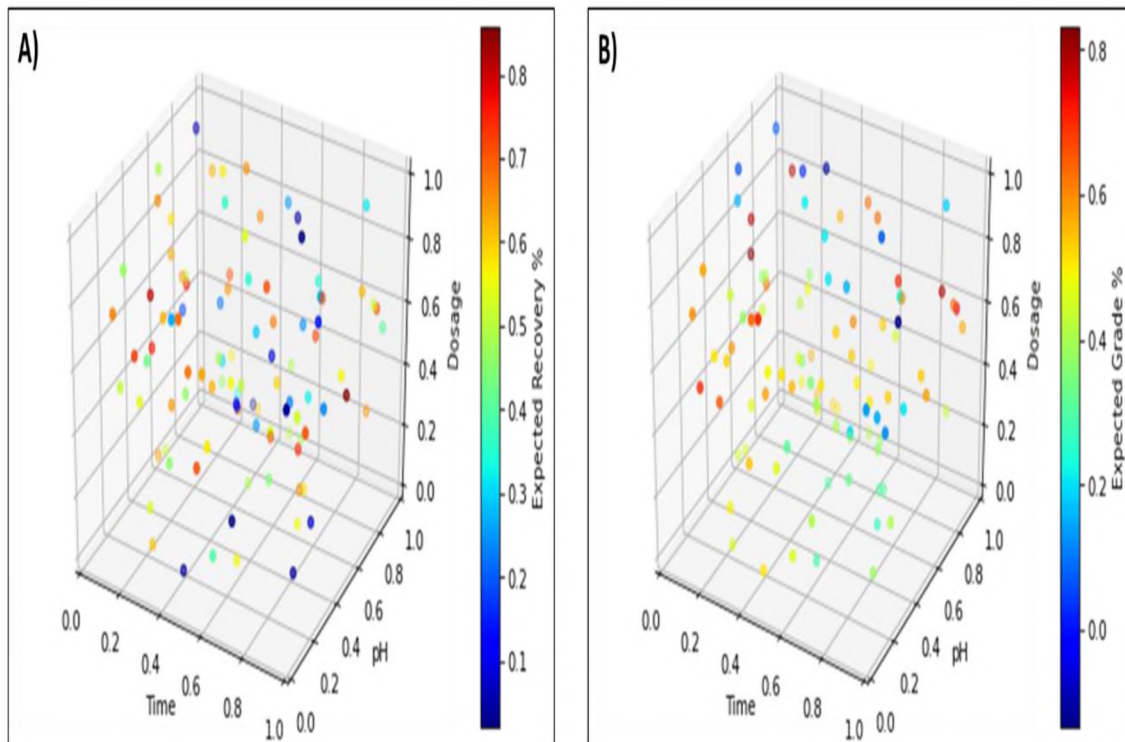


Figure 5.12 The relationship between the flotation inputs and expected flotation outputs in the presence of chitosan, recovery (A), and grade (B).

6. CONCLUSIONS AND RECOMMENDATIONS

6.1. CONCLUSIONS

This research aimed at improving the separation of silicate minerals from phosphate minerals in froth flotation process by utilizing novel and selective reagents.

Functional synthetic polymers and green biodegradable polymer were used as alternatives to conventional inorganic depressants of silicate minerals in the direct flotation of low-grade phosphate ore. Prior to the flotation process, zeta potential measurements on apatite (model phosphate mineral) and quartz (model silicate mineral) were conducted to examine the electrical properties of mineral surfaces in the presence and absence of depressants in order to understand the behavior of the flotation feed. The results showed stronger interactions between the quartz surface and Hy-PAM and chitosan at pH 9 compared to apatite. Bench-scale flotation tests of phosphate ore in the presence of Hy-PAM and chitosan were conducted at different conditions, including dispersant/depressant dosages, pulp's pH, and flotation time. The flotation efficiencies (recovery and grade) of P_2O_5 in the presence of Hy-PAM, chitosan, and sodium silicate (commercial dispersant) were compared. The results showed that at 10 min flotation, the highest recovery of P_2O_5 (86.82%) was observed when the Hy-PAM polymer was used. The second highest recovery was obtained at 66.7% when chitosan polymer was used. Both polymers were more selective than sodium silicate. Also, the highest grade of P_2O_5 (28.4%) was obtained when Hy-PAM was used. These results suggested that Hy-PAM and chitosan can be used as green and sustainable depressants of silicate minerals in the phosphate flotation process.

This research also investigated the potential of ionic liquids (ILs) to serve as selective collectors of silicates in the reverse flotation of phosphate minerals. Two ionic liquids were selected in this study: Tetrahexylammonium iodide (THAI) and 1-Hexyl-3-methylimidazolium hexafluorophosphate (HMLHF). Zeta potential measurements, FTIR, and XPS, were performed on pure and IL-treated minerals (i.e., apatite and quartz) to study the adsorption selectivity and understand the flotation behavior of minerals. The results indicated that ILs had preferential adsorption on the quartz surfaces compared to apatite surfaces. The flotation behavior of apatite (model phosphate mineral) and quartz (model silicate mineral) was investigated in micro-flotation system at different parameters and conditions, including IL type, reagents' dosages, and pulp's pH. In single flotation tests, the best flotation performance was observed at pH 11 and 150 g/ton of THAI with 90% recovery of quartz, while the recovery of apatite was 38% under the same flotation conditions. When HMLHF was used, the recovery of quartz at 150 g/ton of HMLHF was 93% at pH 11. The optimum flotation conditions were obtained at pH 9 and pH 11 in 150 g/ton of THAI and HMLHF in single mineral flotation. These optimum conditions were compared to Dodecylamine (DA) (commercial silicate's collector). The results showed an increase in the recovery of apatite minerals when DA and HMLHF were used. The recovery of apatite was significantly lower (38%) when THAI was used compared to Dodecylamine (47%) and HMLHF (53%). These results were consistent with the adsorption studies. When HMLHF was used in mixed mineral flotation, the quartz's recovery and grade were ~90% and ~64%, respectively, at pH 11. When THAI and DA were used, the recovery and grade of quartz were (87% and 70.3%), and 87% and 65.3%, respectively. Based on the

obtained results, this study demonstrated the potential of using ILs as alternative collector of silicate minerals in the reverse phosphate flotation at specific conditions.

Artificial Neural Network (ANN) model was employed to predict phosphate's flotation behavior in the direct froth flotation process. Mean absolute error (MAE), coefficient of determination (R^2), and root-mean-square error (RMSE) were used as performance indicators of the model. The results showed that good prediction performance was obtained when three-hidden layers were used. The calculated MAE, R^2 , and RMSE for phosphate recoveries were 2.14 %, 97.83%, and 4.03%, respectively. For phosphate grade, the calculated MAE, R^2 , and RMSE were 0.32%, 98.72%, and 0.42%, respectively. A three-dimensional scatter plot was used to present the relationship between the flotation inputs and flotation outputs for optimization purposes. Results indicated that the optimum flotation performance in the presence of sodium silicate could be achieved at longer flotation time, low to medium pH, and higher dosages. Results showed that the optimum flotation performance in the presence of Hy-PAM could be achieved at shorter flotation time, low pH, and higher dosages. Moreover, in the presence of chitosan polymer, longer flotation time, higher pH, and higher dosages were needed to achieve high recovery and high grade.

6.2. RECOMMENDATIONS FOR FUTURE WORK

Findings obtained from this study indicated that using hybrid polyacrylamide polymer (Hy-PAM) and chitosan as alternatives to conventional dispersants in direct froth flotation of phosphate minerals had positively impacted phosphate's recovery and grade.

However, to successfully implement this technology at an industrial scale, more work is recommended as follows:

- 1) Investigations on the flotation performance of phosphates as a function of additional operational variables such as agitation speed, airflow rate, temperature, and water chemistry. More datasets will be produced, which will enhance the accuracy of the developed ML model.
- 2) More investigations on the mechanism that govern the adsorption of polymers on phosphate and silicate minerals. This will allow for structural optimization of these polymers in relation to pulp's attributes.
- 3) Testing other machine learning models such as random forest, adaptive neuro-fuzzy inference system, Mamdani fuzzy logic, and hybrid neural fuzzy inference system, and compare their performances to ANN.
- 4) Detailed cost analysis to evaluate the economic benefits to use these reagents at industrial scale. This cost analysis should take into consideration the tailing disposal, water-treatment costs, energy consumption, and production rates compared to the case where conventional depressants are used.

Moreover, fundamental flotation studies conducted in this work show that tetrahexylammonium iodide (THAI) and 1-hexyl-3-methylimidazoli hexafluorophosphate (HMLHF) could be used as alternatives to conventional amine collectors of silicate minerals in the reverse flotation of phosphate minerals. However, these studies were preliminary and conducted using model minerals (pure minerals) in micro-flotation systems wherein a limited number of physicochemical variables were tested. Therefore, more studies using batch flotation systems have to be conducted to examine the

applicability of IL-based technology at industrial scale. These studies should investigate the impact of other physiochemical and operational variables on the flotation efficiency of phosphate mineral. Cost analysis needs to be done on IL-based technology to evaluate economic feasibility.

BIBLIOGRAPHY

- [1] L. Cisse and T. Mrabet, "World Phosphate Production: Overview and Prospects," 2004.
- [2] H. El-Shall, P. Zhang, N. Abdel Khalek, and S. El-Mofty, "Beneficiation technology of phosphates: Challenges and solutions," *Miner. Metall. Process.*, vol. 21, no. 1, pp. 17–26, Feb. 2004.
- [3] F. Hellal, S. El-Sayed, R. Zewainy, and A. Amer, "Importance of phosphate rock application for sustaining agricultural production in Egypt," *Bull. Natl. Res. Cent.*, vol. 43, no. 1, Dec. 2019.
- [4] and J. T. C. Kawatra, S. Komar, "Beneficiation of Phosphate Ore," 2013.
- [5] R. Houot, "Beneficiation of phosphatic ores through flotation: Review of industrial applications and potential developments," *Int. J. Miner. Process.*, vol. 9, no. 4, pp. 353–384, Oct. 1982.
- [6] A. Z. M. Abouzeid, A. T. Negm, and D. A. Elgillani, "Upgrading of calcareous phosphate ores by flotation: Effect of ore characteristics," *Int. J. Miner. Process.*, vol. 90, no. 1–4, pp. 81–89, Feb. 2009.
- [7] A. Tohry and A. Dehghani, "Effect of sodium silicate on the reverse anionic flotation of a siliceous-phosphorus iron ore," *Sep. Purif. Technol.*, vol. 164, pp. 28–33, May 2016.
- [8] T. R. Boulos, A. Yehia, S. S. Ibrahim, and K. E. Yassin, "A modification in the flotation process of a calcareous-siliceous phosphorite that might improve the process economics," *Miner. Eng.*, vol. 69, pp. 97–101, 2014.
- [9] H. Sis and S. Chander, "Reagents used in the flotation of phosphate ores: A critical review," *Miner. Eng.*, vol. 16, no. 7, pp. 577–585, 2003.
- [10] L. Zhang, "Enhanced phosphate flotation using novel depressants," *Theses Diss. Eng.*, Jan. 2013.
- [11] P. Zhang, R. Snow, Y. Yu, and M. D. Bogan, "A SCREENING STUDY ON PHOSPHATE DEPRESSANTS FOR BENEFICIATING FLORIDA PHOSPHATE MINERALS FINAL REPORT," 2002.
- [12] A. Z. M. Abouzeid, "Physical and thermal treatment of phosphate ores - An overview," *International Journal of Mineral Processing*, vol. 85, no. 4, pp. 59–84, 31-Jan-2008.

- [13] Y. Ruan, D. He, and R. Chi, "Review on beneficiation techniques and reagents used for phosphate ores," *Minerals*, vol. 9, no. 4. MDPI AG, p. 253, 01-Apr-2019.
- [14] A. Z. M. Abouzeid, A. T. Negm, and D. A. Elgillani, "Upgrading of calcareous phosphate ores by flotation: Effect of ore characteristics," *Int. J. Miner. Process.*, vol. 90, no. 1–4, pp. 81–89, Feb. 2009.
- [15] M. S. Oliveira, R. C. Santana, C. H. Ataíde, and M. A. S. Barrozo, "Recovery of apatite from flotation tailings," *Sep. Purif. Technol.*, vol. 79, no. 1, pp. 79–84, May 2011.
- [16] R. C. Santana, A. C. C. Farnese, M. C. B. Fortes, C. H. Ataíde, and M. A. S. Barrozo, "Influence of particle size and reagent dosage on the performance of apatite flotation," *Sep. Purif. Technol.*, vol. 64, no. 1, pp. 8–15, Nov. 2008.
- [17] J. L. Ivey, E. R. Morey, and D. J. Baylink, "The effects of phosphate depletion on bone.," *Adv. Exp. Med. Biol.*, vol. 103, pp. 373–380, 1978.
- [18] E. Takeda, Y. Taketani, N. Sawada, T. Sato, and H. Yamamoto, "The regulation and function of phosphate in the human body," *BioFactors*, vol. 21, no. 1–4, pp. 345–355, Jan. 2004.
- [19] C. A. Grant, D. N. Flaten, D. J. Tomasiewicz, and S. C. Sheppard, "The importance of early season phosphorus nutrition," *Canadian Journal of Plant Science*, vol. 81, no. 2. Agricultural Institute of Canada, pp. 211–224, 2001.
- [20] J. Wisniak, "Phosphorus-From discovery to commodity," *CSIR*, pp. 108–122, 2005.
- [21] A. Chaabouni, C. Chtara, A. Nzihou, and H. EL Feki, "Study the Nature and the Effects of the Impurities of Phosphate Rock in the Plants of Production of Phosphoric Acid," *J. Adv. Chem.*, vol. 7, no. 2, pp. 1296–1299, Jan. 2008.
- [22] J. Driver, D. Lijmbach, and I. Steen, "Why recover phosphorus for recycling, and how?," *Environ. Technol. (United Kingdom)*, vol. 20, no. 7, pp. 651–662, Jul. 1999.
- [23] B. Wills and J. Finch, *Wills' mineral processing technology: an introduction to the practical aspects of ore treatment and mineral recovery*. 2015.
- [24] R. M. Rahman, S. Ata, and G. J. Jameson, "The effect of flotation variables on the recovery of different particle size fractions in the froth and the pulp," *Int. J. Miner. Process.*, vol. 106–109, pp. 70–77, May 2012.
- [25] G. G. Holmes, S. R. Lishmund, and G. M. Oakes, *A review of industrial minerals and rocks in New South Wales*. New South Wales Dept. of Mineral Resources, 1982.

- [26] C. S. Ek, "Energy Usage in Mineral Processing," in *Mineral Processing at a Crossroads*, Dordrecht: Springer Netherlands, 1986, pp. 133–155.
- [27] "Rolla, MO Electricity Rates | Electricity Local." [Online]. Available: <https://www.electricitylocal.com/states/missouri/rolla/>. [Accessed: 28-Nov-2019].
- [28] H. & E. R. A. on ingredients Of and E. household cleaning Products, "Soluble Silicates," *Hum. Environ. Risk Assess. ingredients Eur. Househ. Clean. Prod.*, 2005.
- [29] H. P. Van Dokkum, J. H. J. Hulskotte, K. J. M. Kramer, and J. Wilmot, "Emission, Fate and Effects of Soluble Silicates (Waterglass) in the Aquatic Environment," *Environ. Sci. Technol.*, vol. 38, no. 2, pp. 515–521, Jan. 2004.
- [30] "SODIUM SILICATE - National Library of Medicine HSDB Database." [Online]. Available: <https://toxnet.nlm.nih.gov/cgi-bin/sis/search/a?dbs+hsdb:@term+@DOCNO+5028>. [Accessed: 25-Oct-2019].
- [31] M. A. Mohammed, J. T. M. Syeda, K. M. Wasan, and E. K. Wasan, "An overview of chitosan nanoparticles and its application in non-parenteral drug delivery," *Pharmaceutics*, vol. 9, no. 4. MDPI AG, 01-Dec-2017.
- [32] T. Dai, M. Tanaka, Y. Y. Huang, and M. R. Hamblin, "Chitosan preparations for wounds and burns: Antimicrobial and wound-healing effects," *Expert Review of Anti-Infective Therapy*, vol. 9, no. 7. NIH Public Access, pp. 857–879, Jul-2011.
- [33] S. Mohanty, "Artificial neural network based system identification and model predictive control of a flotation column," *J. Process Control*, vol. 19, no. 6, pp. 991–999, Jun. 2009.
- [34] E. C. Çilek, "Application of neural networks to predict locked cycle flotation test results," *Miner. Eng.*, vol. 15, no. 12, pp. 1095–1104, Dec. 2002.
- [35] S. AL-THYABAT, "On the optimization of froth flotation by the use of an artificial neural network," *J. China Univ. Min. Technol.*, vol. 18, no. 3, pp. 418–426, Sep. 2008.
- [36] F. Nakhaei, M. Irannajad, and M. Yousefikhoshbakht, "Simultaneous optimization of flotation column performance using genetic evolutionary algorithm," *Physicochem. Probl. Miner. Process.*, vol. 52, no. 2, pp. 874–893, 2016.
- [37] M. B. Hayat, L. Alagha, and S. M. Sannan, "Flotation Behavior of Complex Sulfide Ores in the Presence of Biodegradable Polymeric Depressants," *Int. J. Polym. Sci.*, vol. 2017, 2017.

- [38] J. T. McCoy and L. Auret, "Machine learning applications in minerals processing: A review," *Minerals Engineering*, vol. 132. Elsevier Ltd, pp. 95–109, 01-Mar-2019.
- [39] J. Leja, *Surface chemistry of froth flotation*. 2012.
- [40] J. C. Shean, BJ, "A review of froth flotation control," *Int. J. Miner. Process.*, vol. 100, no. 3–4, pp. 57–71, 2011.
- [41] S Farrokhpay, "The significance of froth stability in mineral flotation—A review," *Adv. Colloid Interface Sci.*, vol. 166, no. 1–2, pp. 1–7, 2011.
- [42] S. Rao, *Surface chemistry of froth flotation: Volume 1: Fundamentals*. 2013.
- [43] D Tao, "Role of bubble size in flotation of coarse and fine particles—a review," *Sep. Sci. Technol.*, vol. 39, no. 4, pp. 741–760, 2005.
- [44] C. W. Bakker, C. J. Meyer, and D. A. Deglon, "The development of a cavern model for mechanical flotation cells," in *Minerals Engineering*, 2010, vol. 23, no. 11–13, pp. 968–972.
- [45] R. Klimpel, "The influence of frother structure on industrial coal flotation," 1995.
- [46] R. Houot, "Beneficiation of phosphatic ores through flotation: Review of industrial applications and potential developments," *Int. J. Miner. Process.*, vol. 9, no. 4, pp. 353–384, 1982.
- [47] L. Bergh and J. Yianatos, "Control of rougher flotation circuits aided by industrial simulator," in *Journal of Process Control*, 2013, vol. 23, no. 2, pp. 140–147.
- [48] O. Oney, "Optimization of operating parameters of graphite flotation circuit using box-behnen design," 2018.
- [49] C. Ni, G. Xie, M. Jin, Y. Peng, and W. Xia, "The difference in flotation kinetics of various size fractions of bituminous coal between rougher and cleaner flotation processes," *Powder Technol.*, vol. 292, pp. 210–216, May 2016.
- [50] S. Al-Thyabat, R.-H. Yoon, and D. Shin, "Floatability of fine phosphate in a batch column flotation cell," *Mining, Metall. Explor.*, vol. 28, no. 2, pp. 110–116, May 2011.
- [51] A. Yehia, M. A. Youseff, and T. R. Boulos, "Different alternatives for minimizing the collector consumption in phosphate fatty acid flotation," *Miner. Eng.*, vol. 3, no. 3–4, pp. 273–278, 1990.
- [52] E. N. Peleka, P. P. Mavros, D. Zamboulis, and K. A. Matis, "Removal of phosphates from water by a hybrid flotation-membrane filtration cell," *Desalination*, vol. 198, no. 1–3, pp. 198–207, Oct. 2006.

- [53] X. Wang, "Study on the Flotation Process of Low Grade Phosphorite," *Wuhan Univ. Technol. -China*, 2005.
- [54] A. Alsafasfeh and L. Alagha, "Recovery of Phosphate Minerals from Plant Tailings Using Direct Froth Flotation," *Minerals*, vol. 7, no. 8, p. 145, Aug. 2017.
- [55] J. Kou, D. Tao, and G. Xu, "Fatty acid collectors for phosphate flotation and their adsorption behavior using QCM-D," *Int. J. Miner. Process.*, vol. 95, no. 1–4, pp. 1–9, Jul. 2010.
- [56] M. Khodakarami, O. Molatlhegi, and L. Alagha, "Evaluation of Ash and Coal Response to Hybrid Polymeric Nanoparticles in Flotation Process: Data Analysis Using Self-Learning Neural Network," *Int. J. Coal Prep. Util.*, vol. 39, no. 4, pp. 199–218, May 2019.
- [57] Q. Liu, Y. Zhang, and J. S. Laskowski, "The adsorption of polysaccharides onto mineral surfaces: An acid/base interaction," *Int. J. Miner. Process.*, vol. 60, no. 3–4, pp. 229–245, Dec. 2000.
- [58] L. A. F. Barros, E. E. Ferreira, and A. E. C. Peres, "Floatability of apatites and gangue minerals of an igneous phosphate ore," *Miner. Eng.*, vol. 21, no. 12–14, pp. 994–999, Nov. 2008.
- [59] A. Alsafasfeh, M. Khodakarami, L. Alagha, M. Moats, and O. Molatlhegi, "Selective depression of silicates in phosphate flotation using polyacrylamide-grafted nanoparticles," *Miner. Eng.*, vol. 127, pp. 198–207, Oct. 2018.
- [60] A. C. Araujo, P. R. M. Viana, and A. E. C. Peres, "Reagents in iron ores flotation," in *Minerals Engineering*, 2005, vol. 18, no. 2 SPEC. ISS., pp. 219–224.
- [61] B. Kar, H. Sahoo, S. S. Rath, and B. Das, "Investigations on different starches as depressants for iron ore flotation," *Miner. Eng.*, vol. 49, pp. 1–6, Aug. 2013.
- [62] B. Nanthakumar, D. Grimm, and M. Pawlik, "Anionic flotation of high-iron phosphate ores-Control of process water chemistry and depression of iron minerals by starch and guar gum," *Int. J. Miner. Process.*, vol. 92, no. 1–2, pp. 49–57, Jul. 2009.
- [63] E. T. Woodburn, R. P. King, and R. P. Colborn, "The Effect of Particle Size Distribution on the Performance of a Phosphate Flotation Process," 1971.
- [64] F. Hernáinz, M. Calero, and G. Blázquez, "Flotation of low-grade phosphate ore," *Adv. Powder Technol.*, vol. 15, no. 4, pp. 421–433, Jan. 2004.
- [65] R. Singh, Pradip, and T. A. P. Sankar, "Selective flotation of Maton (India) phosphate ore slimes with particular reference to the effects of particle size," *Int. J. Miner. Process.*, vol. 36, no. 3–4, pp. 283–293, Oct. 1992.

- [66] X. Liu, Y. Zhang, T. Liu, Z. Cai, T. Chen, and K. Sun, "Beneficiation of a sedimentary phosphate ore by a combination of spiral gravity and direct-reverse flotation," *Minerals*, vol. 6, no. 2, Apr. 2016.
- [67] Z. Huang *et al.*, "Utilization of a new Gemini surfactant as the collector for the reverse froth flotation of phosphate ore in sustainable production of phosphate fertilizer," *J. Clean. Prod.*, vol. 221, pp. 108–112, Jun. 2019.
- [68] P. Huang, L. Wang, and Q. Liu, "Depressant function of high molecular weight polyacrylamide in the xanthate flotation of chalcopyrite and galena," *Int. J. Miner. Process.*, vol. 128, pp. 6–15, Apr. 2014.
- [69] H. T. Chen, S. A. Ravishankar, and R. S. Farinato, "Rational polymer design for solid-liquid separations in mineral processing applications," *Int. J. Miner. Process.*, vol. 72, no. 1–4, pp. 75–86, Sep. 2003.
- [70] O. Molatlhegi and L. Alagha, "Ash Depression in Fine Coal Flotation Using a Novel Polymer Aid," *Int. J. Clean Coal Energy*, vol. 5, pp. 65–85, 2016.
- [71] L. Alagha, S. Wang, Z. Xu, and J. Masliyah, "Adsorption kinetics of a novel organic-inorganic hybrid polymer on silica and alumina studied by quartz crystal microbalance," *J. Phys. Chem. C*, vol. 115, no. 31, pp. 15390–15402, Aug. 2011.
- [72] P. Huang, M. Cao, and Q. Liu, "Using chitosan as a selective depressant in the differential flotation of Cu-Pb sulfides," *Int. J. Miner. Process.*, vol. 106–109, pp. 8–15, May 2012.
- [73] M. Hayat, "Mitigation of environmental hazards of sulfide mineral flotation with an insight into froth stability and flotation performance," *Dr. Diss.*, Jan. 2018.
- [74] A. Burke, E. Yilmaz, N. Hasirci, and O. Yilmaz, "Iron(III) ion removal from solution through adsorption on chitosan," *J. Appl. Polym. Sci.*, vol. 84, no. 6, pp. 1185–1192, Feb. 2002.
- [75] R. Bassi, S. O. Prasher, and B. K. Simpson, "Removal of selected metal ions from aqueous solutions using chitosan flakes," *Sep. Sci. Technol.*, vol. 35, no. 4, pp. 547–560, 2000.
- [76] H. S. Blair and T.-C. Ho, "Studies in the adsorption and diffusion of ions in chitosan," *J. Chem. Technol. Biotechnol.*, vol. 31, no. 1, pp. 6–10, May 2007.
- [77] A. Findon, G. McKay, and H. S. Blair, "Transport Studies for the Sorption of Copper Ions by Chitosan," *J. Environ. Sci. Heal. Part A Environ. Sci. Eng. Toxicol.*, vol. 28, no. 1, pp. 173–185, 1993.

- [78] M. Rhazi *et al.*, “Contribution to the study of the complexation of copper by chitosan and oligomers,” *Polymer (Guildf)*, vol. 43, no. 4, pp. 1267–1276, Dec. 2001.
- [79] J. C. Liu, Warmadewanthi, and C. J. Chang, “Precipitation flotation of phosphate from water,” *Colloids Surfaces A Physicochem. Eng. Asp.*, vol. 347, no. 1–3, pp. 215–219, Sep. 2009.
- [80] W. S. Wan Ngah, L. C. Teong, and M. A. K. M. Hanafiah, “Adsorption of dyes and heavy metal ions by chitosan composites: A review,” *Carbohydrate Polymers*, vol. 83, no. 4, pp. 1446–1456, 01-Feb-2011.
- [81] O. Molatlhegi, S. Khatibi, and L. Alagha, “Studies on the role of organic/inorganic polyacrylamides in fine coal flotation,” *2015 SME Annu. Conf. Expo C. 117th Natl. West. Min. Conf. - Min. Navig. Glob. Waters*, 2015.
- [82] “Metallurgical Accounting Formulas | Concentration and Recovery in Mineral Processing.” [Online]. Available: <https://www.911metallurgist.com/blog/metallurgical-accounting-formulas>. [Accessed: 06-Oct-2020].
- [83] A. Kaya and Y. Yukselen, “Zeta potential of clay minerals and quartz contaminated by heavy metals,” *Can. Geotech. J.*, vol. 42, no. 5, pp. 1280–1289, Oct. 2005.
- [84] I. Billard, “Ionic Liquids: New Hopes for Efficient Lanthanide/Actinide Extraction and Separation?,” in *Handbook on the Physics and Chemistry of Rare Earths*, vol. 43, Elsevier B.V., 2013, pp. 213–273.
- [85] F. Yang, F. Kubota, Y. Baba, N. Kamiya, and M. Goto, “Selective extraction and recovery of rare earth metals from phosphor powders in waste fluorescent lamps using an ionic liquid system,” *J. Hazard. Mater.*, vol. 254–255, no. 1, pp. 79–88, Jun. 2013.
- [86] S. Werner, M. Haumann, and P. Wasserscheid, “Ionic Liquids in Chemical Engineering,” *Annu. Rev. Chem. Biomol. Eng.*, vol. 1, no. 1, pp. 203–230, Jun. 2010.
- [87] M. Khodakarami and L. Alagha, “Separation and recovery of rare earth elements using novel ammonium-based task-specific ionic liquids with bidentate and tridentate O-donor functional groups,” *Sep. Purif. Technol.*, vol. 232, p. 115952, Feb. 2020.
- [88] J. Dupont, R. F. De Souza, and P. A. Z. Suarez, “Ionic liquid (molten salt) phase organometallic catalysis,” *Chem. Rev.*, vol. 102, no. 10, pp. 3667–3692, Oct. 2002.

- [89] A. M. Ferreira, J. A. P. Coutinho, A. M. Fernandes, and M. G. Freire, "Complete removal of textile dyes from aqueous media using ionic-liquid-based aqueous two-phase systems," *Sep. Purif. Technol.*, vol. 128, pp. 58–66, May 2014.
- [90] J. Pernak *et al.*, "Long alkyl chain quaternary ammonium-based ionic liquids and potential applications," *Green Chem.*, vol. 8, no. 9, pp. 798–806, 2006.
- [91] J. Weng, C. Wang, H. Li, and Y. Wang, "Novel quaternary ammonium ionic liquids and their use as dual solvent-catalysts in the hydrolytic reaction," *Green Chem.*, vol. 8, no. 1, pp. 96–99, 2006.
- [92] H. Sahoo, S. S. Rath, and B. Das, "Use of the ionic liquid-tricaprylmethyl ammonium salicylate (TOMAS) as a flotation collector of quartz," *Sep. Purif. Technol.*, vol. 136, pp. 66–73, Nov. 2014.
- [93] X. Zhu, H. Wei, M. Hou, Q. Wang, X. You, and L. Li, "Thermodynamic behavior and flotation kinetics of an ionic liquid microemulsion collector for coal flotation," *Fuel*, vol. 262, p. 116627, Feb. 2020.
- [94] H. Sahoo, N. Sinha, S. S. Rath, and B. Das, "Ionic liquids as novel quartz collectors: Insights from experiments and theory," *Chem. Eng. J.*, vol. 273, pp. 46–54, Aug. 2015.
- [95] D. Azizi, F. Larachi, and M. Latifi, "Ionic-liquid collectors for rare-earth minerals flotation—Case of tetrabutylammonium bis(2-ethylhexyl)-phosphate for monazite and bastnäsite recovery," *Colloids Surfaces A Physicochem. Eng. Asp.*, vol. 506, pp. 74–86, Oct. 2016.
- [96] H. Sahoo, S. S. Rath, S. K. Jena, B. K. Mishra, and B. Das, "Aliquat-336 as a novel collector for quartz flotation," *Adv. Powder Technol.*, vol. 26, no. 2, pp. 511–518, Mar. 2015.
- [97] H. Sahoo, S. S. Rath, B. Das, and B. K. Mishra, "Flotation of quartz using ionic liquid collectors with different functional groups and varying chain lengths," *Miner. Eng.*, vol. 95, pp. 107–112, Sep. 2016.
- [98] R. Peter King, *Modeling and Simulation of Mineral Processing Systems*. 2012.
- [99] J. Labidi, M. À. Pèlach, X. Turon, and P. Mutjé, "Predicting flotation efficiency using neural networks," *Chem. Eng. Process. Process Intensif.*, vol. 46, no. 4, pp. 314–322, Apr. 2007.
- [100] E. Jorjani, S. Mesroghli, and S. C. Chelgani, "Prediction of operational parameters effect on coal flotation using artificial neural network," *J. Univ. Sci. Technol. Beijing Miner. Metall. Mater. (Eng Ed)*, vol. 15, no. 5, pp. 528–533, Oct. 2008.

- [101] D. Ali, M. B. Hayat, L. Alagha, and O. K. Molatlhegi, “An evaluation of machine learning and artificial intelligence models for predicting the flotation behavior of fine high-ash coal,” *Adv. Powder Technol.*, vol. 29, no. 12, pp. 3493–3506, Dec. 2018.
- [102] X. Dou and Y. Yang, “Comprehensive Evaluation of Machine Learning Techniques for Estimating the Responses of Carbon Fluxes to Climatic Forces in Different Terrestrial Ecosystems,” *Atmosphere (Basel)*., vol. 9, no. 3, p. 83, Feb. 2018.

VITA

Ashraf Alsafasfeh grew up in Tafila, Jordan. In May 2014, he received his B.S with honors in Mining Engineering from Tafila Technical University, Jordan. In May 2017, he received his M.S degree in Mining Engineering from Missouri University of Science and Technology, MO, USA. After that, he started his Ph.D. in Mining Engineering at Missouri University of Science & Technology (Missouri S&T) in Rolla, Missouri, USA. In December 2020, he received his Ph.D. in Mining Engineering from Missouri S&T. During his Ph.D., he worked as a research and teaching assistant at Missouri S&T for environment and mine safety courses. He was awarded outstanding graduate research from Missouri S&T in 2020 and a stipend funding research award from Rock Mechanics and Explosives Research Center at Missouri S&T. Alongside his studying, he had two great opportunities to work as an intern with one of the biggest coal companies in USA, Peabody Energy-Peabody Corporate Headquarters, in 2019. And, with one of the biggest salt company in USA, Compass Minerals-Underground Salt Mine, as a mine engineer intern. Ashraf Alsafasfeh has been a member of the Jordan Engineers Association since 2014 and a member of the Society of Mining, Metallurgy, and Exploration (SME) since 2017.